PUBLICATIONS OF
THE UNIVERSITY OF EASTERN FINLAND

Dissertations in Forestry and Natural Sciences

MATIAS KOIVUROVA

COHERENCE OF PULSED LIGHT:
THEORY, MODELING, AND EXPERIMENTS

UNIVERSITY OF
EASTERN FINLAND

PUBLICATIONS OF THE UNIVERSITY OF EASTERN FINLAND
DISSERTATIONS IN FORESTRY AND NATURAL SCIENCES

N:o 345

Matias Koivurova

COHERENCE OF PULSED LIGHT:

THEORY, MODELING, AND EXPERIMENTS

ACADEMIC DISSERTATION

To be presented by the permission of the Faculty of Science and Forestry for public examination in the Auditorium M100 in Metria Building at the University of Eastern Finland, Joensuu, on June 26th, 2019, at 12 o'clock.

University of Eastern Finland
Department of Physics and Mathematics
Joensuu 2019

Grano Oy
Jyväskylä, 2019
Editors: Pertti Pasanen, Jukka Tuomela,
Matti Vornanen, and Pekka Toivanen

Distribution:
University of Eastern Finland Library / Sales of publications
julkaisumyynti@uef.fi
http://www.uef.fi/kirjasto

ISBN: 978-952-61-3115-3 (print)
ISSNL: 1798-5668
ISSN: 1798-5668
ISBN: 978-952-61-3116-0 (pdf)
ISSNL: 1798-5668
ISSN: 1798-5668

Author's address:
University of Eastern Finland
Department of Physics and Mathematics
P. O. Box 111
80101 JOENSUU
FINLAND
email: Matias.Koivurova@uef.fi

Supervisors:
Professor Ari T. Friberg
University of Eastern Finland
Department of Physics and Mathematics
P. O. Box 111
80101 JOENSUU
FINLAND
email: Ari.Friberg@uef.fi

Professor Jari Turunen
University of Eastern Finland
Department of Physics and Mathematics
P. O. Box 111
80101 JOENSUU
FINLAND
email: Jari.Turunen@uef.fi

Reviewers:
Professor Juha Toivonen
Tampere University of Technology
Photonics Laboratory
P. O. Box 692
33101 TAMPERE
FINLAND
email: Juha.Toivonen@tuni.fi

Professor Klas Lindfors
University of Cologne
Department of Chemistry
Greinstraße 4-6
50939 KÖLN
GERMANY
email: Klas.Lindfors@uni-koeln.de

Opponent:
Professor Ivan A. Vartanyants
Deutsches Elektronen-Synchrotron DESY
Photon Science
Notkestraße 85
22607 HAMBURG
GERMANY
email: Ivan.Vartaniants@desy.de

Matias Koivurova
Coherence of Pulsed Light: Theory, Modeling, and Experiments
Joensuu: University of Eastern Finland, 2019
Publications of the University of Eastern Finland
Dissertations in Forestry and Natural Sciences
N:o 345

ABSTRACT

This work contains extensions of theoretical ideas to nonstationary fields, along with the detailed study of some correlation induced effects. Furthermore, several measurement schemes in spatial, temporal, as well as spectral domains are introduced, and the generation of model fields is considered.

The concept of cross-spectral purity is extended to nonstationary fields, and it is investigated whether this property is conserved upon propagation. Later on, it is shown how such fields could be generated, and a peculiar duality with fields satisfying Wolf's scaling law is found. Fields that are not cross-spectrally pure are studied in detail, and the resulting spatiotemporal effects are investigated. It is found that such fields mix their spatial and temporal coherence properties, and in the considered scheme, the coupling becomes stronger with shorter pulses. Additionally, it is established that pulses generated in stable cavities that are longer than a few optical cycles may be approximated as being cross-spectrally pure. Several partially coherent model fields are discussed, in both spatial and temporal domains. Their correlation-induced properties are investigated, with an emphasis on spatial self-focusing and temporal self-splitting. Additionally, the theoretical framework for self-Fourier transforming beams is developed.

Several measurement schemes for characterizing nonstationary fields in spatial, temporal, as well as spectral domain are considered in detail, and some novel extensions are found. New methods that are able to measure the two-coordinate spatial coherence function are demonstrated, which are applicable for measuring nonstationary fields as well. In particular, it is shown what information can be extracted from simple linear time-domain interferometric measurements. Some nonlinear pulse measurement schemes are improved upon, and a novel method for measuring the spectral correlations of pulsed light is found.

Finally, schemes for generating partially coherent fields are examined. Starting from a setup for decreasing the temporal coherence of completely coherent input pulse trains, it is then shown that increasing temporal or spectral coherence is feasible. Particularly simple experimental methods for generating partially coherent beams with rotating elements are discussed and the generation of cross-spectrally pure fields is studied.

Universal Decimal Classification: *535.1, 535.3, 535.4, 53.084.85, 681.7.*
OCIS codes: *030.1640, 030.4070, 030.6600, 050.1950, 050.2230, 140.3538, 140.7090, 190.7220, 230.1040, 230.1980, 230.4110, 320.5540, 320.6629, 350.5500.*
Keywords: *Pulsed light, coherence, spatiotemporal coupling, ultrashort pulses, sub-cycle pulses, stability, correlation induced phenomena, model fields, interferometry, optical metrology, nonlinear optics, rotating optical elements.*

ACKNOWLEDGMENTS

This thesis embodies the academic journey I have traversed during my years at the University of Eastern Finland. In 2011, I began my studies at the Bachelor level, although my knowledge of physics was nearly zero at the time. I chose this field only because I didn't know what to do with my life, and I thought it would be simple to transfer to other technological areas from here. However, during the summer between the first and second study years, I felt something physically change in my brain. It was as if something finally fell into place. Ever since then, I have looked at the world in a whole new way: all unanswered questions relating to the way the world works are but puzzles waiting to be solved, where the difficulty increases the further you go – physics is the ultimate game of wits. As such, I have had the good fortune of getting a job that is also my hobby. This journey would not have been complete, or even possible without the influence of several people, both inside and outside the workplace.

First and foremost, I want to thank my supervisor, Prof. Ari T. Friberg, for not taking everything I say for granted and giving me a fair amount of fresh scepticism. The several discussions on science, life, politics, etc., have been thought provoking, and the way you underline the importance of communication skills in research has developed my expression style considerably. I am also indebted to my other supervisor, Prof. Jari Turunen, whose enthusiasm and experience have been an almost unending source of new ideas. There was a time when I couldn't leave Jaris office without something new to do, which showed me how deep this area of research is. A special thanks goes also to Dr. Henri Partanen, who has provided me with a fine example on experimental work procedures. I still strive to get results that are on par with yours. Additionally, I thank Prof. Tero Setälä, Prof. Tommi Hakala, Dr. Kimmo Saastamoinen, Dr. Lasse-Petteri Leppänen, Dr. Lutful Ahad, and Antti Hannonen for the many chances to work on new research projects.

Additionally, my current office mate Henri Pesonen deserves an honorary mention for excellent performance in making sure that I do not run out of caffeine. I also had some fine moments with Dr. Andreas Norrman, Antonie Verhoeven, and Olli Ovaskainen. As for other people at the workplace, I am thankful to Dr. Noora Heikkilä, Hannele Karppinen, Marita Ratilainen, and Katri Mustonen, for having the patience and skills to deal with the bureuacratic side of academia. These tasks were also carried out by the ever changing heads of the department, Prof. Pasi Vahimaa, Prof. Seppo Honkanen, Prof. Timo Jääskeläinen, and most recently Prof. Jyrki Saarinen. I am also grateful to my former students, Taher Khan, Atri Halder, Julien Lahyani, and Nathan Cariou, as well as the dozens of others who have been the subjects of my teachings. As I taught you, I also learned so much more.

Out of the people outside the University of Eastern Finland, I am especially thankful to Prof. Chaoliang Ding from Luoyang University, with whom we obtained many great results; I hope our collaboration will carry on for years to come. Other collaborations that I am grateful for include the work with Dr. Gianluca Geloni from European X-FEL, as well as with Prof. Sergei Popov, Prof. Lars Berglund, Dr. Elena Vasileva, and Dr. Yuanyuan Li from KTH. Without these people, many of the results in this thesis would not exist, and I am sure we will work together in the future as well. The insightful comments by Prof. Juha Toivonen and Prof. Klas Lindfors are highly appreciated, and I am thankful to Prof. Ivan Vartanyants for accepting to be my opponent. I am also indebted for the intership opportunities at the Radiation and Nuclear Safety Authority of Finland, and at Microsoft Research Cambridge,

both of which gave me very different but extremely valuable experiences. Finally, I gratefully acknowledge the support of KAUTE foundation and UEF Doctoral School for funding my research.

Apart from workplace relations, I am also grateful to my friends and family, for occasionally pulling my head out of academia and science. We all need to reboot at some point, and the friends I gained throughout my study years have been an invaluable help at that. As for my family, I am thankful to my parents for teaching me the importance of hard work and dedication, which has greatly helped me in life. In addition, I have learned a great many things from my older brother, who I know still enjoys educating me; let us never stop learning. Last but certainly not the least, I am thankful to my wife, without whom I would have never gone down this path. You made all this, and many other things possible.

Joensuu, May 24, 2019

Matias Koivurova

LIST OF PUBLICATIONS

This thesis consists of the present review of the author's work in the field of coherence of nonstationary light and the following selection of the author's publications:

I M. Koivurova, C. Ding, J. Turunen, and A. T. Friberg, "Cross-spectral purity of nonstationary light," *Phys. Rev. A* **99**, 043842 (2019).

II M. Koivurova, C. Ding, J. Turunen, and L. Pan, "Partially coherent isodiffracting pulsed beams," *Phys. Rev. A* **97**, 023825 (2018).

III M. Koivurova, A. Halder, H. Partanen, and J. Turunen, "Bessel-correlated supercontinuum fields," *Opt. Express* **25**, 23974–23988 (2017).

IV A. Halder, M. Koivurova, H. Partanen, and J. Turunen, "Paraxial propagation of a class of Bessel-correlated fields," *Opt. Express* **26**, 11055–11067 (2018).

V C. Ding, M. Koivurova, J. Turunen, and L. Pan, "Self-focusing of a partially coherent beam with circular coherence," *J. Opt. Soc. Am. A* **34**, 1441–1447 (2017).

VI C. Ding, M. Koivurova, J. Turunen, and L. Pan, "Temporal self-splitting of optical pulses," *Phys. Rev. A* **97**, 053838 (2018).

VII M. Koivurova, H. Partanen, J. Turunen, and A. T. Friberg, "Grating interferometer for light-efficient spatial coherence measurement of arbitrary sources," *Appl. Opt.* **56**, 5216–5227 (2017).

VIII M. Koivurova, E. Vasileva, Y. Li, L. Berglund and S. Popov, "Complete spatial coherence characterization of quasi-random laser emission from dye doped transparent wood," *Opt. Express* **26**, 13474–13482 (2018).

IX M. Koivurova, H. Partanen, J. Lahyani, N. Cariou, and J. Turunen, "Scanning wavefront folding interferometers," *Opt. Express* **27**, 7738–7750 (2019).

X M. Koivurova, L. Ahad, G. Gianluca, T. Setälä, J. Turunen, and A. T. Friberg, "Interferometry and coherence of nonstationary light," *Opt. Lett.* **44**, 522–525 (2019).

XI C. Ding, M. Koivurova, J. Turunen, T. Setälä and A. T. Friberg, "Coherence control of pulse trains by spectral phase modulation," *J. Opt.* **19**, 095501 (2017).

XII H. Pesonen, K. Saastamoinen, M. Koivurova, T. Setälä, and J. Turunen, "Temporal coherence modulation of pulsed, scalar light with a Fabry-Pérot interferometer," *J. Opt. Soc. Am. A* **36**, 1137–1145 (2019).

Throughout the overview, these papers will be referred to by Roman numerals.

AUTHOR'S CONTRIBUTION

The publications selected in this dissertation are original research papers in the field of optical coherence, with a special emphasis on pulsed light. The publications reported within this thesis are results of group efforts, but the author had a key role in the theoretical, experimental, and numerical aspects of the research that lead to papers **I**–**XII**. The mathematical derivations in papers **I**, **II**, **V**, **VI**, and **XI**, were carried out by the author in close collaboration with Prof. Chaoliang Ding. In papers **VIII**–**X**, the theoretical work was mainly carried out by the author. The author had a large influence on the experimental aspects in papers **III** and **IV**, which were performed together with Dr. Henri Partanen and Atri Halder. The experiments in papers **VII** and **IX** were carried out by author with Dr. Henri Partanen, while the measurements in paper **VIII** were performed by the author. Additionally, large part of the numerical simulations in papers **XI** and **XII** were done by the author. The majority of the international collaboration performed throughout the works was coordinated by the author, and all of the manuscripts have been written together in close cooperation with the co-authors. In particular, the original ideas for papers **IX**–**XI** came from the author.

TABLE OF CONTENTS

1 Introduction

Nature has demonstrated time and again that perfection does not exist. All physical phenomena are subject to some fluctuations; randomness that is woven into the fabric of reality. Researching the coherence of light is the attempt at quantifying the inherent noise and instabilities found in electromagnetic fields, and to harness their properties. As should be expected, this is not an easy task. Some of the most extreme quantities are found in photonics, such as time scales below 10^{-15} seconds, or peak powers above 10^{15} watts. But it is precisely because of these properties that the research carried out in this domain is so fruitful. Many of the greatest breakthroughs in the history of science have resulted from improved understanding of light, and nowadays we can routinely use telescopes to look deep into the cosmos, or microscopes to sneak a peek at the smallest constituents of life. We can even image inside opaque objects, and the speed of light has been harnessed for telecommunication, allowing the realization of the internet. Light is, in many ways, the cornerstone of modern society.

Research on the properties of light has continued for millennia, and the oldest known lenses date back over 3000 years to ancient Greece, Egypt, and Assyria [1]. Some of the first written accounts on the characteristics of light were given by Euclid around 300 BCE, which have fortunately survived to modern times [2]. Around the year 160, Ptolemy wrote works which influenced later investigations greatly, though a large part of them have been lost. Progress stalled for several hundred years, until Ibn al-Haytham wrote his series of books on optics during his incarceration between 1011–1021. His work consisted of a description on the magnifying properties of convex lenses, the correct theory of sight, experimental considerations on dispersion of light, as well as the first known use of camera obscura [3–5]. No large advances were made until the advent of Renaissance, after which European scientists rediscovered many results and further advanced the field greatly.

Willebrord Snellius discovered the law of reflection (now known as Snell's law) in 1621, and the term "diffraction" was coined by Francesco Grimaldi during his studies in the mid 1650s. In 1666, Isaac Newton showed that colors are an intrinsic property of light, and later he posited that light is composed of corpuscles, or particles of light. Christian Huygens made arguments towards the wave theory of light in 1690, and Thomas Young performed his famous double-slit experiment in 1803, which he believed to be a definitive proof of the wave nature of light. Augustin-Jean Fresnel improved on the theoretical foundations of the wave theory, and François Arago experimentally confirmed some of the theoretical predictions during the 19th century. In 1861, James Maxwell had already derived his famous set of equations. Albert Michelson and Edward Morley then produced the most well-known null result in the history of science, when they didn't find any signs of luminoferous ether in 1887. In the very beginning of the 20th century, Max Planck derived the correct formula for blackbody radiation by assuming that the energy of the electromagnetic wave is quantized, which sparked a revolution in physics. During the last hundred years, research of light has exploded to several active subfields, out of which coherence of light is the main topic of this dissertation.

1.1 PAST RESEARCH ON COHERENCE AND PULSED LIGHT

Coherence of light is arguably one of the most difficult subjects in modern physics. It is essentially a combination of two theoretically demanding fields – electromagnetism and statistical mechanics – although this is not the main source of difficulty. In fact, it is the interpretations and underlying physics which may cause problems. This includes questions such as: what are general properties of light? How to produce light with certain attributes? What kind of information can be extracted from light? What should we expect to see in experiments? And what are we really measuring? The first self-contained description of coherence of stationary light was given in the seminal work *Principles of Optics*, by Max Born and Emil Wolf [6]. The project started in 1951, when Born hired Wolf – who is now known as the father of coherence theory – to work as a private assistant on the book. Accounts given by Wolf's students later on reveal that getting all of the relevant results into the same book took longer than expected, and Born got impatient. Born would have left the discussion out, but Wolf insisted on having a section on coherence theory within the book. After additional publishing delays, the first edition finally came out in 1959. This was fortunate, since the first laser was built in 1960 by Theodore Maiman, based on the theoretical work of Charles Townes and Arthur Schawlow [7], which relied heavily on the theory of coherence for stationary sources. Thus, *Principles of Optics* became a landmark in optics research, and one of the main sources of information on coherence of light. To this day, it remains the all time most cited scientific work accross all disciplines in physics.

By the mid-1960's, the first mode-locked lasers had already been built, which could generate pulses far shorter than any earlier methods [8]. Although the time between the first laser and the first ultrashort pulse is only a couple of years, the gap between stationary and nonstationary coherence theory is quite large. For decades it was unclear what is the correct theoretical framework for nonstationary fields, and even experimental aspects were uncertain. For stationary fields, the main metric with which the degree of temporal coherence is probed is the coherence time, and it forms a Fourier transform relationship with the power spectrum. Thus, a wide spectrum entails short coherence time, and vice versa. However, this is not true for nonstationary fields. In fact, research into the coherence properties of nonstationary light is a very diverse field, and it is the main area of interest in the quest for ever shorter and more stable pulses. Recently, the length of the shortest optical pulses have been pushed all the way down to single optical cycles and even sub-cycle pulses have been demonstrated [9–15].

The production of pulses experienced large advances in the next decades, but corresponding measurement schemes lagged behind. After the first demonstrations of mode-locked lasers, it was quickly realized that conventional detectors were not nearly fast enough to record the pulse shape, and alternative methods were needed to examine these newly generated ultrashort pulses [8]. One of the first setups which could be used to estimate the pulse length was the intensity autocorrelation, but it featured a serious problem: every autocorrelation trace had several pulse shapes that could produce it. Thus, finding the shape of the pulse was in fact not possible at all, and in many studies a pulse shape with a short width was assumed with little justification. It wasn't until the 1990s that better measurement methods were invented, which could retrieve the pulse shape unambigiously [16, 17]. These methods have been improved upon, and they can now be found even as commercial devices. However, as of yet, there is no general method to measure the temporal

and spectral coherence properties of nonstationary light. Currently, the only way to achieve this is to measure pulses in a single-shot manner and construct the correlation functions numerically.

The coherence properties (or in other words, stability) of pulsed light is an important subject, since stable and short pulses have several uses. For example, ultrashort pulses can be utilized for femtochemistry, where chemical reactions are observed on extremely short timescales [18, 19]. Ahmed Zewail pioneered this technique, for which he was awarded the Nobel Prize in Chemistry in 1999 [20]. Additionally, stable pulse trains allow the realization of frequency metrology with an unprecedented resolution [21–26], that can be utilized for optical clocks and spectrographic astronomy. Work in this field led to the Nobel Prize in Physics for John Hall and Theodor Hänsch in 2005 [27]. Ultrashort pulses can also be utilized for micromachining [28] and the modification of matter to synthesize novel materials [29], as well as to realize rewritable optical memory [30]. Short and intense optical pulses are such important tools that even discovering a method for amplifying them led to the 2018 Nobel Prize in physics being granted to Donna Strickland and Gerard Mourou.

1.2 SCOPE OF THE THESIS

This thesis was written to be a self-contained work on the properties of pulsed scalar light, and its goal is to expand upon, as well as clarify, the central attributes of nonstationary fields and their coherence properties. The text is divided into four distinct chapters, each of which serves a particular purpose, but are intimately linked to each other.

In chapter 2, we introduce the fundamental concepts of pulsed light and the theoretical framework of nonstationary coherence. The correlation functions used to characterize pulsed fields are established and their mathematical properties are investigated. The connections between correlation functions in different domains, as well as methods to transform them are deliberated on. It is then noted that there are some physically realizable ways to produce light with desired correlations, namely, the genuine representation. The concept of cross-spectral purity is laid out for the case of stationary fields, which we extend to the nonstationary case (paper **I**). Chapter 3 considers some important partially coherent model fields. We start by introducing a rigorous mathematical model for pulsed beams, and examine its spatiotemporal properties (paper **II**). We then move to some simpler models, which feature correlation-induced effects, such as self-Fourier transforming (papers **III** and **IV**), self-focusing (paper **V**), and self-splitting (paper **VI**). The mathematical frameworks and the interpretations for these phenomena are discussed in detail. Further, numerical simulations are carried out to exemplify the effects.

Schemes for measuring nonstationary light are given in chapter 4. We begin by formulating the basic principles for Young's interferometer and proceed to investigate new methods for quantifying the spatial coherence of light (papers **VII–IX**). We then show that field interferometric measurements carried out in the temporal domain yield spectral domain information, and a method for quantifying spectral coherence is developed (paper **X**). Furthermore, we extend the usage of well-known pulse characterization methods and formulate a novel method for quantifying spectral correlations. Generation of partially coherent model fields is analyzed in chapter 5, where we begin by introducing a method for generating partially coherent pulse

trains (paper **XI**) and a scheme for increasing the temporal coherence of pulsed light (paper **XII**). We then continue to evaluate the effect of rotating optical elements on coherence, and show a simple method for generating Bessel-correlated and self-Fourier transforming beams. In the last part of the chapter, we elucidate on methods that generate cross-spectrally pure fields, and certain duality is found.

Finally, chapter 6 gives some concluding remarks, and the main results are summarized. In addition, some possibilities for future investigations are discussed. The research outlined in this thesis is expected to have far-reaching impact in future investigations of pulsed sources. The theoretical results show when certain approximations are valid, and what types of effects can be produced with partially coherent fields. However, the experimental considerations have an especially high importance. Methods for measuring the temporal and spectral correlation properties of light are in high demand, and schemes for stabilizing pulse trains are attractive for pulse generation. Both of these aspects are explored in this thesis and novel methods are found.

2 Coherence of nonstationary light

In the case of statistically stationary light, one assumes that the intensity of the field is constant with respect to time [6, 31]. Obviously, this is never true if we are able to perfectly resolve the field, because it is actually an oscillating electromagnetic signal and it has a beginning and an end. Thus, it is more accurate to say that one assumes that the field is statistically stationary with respect to some relevant time scale, which is much longer than the period of the oscillation and shorter than the length of the signal. This greatly simplifies the theoretical expressions, since it turns out that the correlations depend only on one temporal or spectral coordinate. Stationary coherence theory has yielded a wealth of important results, such as an explanation of why lasers are so special [6], whether the spectrum of light changes on propagation [32–35], or how a turbulent medium affects partially coherent beams [36–42]. Additionally, it has been shown how propagation invariance and partial coherence are linked [43–46] and that directionality is not limited to completely coherent fields [47–50]. Furthermore, the realization of twisted beams [51,52], as well as improving the resolution of optical microscopes [53, 54] are within the domain of stationary coherence theory.

However, nature is inherently nonstationary: light sources fluctuate in intensity and ultimately their signals will begin and end at some point. This is not a problem when the signal is very long and stable, but what if we have clearly pulsed signals? Such fields are obviously not stationary, especially if we are looking at ultrashort pulses, which may have pulse lengths on the order of optical cycles [55–59]. Transition to nonstationary theory is simple in principle: we just say that the field is not constant with respect to time anymore, which introduces a second coordinate to the correlation functions. However, this also entails that many of the results from stationary theory are not exactly valid for such fields, which may produce conceptual difficulties when attempting to grasp the multitude of new results.

2.1 PULSED BEAMS

Let us start by introducing the type of fields we are interested in. When we talk about the coherence of pulse trains, we are concerned with fields where a single temporal realization taken from the train can be expressed with a complex analytic signal $E(\mathbf{r};t)$, where $\mathbf{r} = (x, y, z)$ is the cartesian position vector in three dimensional space, and the field propagates towards the positive half-space $z > 0$. This forms a Fourier transform pair with the spectral field realization

$$E(\mathbf{r};\omega) = \frac{1}{2\pi}\int_{-\infty}^{\infty} E(\mathbf{r};t)\exp\left(i\omega t\right)\mathrm{d}t, \tag{2.1}$$

$$E(\mathbf{r};t) = \int_{0}^{\infty} E(\mathbf{r};\omega)\exp\left(-i\omega t\right)\mathrm{d}\omega. \tag{2.2}$$

The lower integration limit of zero in Eq. (2.2) is due to analyticity (Ref. [6], section 10.2), since we can neglect the negative frequencies. In the general case, the electric field is a vector quantity, but we are considering only scalar fields for simplicity. In

addition to these properties, the signal $E(\mathbf{r};t)$ is taken to be square integrable, i.e., the identity

$$\int_{-\infty}^{\infty} |E(\mathbf{r};t)|^2 \mathrm{d}t < \infty \tag{2.3}$$

is satisfied. This essentially means that a single realization taken from the train is not infinite in extent, but rather, it is a pulse. The complete train of pulses, $\tilde{E}(\mathbf{r};t)$, is then reconstructed when these single realizations are arranged in a line along the propagation direction, as in

$$\tilde{E}(\mathbf{r};t) = \sum_{m=0}^{N} E_m(\mathbf{r};t + m\Delta\tau_m), \tag{2.4}$$

where the pulse separation, $\Delta\tau_m$, and each realization, $E_m(\mathbf{r};t)$, are potentially different in a shot-to-shot manner, i.e., the train may fluctuate in both shape and timing of the pulses.

When the pulse train is completely stable, the pulses are all identical and equally spaced. As can be seen from Eq. (2.4), a single pulse is square integrable, but the whole train might not be, if we take the limit $M \to \infty$. This is of little consequence, since a realistic pulse train is always finite. More importantly, the pulse train $\tilde{E}(\mathbf{r};t)$ forms a Fourier transform pair with

$$\tilde{E}(\mathbf{r};\omega) = \sum_{m=0}^{M} E_m(\mathbf{r};\omega) \exp(i\omega m\Delta\tau_m). \tag{2.5}$$

When all of the pulse realizations $E_m(\mathbf{r};\omega)$ are identical and $\Delta\tau_m$ is constant, the train becomes completely coherent and it can be written as

$$\tilde{E}(\mathbf{r};\omega) = E(\mathbf{r};\omega) D_M(\omega,\Delta\nu) \tag{2.6}$$

where $D_M(\omega,\Delta\nu)$ is a Dirichlet kernel

$$D_M(\omega,\Delta\nu) = \frac{\sin[(M+1)\omega\pi/\Delta\nu]}{\sin(\omega\pi/\Delta\nu)} \exp\left(i\frac{M\omega}{\Delta\nu}\right), \tag{2.7}$$

with $\Delta\nu = 2\pi/\Delta\tau$ being a constant separation between spectral components. This ideal identity is called a frequency comb [21, 22], and it is extremely important for high precision optical frequency metrology [23]. Whenever there is a temporal field that consists of more than one pulse, its spectral domain counterpart will feature strong modulation, which is depicted in Fig. 2.1. The two extremes are a pair of pulses and infinitely many pulses, where the former case produces sinusoidal modulation, and the latter contains spectral components that are equally spaced and infinitesimally thin spikes. In other words, when the number of pulses tends towards infinity, the Dirichlet kernel assumes the form of a perfect delta comb

$$D_\infty(\omega,\Delta\nu) = \sum_{m=0}^{\infty} \delta(\omega - m\Delta\nu). \tag{2.8}$$

The kind of delta comb in the limit of $M \to \infty$ in Eq. (2.6) would be highly advantageous in many experimental settings, but we can never truly achieve it. The

most obvious reason for this is that it would require an infinite space to produce a train with infinitely many pulses. Secondly, a realistic light source always features noise – that is, partial coherence – and the comb will also inherit some of those fluctuations [60]. Even if we have the most stable source imaginable, the shot-noise caused by the quantum nature of light fundamentally limits the width of the comb lines [7, 24–26].

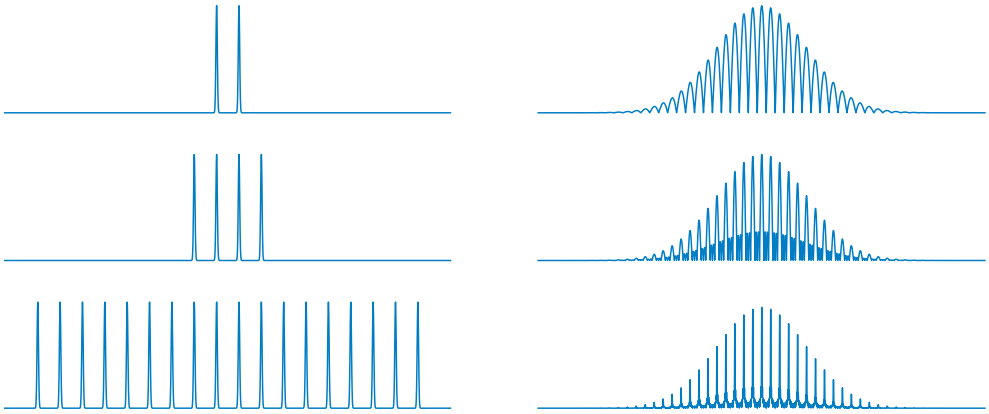

Figure 2.1: Depiction of pulse trains (left) of varying lengths, with their corresponding spectra (right). The pulse shape and envelope of the power spectrum is constant in all cases.

2.2 CORRELATION FUNCTIONS

The stability of a pulse train can be characterized with the use of the mutual coherence function (MCF) in the temporal domain, and the cross spectral density (CSD) function in the spectral domain, defined as

$$\Gamma(\mathbf{r}_1, \mathbf{r}_2; t_1, t_2) = \langle E^*(\mathbf{r}_1; t_1) E(\mathbf{r}_2; t_2) \rangle \tag{2.9}$$

and

$$W(\mathbf{r}_1, \mathbf{r}_2; \omega_1, \omega_2) = \langle E^*(\mathbf{r}_1; \omega_1) E(\mathbf{r}_2; \omega_2) \rangle, \tag{2.10}$$

respectively. The mean intensity is defined as $I(\mathbf{r}; t) = \Gamma(\mathbf{r}, \mathbf{r}; t, t)$, and the average power spectrum is $S(\mathbf{r}; \omega) = W(\mathbf{r}, \mathbf{r}; \omega, \omega)$. Here the angle brackets denote averaging over an ensemble of single pulse realizations picked from the train, as in

$$\Gamma(\mathbf{r}_1, \mathbf{r}_2; t_1, t_2) = \frac{1}{N} \sum_{n=1}^{N} E_n^*(\mathbf{r}_1; t_1) E_n(\mathbf{r}_2; t_2). \tag{2.11}$$

Theoretically speaking, the single pulse realizations are picked from the train with a moving sampling window, with a period that is equal to the average value of the pulse separation. This way, it is possible to account also for random variations of $\Delta\tau_m$ in Eq. (2.5) (timing jitter), as well as any changes in the pulse shape or phase.

One might think that looking at an ensemble average over single pulses rather than the whole pulse train would reduce the amount of available information on

the stability of the field, but this is not the case. In the temporal domain, as long as the fluctuations are truly caused by partial coherence, ensemble averaging over long sections of the pulse train would lead to a correlation function that periodically repeats [60]. In the spectral domain, it would actually decrease the amount of available information: if we take Eq. (2.6) with no timing jitter, and substitute into Eq. (2.10), we get

$$W(\mathbf{r}_1, \mathbf{r}_2; \omega_1, \omega_2) = D_M^*(\omega_1, \Delta\nu) D_M(\omega_2, \Delta\nu) W_0(\mathbf{r}_1, \mathbf{r}_2; \omega_1, \omega_2), \tag{2.12}$$

where $W_0(\mathbf{r}_1, \mathbf{r}_2; \omega_1, \omega_2)$ is the CSD averaged over single pulse realizations. Equation (2.12) depicts a correlation function that is periodically sampled, and therefore it does not yield any information on the parts that have been left out, although single pulses isolated from the train do contain contributions from the unsampled parts.

The MCF and CSD are connected via the generalized Wiener–Khintchine theorem, which is a Fourier-type relationship of the form

$$\Gamma(\mathbf{r}_1, \mathbf{r}_2; t_1, t_2) = \iint_0^\infty W(\mathbf{r}_1, \mathbf{r}_2; \omega_1, \omega_2) \exp\left[i(\omega_1 t_1 - \omega_2 t_2)\right] \mathrm{d}\omega_1 \mathrm{d}\omega_2, \tag{2.13}$$

$$W(\mathbf{r}_1, \mathbf{r}_2; \omega_1, \omega_2) = \frac{1}{(2\pi)^2} \iint_{-\infty}^\infty \Gamma(\mathbf{r}_1, \mathbf{r}_2; t_1, t_2) \exp\left[-i(\omega_1 t_1 - \omega_2 t_2)\right] \mathrm{d}t_1 \mathrm{d}t_2, \tag{2.14}$$

that can be constructed by inserting from Eqs. (2.1) and (2.2), into the definitions (2.9) and (2.10). Thus, the two correlation functions feature properties common to Fourier transform pairs. When the different frequency components are uncorrelated, the CSD can be formally written as

$$W(\mathbf{r}_1, \mathbf{r}_2; \omega_1, \omega_2) = W(\mathbf{r}_1, \mathbf{r}_2; \omega_1) \delta(\omega_2 - \omega_1), \tag{2.15}$$

which corresponds to a stationary field. In this case, the Wiener–Khintchine theorem results in

$$\begin{aligned} \Gamma(\mathbf{r}_1, \mathbf{r}_2; t_1, t_2) &= \iint_0^\infty W(\mathbf{r}_1, \mathbf{r}_2; \omega_1) \delta(\omega_2 - \omega_1) \exp\left[i(\omega_1 t_1 - \omega_2 t_2)\right] \mathrm{d}\omega_1 \mathrm{d}\omega_2 \\ &= \int_0^\infty W(\mathbf{r}_1, \mathbf{r}_2; \omega_1) \exp\left[-i\omega_1(t_2 - t_1)\right] \mathrm{d}\omega, \end{aligned} \tag{2.16}$$

that is, the MCF depends only on the time difference $t_2 - t_1$, and the temporal correlation properties are completely dictated by the power spectrum [6, 31]. Since the stationary case can be derived from nonstationary theory, the latter is thus more general than the former.

The mean intensity $I(\mathbf{r}; t)$ and spectral density $S(\mathbf{r}; \omega)$ can be used to normalize the MCF and CSD, which yields the complex degrees of temporal and spectral coherence, as in

$$\gamma(\mathbf{r}_1, \mathbf{r}_2; t_1, t_2) = \frac{\Gamma(\mathbf{r}_1, \mathbf{r}_2; t_1, t_2)}{\sqrt{I(\mathbf{r}_1; t_1) I(\mathbf{r}_2; t_2)}} \tag{2.17}$$

and

$$\mu(\mathbf{r}_1, \mathbf{r}_2; \omega_1, \omega_2) = \frac{W(\mathbf{r}_1, \mathbf{r}_2; \omega_1, \omega_2)}{\sqrt{S(\mathbf{r}_1; \omega_1) S(\mathbf{r}_2; \omega_2)}}. \tag{2.18}$$

The absolute values of the temporal and spectral degrees of coherence can take on values ranging from zero to unity within a four dimensional space, signifying complete incoherence and coherence at the given coordinates, respectively. For example, a completely coherent field has a value of unity at all possible coordinate combinations, whereas a partially coherent field may attain a range of values. To get a single numerical value for the coherence characterized by the MCF and CSD, one can compute the overall degree of coherence, defined as [61]

$$\bar{\gamma}^2 = \frac{\iint_D \int\int_{-\infty}^{\infty} |\Gamma(\mathbf{r}_1, \mathbf{r}_2; t_1, t_2)|^2 \mathrm{d}t_1 \mathrm{d}t_2 \mathrm{d}^3 r_1 \mathrm{d}^3 r_2}{\iint_D \int\int_{-\infty}^{\infty} I(\mathbf{r}_1; t_1) I(\mathbf{r}_2; t_2) \mathrm{d}t_1 \mathrm{d}t_2 \mathrm{d}^3 r_1 \mathrm{d}^3 r_2} \tag{2.19}$$

in the temporal domain, and

$$\bar{\mu}^2 = \frac{\iint_D \int\int_{0}^{\infty} |W(\mathbf{r}_1, \mathbf{r}_2; \omega_1, \omega_2)|^2 \mathrm{d}\omega_1 \mathrm{d}\omega_2 \mathrm{d}^3 r_1 \mathrm{d}^3 r_2}{\iint_D \int\int_{0}^{\infty} S(\mathbf{r}_1; \omega_1) S(\mathbf{r}_2; \omega_2) \mathrm{d}\omega_1 \mathrm{d}\omega_2 \mathrm{d}^3 r_1 \mathrm{d}^3 r_2} \tag{2.20}$$

in the spectral domain. Here the integration over space is done over the spatial extent of the pulse, D. The overall degrees of coherence are essentially root-mean-squared averages over the corresponding degrees of coherence, and as such they can have only values between zero and one. At times it is useful to map out how the overall degree of temporal or spectral coherence changes as a function of spatial/temporal/spectral position, by setting two coordinates equal and neglecting the integration over the corresponding dimension.

Equations (2.9) and (2.10) uniquely define the temporal and spectral characteristics of any arbitrary pulsed field. They are often defined with the absolute coordinates t_1, t_2 and ω_1, ω_2, although it is possible – and sometimes favorable – to rotate the coordinate system by 45 degrees, so that we can write

$$\Gamma(\mathbf{r}_1, \mathbf{r}_2; \bar{t}, \Delta t) = \langle E^*(\mathbf{r}_1; \bar{t} - \Delta t/2) E(\mathbf{r}_2; \bar{t} + \Delta t/2) \rangle, \tag{2.21}$$

$$W(\mathbf{r}_1, \mathbf{r}_2; \bar{\omega}, \Delta\omega) = \langle E^*(\mathbf{r}_1; \bar{\omega} - \Delta\omega/2) E(\mathbf{r}_2; \bar{\omega} + \Delta\omega/2) \rangle, \tag{2.22}$$

where $\bar{t} = (t_1 + t_2)/2$ and $\bar{\omega} = (\omega_1 + \omega_2)/2$ are the average temporal and spectral coordinates, whereas $\Delta t = t_2 - t_1$ and $\Delta\omega = \omega_2 - \omega_1$ are the corresponding difference coordinates. These expressions can be reduced to those used in stationary theory, by considering the integral over the average time in the MCF

$$\Gamma^{(\mathrm{int})}(\mathbf{r}_1, \mathbf{r}_2; \Delta t) = \int_{-\infty}^{\infty} \langle E^*(\mathbf{r}_1; \bar{t} - \Delta t/2) E(\mathbf{r}_2; \bar{t} + \Delta t/2) \rangle \mathrm{d}\bar{t}. \tag{2.23}$$

Substituting Eq. (2.23) into (2.14) we can derive the standard Wiener–Khintchine theorem for stationary fields

$$\Gamma^{(\mathrm{int})}(\mathbf{r}_1, \mathbf{r}_2; \Delta t) = \int_{0}^{\infty} W(\mathbf{r}_1, \mathbf{r}_2; \bar{\omega}, 0) \exp\left(-i\bar{\omega}\Delta t\right) \mathrm{d}\bar{\omega}, \tag{2.24}$$

which has the same functional form as Eq. (2.16). It needs to be noted that since we are integrating over average time, we lose a major part of the correlation information required to completely characterize a pulsed field. This is allowed only in one case: when the complex degree of coherence in the temporal domain is invariant along the average time axis. Fields with this property are said to obey the Schell model [62],

which contains a wide range of different types of light sources. It is notable that by definition, stationary light can only be of the Schell-model type in temporal space, whereas nonstationary fields can feature any kinds of temporal correlations.

This leads us to one of the concepts that causes confusion in the context of nonstationary coherence theory: the coherence time. It is usually defined as the time difference Δt, for which $\Gamma^{(\mathrm{int})}(\Delta t)$ reduces appreciably. The main problem here is that coherence time is poorly defined for pulsed fields, which is examined in Fig. 2.2, and this definition actually yields a time that is related to the length of a transform limited pulse (Ref. [16], section 2). If we have a pulse train that shows no fluctuations (either in intensity or phase) over any observation time, then what is the coherence time? Stationary theory would suggest that it is the length of the transform limited pulse – no matter how short that pulse is. But obviously such a train of pulses is almost completely coherent and coherence time should tend toward infinity. On the other hand, what if we have a pulse train where all of the individual pulses are completely correlated with each other near the peak intensity, but not at the edges, then what is the coherence time? Is it the time from the peak to the edge, or the time between subsequent pulses? The two-coordinate nature of nonstationary fields is the source of these problems, and a single temporal variable is never enough to completely characterize the properties of pulsed light. Of course, if the definition of coherence time is first stated and then used to compare fields, the problem becomes less significant, depending on the definition and the field in question.

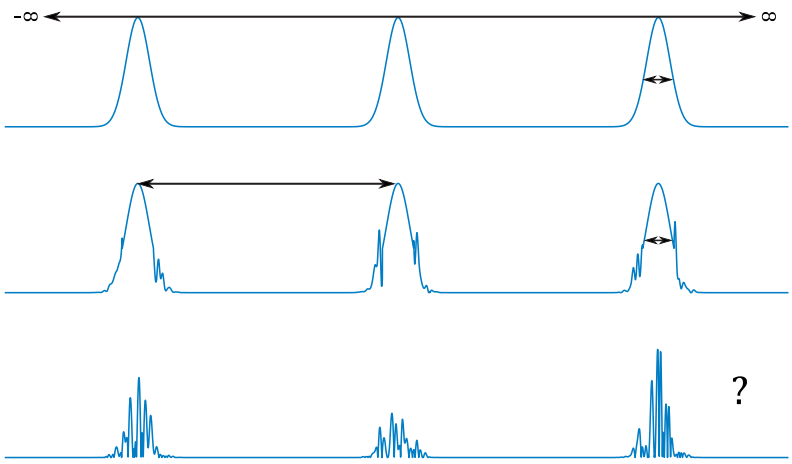

Figure 2.2: Different types of pulse trains and definitions of coherence time.

What about the coherence of a single pulse? Looking at the definitions of the overall degrees of coherence in Eqs. (2.17) and (2.18), we see that a single pulse is always completely coherent, no matter what type of phase or intensity fluctuations it contains. This sounds rather counterintuitive, but it is actually very clear: partial coherence in the nonstationary theory always arises from ensemble averaging. Coherence of pulse trains is essentially a measure of the statistical similarity of the realizations that make up the train. Furthermore, looking at a single pulse realization is actually equivalent to stopping time. If a field – any field – is stopped in time, then any spatiotemporal point along the field is completely correlated with all other points within the field. Coherence theory does not inspect such things, but rather

situations that are experimentally accessible via averages, either over an ensemble or time.

One may wonder that if the two-time nature of the nonstationary theory is more general, then why don't we use it also to characterize stationary fields? That is simply because one temporal coordinate is enough for stationary sources. If we have a stationary field and look at it's two-coordinate MCF, we will see that it is invariant along the average time axis. In that case, the time integrated MCF – or any slice in the direction of the time difference axis – completely characterizes the correlation properties of the field.

2.2.1 Connections between different domains

Because of the Fourier-type relationship between the MCF and CSD, the temporal and spectral degrees of coherence are also deeply linked. With the help of the Wiener–Khintchine theorem, we can find the Friberg–Wolf theorem [63] for nonstationary fields:

$$\gamma(\mathbf{r}_1,\mathbf{r}_2;t_1,t_2) = \iint_0^\infty \left[s(\mathbf{r}_1;\omega_1;t_1)s(\mathbf{r}_2;\omega_2;t_2)\right]^{1/2} \times \mu(\mathbf{r}_1,\mathbf{r}_2;\omega_1,\omega_2)\exp\left[i(\omega_1 t_1-\omega_2 t_2)\right]\mathrm{d}\omega_1\mathrm{d}\omega_2, \tag{2.25}$$

$$\mu(\mathbf{r}_1,\mathbf{r}_2;\omega_1,\omega_2) = \iint_{-\infty}^\infty \left[s(\mathbf{r}_1;\omega_1;t_1)s(\mathbf{r}_2;\omega_2;t_2)\right]^{-1/2} \times \gamma(\mathbf{r}_1,\mathbf{r}_2;t_1,t_2)\exp\left[-i(\omega_1 t_1-\omega_2 t_2)\right]\mathrm{d}t_1\mathrm{d}t_2, \tag{2.26}$$

where $s(\mathbf{r};\omega;t) = S(\mathbf{r};\omega)/I(\mathbf{r};t)$ is the time-dependent normalized spectrum of the field. It needs to be noted that $s(\mathbf{r};\omega;t)$ does not correspond to any real physical entity, and it is actually pathological on it's own. Within the integral it behaves smoothly. This connection between the complex degrees of coherence in time and frequency domains raises the question whether the overall degrees of coherence are also related. Recalling the definitions in Eqs. (2.19) and (2.20) and employing the Wiener–Khintchine theorem indeed provides a connection between the two domains. It is straightforward to show that

$$2\pi\int_D\int_0^\infty S(\mathbf{r};\omega)\mathrm{d}\omega\mathrm{d}^3r = \int_D\int_{-\infty}^\infty I(\mathbf{r};t)\mathrm{d}t\mathrm{d}^3r, \tag{2.27}$$

which basically amounts to conservation of energy in the Fourier transformations. Employing this identity and the Wiener–Khintchine theorem, one can easily show that the overall degrees of coherence in the two domains are equal, that is $\bar{\gamma} = \bar{\mu}$. Therefore, it does not matter whether it is the temporal or the spectral domain where the overall degree of coherence is computed.

Another convenient transformation we can do is to consider the spatial frequencies of the field. At the initial plane $z = 0$, the complex analytic field of Eq. (2.1) forms a Fourier-type relation accross the transverse plane (x, y) with the time domain angular field

$$E(\boldsymbol{\kappa};t) = \frac{1}{2\pi}\int_{-\infty}^\infty E(\boldsymbol{\rho};t)\exp\left(-i\boldsymbol{\kappa}\cdot\boldsymbol{\rho}\right)\mathrm{d}^2\rho, \tag{2.28}$$

where $\boldsymbol{\kappa} = (k_x, k_y)$ contains the transverse wave vector components and $\boldsymbol{\rho} = (x, y)$. The coherence properties of the angular field are characterized by the time domain angular correlation function (ACF), defined as

$$T(\boldsymbol{\kappa}_1, \boldsymbol{\kappa}_2; t_1, t_2) = \langle E^*(\boldsymbol{\kappa}_1; t_1) E(\boldsymbol{\kappa}_2; t_2) \rangle, \tag{2.29}$$

and the average angular intensity is now given by $A(\boldsymbol{\kappa}; t) = T(\boldsymbol{\kappa}, \boldsymbol{\kappa}; t, t)$. Similarly as in the case of Eqs. (2.9) and (2.10), the ACF is also connected to the tranverse components of the MCF via the generalized Wiener–Khintchine theorem, which can be written as

$$\Gamma(\boldsymbol{\rho}_1, \boldsymbol{\rho}_2; t_1, t_2) = \iint_{-\infty}^{\infty} T(\boldsymbol{\kappa}_1, \boldsymbol{\kappa}_2; t_1, t_2) \exp\left[i(\boldsymbol{\kappa}_1 \cdot \boldsymbol{\rho}_1 - \boldsymbol{\kappa}_2 \cdot \boldsymbol{\rho}_2)\right] \mathrm{d}^2\kappa_1 \mathrm{d}^2\kappa_2, \tag{2.30}$$

$$T(\boldsymbol{\kappa}_1, \boldsymbol{\kappa}_2; t_1, t_2) = \frac{1}{(2\pi)^2} \iint_{-\infty}^{\infty} \Gamma(\boldsymbol{\rho}_1, \boldsymbol{\rho}_2; t_1, t_2) \exp\left[-i(\boldsymbol{\kappa}_1 \cdot \boldsymbol{\rho}_1 - \boldsymbol{\kappa}_2 \cdot \boldsymbol{\rho}_2)\right] \mathrm{d}^2\rho_1 \mathrm{d}^2\rho_2. \tag{2.31}$$

The angular intensity $A(\boldsymbol{\kappa}; t)$ can again be used to normalize the ACF, yielding the complex degree of time domain angular coherence, as in

$$\alpha(\boldsymbol{\kappa}_1, \boldsymbol{\kappa}_2; t_1, t_2) = \frac{T(\boldsymbol{\kappa}_1, \boldsymbol{\kappa}_2; t_1, t_2)}{\sqrt{A(\boldsymbol{\kappa}_1; t_1), A(\boldsymbol{\kappa}_2; t_2)}} \tag{2.32}$$

Similarly to the earlier coherence functions, the absolute value of the degree of angular coherence can take on values that range from zero to unity, signifying complete incoherence and coherence, respectively. We can also compute the overall degree of coherence, which is defined as

$$\bar{\alpha}^2 = \frac{\int\int_{-\infty}^{\infty} \int\int_{-\infty}^{\infty} |T(\boldsymbol{\kappa}_1, \boldsymbol{\kappa}_2; t_1, t_2)|^2 \mathrm{d}^2\kappa_1 \mathrm{d}^2\kappa_2 \mathrm{d}t_1 \mathrm{d}t_2}{\int\int_{-\infty}^{\infty} \int\int_{-\infty}^{\infty} A(\boldsymbol{\kappa}_1; t_1) A(\boldsymbol{\kappa}_2; t_2) \mathrm{d}^2\kappa_1 \mathrm{d}^2\kappa_2 \mathrm{d}t_1 \mathrm{d}t_2}. \tag{2.33}$$

Furthermore, we can extend the usual Friberg–Wolf theorem to account for the connection between spatial and angular domains, as in

$$\begin{aligned} \gamma(\boldsymbol{\rho}_1, \boldsymbol{\rho}_2; t_1, t_2) = \iint_{-\infty}^{\infty} &\left[a(\boldsymbol{\kappa}_1; \boldsymbol{\rho}_1; t_1) a(\boldsymbol{\kappa}_2; \boldsymbol{\rho}_2; t_2)\right]^{1/2} \\ &\times \alpha(\boldsymbol{\kappa}_1, \boldsymbol{\kappa}_2; t_1, t_2) \exp\left[i(\boldsymbol{\kappa}_1 \cdot \boldsymbol{\rho}_1 - \boldsymbol{\kappa}_2 \cdot \boldsymbol{\rho}_2)\right] \mathrm{d}^2\kappa_1 \mathrm{d}^2\kappa_2, \end{aligned} \tag{2.34}$$

$$\begin{aligned} \alpha(\boldsymbol{\kappa}_1, \boldsymbol{\kappa}_2; t_1, t_2) = \iint_{-\infty}^{\infty} &\left[a(\boldsymbol{\kappa}_1; \boldsymbol{\rho}_1; t_1) a(\boldsymbol{\kappa}_2; \boldsymbol{\rho}_2; t_2)\right]^{-1/2} \\ &\times \gamma(\boldsymbol{\rho}_1, \boldsymbol{\rho}_2; t_1, t_2) \exp\left[-i(\boldsymbol{\kappa}_1 \cdot \boldsymbol{\rho}_1 - \boldsymbol{\kappa}_2 \cdot \boldsymbol{\rho}_2)\right] \mathrm{d}^2\rho_1 \mathrm{d}^2\rho_2, \end{aligned} \tag{2.35}$$

where $a(\boldsymbol{\kappa}; \boldsymbol{\rho}; t) = A(\boldsymbol{\kappa}; t) / I(\boldsymbol{\rho}; t)$ is the spatially-dependent normalized angular intensity of the field. We can straightforwardly show that energy is conserved also in these Fourier transformations, so that

$$2\pi \iint_{-\infty}^{\infty} A(\boldsymbol{\kappa}; t) \mathrm{d}^2\kappa \mathrm{d}t = \iint_{-\infty}^{\infty} I(\boldsymbol{\rho}; t) \mathrm{d}^2\rho \mathrm{d}t, \tag{2.36}$$

and using this identity and the generalized Wiener–Khintchine theorem, it can be shown that the overall degrees of coherence in the spatial and angular domains are also equal, $\bar{\gamma} = \bar{\alpha}$. Performing this transformation is useful in solving propagation problems, for example, and stationary fields can be propagated to any distance z with these expressions. A similar analysis can be made to obtain the spectral domain ACF, $A(\boldsymbol{\kappa}_1, \boldsymbol{\kappa}_2, \omega_1, \omega_2)$, which is convenient for the propagation of nonstationary fields, as will be shown later on.

Obviously, we can construct a large number of correlation functions, not only by considering the Fourier trasnformations but also coordinate rotations. For example, if the MCF is rotated 45° degrees to obtain $(\bar{t}, \Delta t)$ coordinates and then transformed along the difference time, we will end up at the well-known Wigner distribution $W(\bar{\omega}, \bar{t})$. On the other hand, if the MCF is transformed along the average time coordinate, then the result will be the ambiguity function $A(\Delta t, \Delta\omega)$. Both of these can be converted to the CSD by transforming the remaining coordinate, or back to the MCF via inverse Fourier transform. Figure 2.3 depicts some of the possible connections between the different domains, which were mentioned here.

$$
\begin{array}{ccccc}
W(\boldsymbol{\rho}_1, \boldsymbol{\rho}_2; \omega_1, \omega_2) & \leftarrow & \Gamma(\boldsymbol{\rho}_1, \boldsymbol{\rho}_2; t_1, t_2) & \qquad W(\bar{\omega}, \Delta\omega) & \leftarrow \quad A(\Delta t, \Delta\omega) \\
\downarrow & & \uparrow & \downarrow & \uparrow \\
A(\boldsymbol{\kappa}_1, \boldsymbol{\kappa}_2; \omega_1, \omega_2) & \rightarrow & A(\boldsymbol{\kappa}_1, \boldsymbol{\kappa}_2; t_1, t_2) & \qquad W(\bar{\omega}, \bar{t}) & \rightarrow \quad \Gamma(\bar{t}, \Delta t)
\end{array}
$$

Figure 2.3: Some of the possible transformations between different domains. Arrows denote Fourier transform relationships, which are all reversible.

2.2.2 Genuine representations

A correlation function is physically realizable, when the MCF is Hermitian and non-negative definite. Such functions are called genuine, and they can be represented, for example, as [64]

$$\Gamma(\mathbf{r}_1, \mathbf{r}_2; t_1, t_2) = \int_{-\infty}^{\infty} p(v) h^*(\mathbf{r}_1; t_1; v) h(\mathbf{r}_2; t_2; v) \mathrm{d}v, \tag{2.37}$$

where $p(v)$ is a non-negative weight function and $h(\mathbf{r}; t; v)$ is an arbitrary and possibly complex-valued kernel. This is one of the experimentally realizable pathways to produce partially coherent fields. The weight function – which is essentially a probability density – describes how the kernels – electric fields – should be distributed in order to produce the desired correlation function.

Let us now ignore the spatial dependence for simplicity, and take a time-domain kernel that has the specific Fourier-type form $h(t; v) = f(t) \exp(-itv)$, where $f(t)$ is the complex envelope of the field. In this case, using Eq. (2.37), we find that the MCF of the pulse train is of the Schell-model form

$$\Gamma(t_1, t_2) = f^*(t_1) f(t_2) g(\Delta t), \tag{2.38}$$

where

$$g(\Delta t) = \int_{-\infty}^{\infty} p(v) \exp\left(-i\Delta t v\right) \mathrm{d}v \tag{2.39}$$

satisfies the condition $g(0) = 1$. Under these assumptions, the mean temporal intensity of the pulse train is $I(t) = \Gamma(t,t) = |f(t)|^2$ and its complex degree of temporal coherence can be written as

$$\gamma(t_1, t_2) = \frac{\Gamma(t_1, t_2)}{\sqrt{I(t_1) I(t_2)}} = g(\Delta t) \exp\left\{i\left[\phi(t_2) - \phi(t_1)\right]\right\}, \tag{2.40}$$

where $\phi(t) = \arg[f(t)]$. If we take the absolute value of the complex degree of coherence, we find that $|\gamma(t_1, t_2)| = |g(\Delta t)|$. Thus, in the case of Schell-model fields, the weight function completely determines the correlation function. Again, it is simple to move between the temporal and spectral domains, as outlined in the earlier section.

If we know the type of correlation function we wish to get, it is possible to find the weight function by a simple inversion of Eq. (2.39), as in

$$p(v) = \frac{1}{2\pi} \int_{-\infty}^{\infty} g(\Delta t) \exp\left(iv\Delta t\right) \mathrm{d}\Delta t. \tag{2.41}$$

As a fundamental example, we consider the well-known Gaussian Schell-model (GSM) pulses [65], for which the MCF is expressed as

$$\Gamma(t_1, t_2) = \sqrt{I(t_1) I(t_2)}\gamma(\Delta t), \tag{2.42}$$

where both the temporal intensity and the complex degree of temporal coherence are Gaussian functions

$$I(t) = I_0 \exp\left(-\frac{2t^2}{T^2}\right), \tag{2.43}$$

$$\gamma(\Delta t) = \exp\left(-\frac{\Delta t^2}{2T_c^2}\right), \tag{2.44}$$

where T is the pulse length and T_c is the coherence time. Note that in this case, since the coherence properties of the pulse train depend only on the time difference coordinate Δt, the coherence time is well defined. This feature is limited only to Schell-model sources.

The CSD is obtained with the Wiener–Khintchine theorem, as

$$W(\omega_1, \omega_2) = W_0 \sqrt{S(\omega_1) S(\omega_2)}\mu(\Delta\omega) \tag{2.45}$$

where $W_0 = I_0 T/\pi\Omega$, with Ω being the spectral bandwidth. The spectral density and degree of spectral coherence are yet again Gaussian functions given by

$$S(\omega) = W_0 \exp\left(-\frac{\omega^2}{2\Omega^2}\right), \tag{2.46}$$

$$\mu(\Delta\omega) = \exp\left(-\frac{\Delta\omega^2}{2\Omega_c^2}\right), \tag{2.47}$$

respectively, and Ω_c is the spectral coherence width. Furthermore, the pulse duration T, coherence time T_c, spectral bandwidth Ω, and the coherence width Ω_c are related by

$$\frac{\Omega^2}{4} = \frac{1}{T^2} + \frac{1}{T_c^2}, \tag{2.48}$$

$$\frac{\Omega_c}{T_c} = \frac{\Omega}{T}. \tag{2.49}$$

For pulses such as these, it is convenient to introduce the auxiliary function

$$\beta = \left(1 + \frac{T^2}{T_c^2}\right)^{-1/2} = \left(1 + \frac{\Omega^2}{\Omega_c^2}\right)^{-1/2}. \tag{2.50}$$

Inputting Eqs. (2.42)–(2.44) into the definition of the overall degree of coherence in Eq. (2.19), it turns out that $\bar{\gamma} = \sqrt{\beta}$. Consequently, with the use of genuine representations, it is straightforward to engineer an almost unlimited amount of different types of correlation functions.

2.3 CROSS-SPECTRAL PURITY

The concept of cross-spectral purity was originally introduced by Mandel in 1961 [66], in the context of the Hanbury Brown–Twiss experiment. It is one of the most profound concepts in coherence theory, though not very well known. The basic principle is that one samples the field at two points accross the wavefront, and then inspects their superposition. If the spectral properties are conserved in all three points, then the field is cross-spectrally pure by definition. Mandel showed that if a stationary field is cross-spectrally pure, then the complex degree of coherence is separable into spatial and temporal contributions. He realized that such a property is not general among light fields, but rather a special case applicable only to cross-spectrally pure light. Afterwards, the concept of cross-spectral purity has been studied in the framework of stationary coherence theory [67–71] and extensions have been made to the electromagnetic case [72, 73], partial polarization [73, 74], and the Stokes parameters [75, 76]. No investigations on nonstationary fields have been made in the context of cross-spectral purity.

Up to this day, cross-spectral purity is often implicitly assumed in theoretical studies [77–83], although such fields are rare in practice. In this section, we will briefly consider cross-spectrally pure stationary fields, and then extend the concept of cross-spectral purity to nonstationary fields in accordance with Paper **I**. Additionally, we will consider the propagation properties of cross-spectrally pure fields here, and some methods for the generation of cross-spectrally pure light are described later in chapter 5.

2.3.1 Cross-spectrally pure stationary light

Mandel based his analysis on Young's two pinhole experiment, which is illustrated in Fig. 2.4. He stated that a field is cross-spectrally pure, if the superposition of light

produces the same normalized spectrum at some point in the observation plane as in the pinholes. Basing the analysis on Young's interferometer allows for an easily realizable experimental setting, but it requires relatively narrowband light [66, 67]. In the case of pulsed sources, the spectral bandwidth can be very wide and the Young's interferometer is no longer the tool of choice for measuring the degree of cross-spectral purity. There are other schemes, such as wavefront folding or shearing interferometers, that can be used to measure the purity of wide bandwidth light. For the sake of generality, we will consider only the superposition of fields, and not the device with which they are produced.

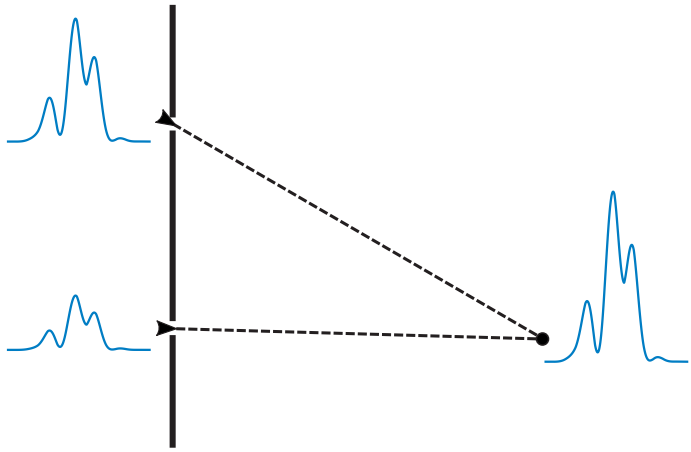

Figure 2.4: Illustration of the concept of cross-spectral purity for stationary fields, as originally defined by Mandel.

Let us take the spectral representation $E(\mathbf{r};\omega)$ and form a superposition between the fields at $\mathbf{r}_1$ and $\mathbf{r}_2$ at some observation point $\mathbf{R}$. We will denote the temporal delay between the fields arising from the two points as τ, and thus the superposed field has the spectral representation

$$E(\mathbf{R};\omega) = E(\mathbf{r}_1;\omega) + E(\mathbf{r}_2;\omega)\exp\left(i\omega\tau\right). \tag{2.51}$$

A stationary light field is called cross-spectrally pure if the normalized spectral densities

$$s(\mathbf{r};\omega) = \frac{S(\mathbf{r};\omega)}{\int_0^\infty S(\mathbf{r};\omega)\mathrm{d}\omega} \tag{2.52}$$

at the three points are equal around some value $\tau = \tau_0$ of the time delay, that is, if the condition

$$s(\mathbf{R};\omega) = s(\mathbf{r}_1;\omega) = s(\mathbf{r}_2;\omega) \tag{2.53}$$

is fulfilled. It is straightforward to show that when these conditions hold, cross-spectrally pure stationary light can be factored in two distinct contributions according to the reduction formula

$$\gamma(\mathbf{r}_1,\mathbf{r}_2;\tau) = \gamma(\mathbf{r}_1,\mathbf{r}_2;\tau_0)\gamma(\mathbf{r},\mathbf{r};\tau-\tau_0), \tag{2.54}$$

where $\mathbf{r} = \mathbf{r}_1$ or $\mathbf{r} = \mathbf{r}_2$ holds, and $\gamma(\mathbf{r}_1, \mathbf{r}_2; \tau)$ is essentially the normalized form of Eq. (2.23). This formula expresses the complex degree of coherence as a product of a term that characterizes the spatial coherence (between points $\mathbf{r}_1$ and $\mathbf{r}_2$) and a term that characterizes the temporal coherence of the field at a single point ($\mathbf{r}_1$ or $\mathbf{r}_2$).

2.3.2 Cross-spectrally pure nonstationary light

In the case of nonstationary light, the situation is more involved. In contrast to the stationary case, the coherence in the space-frequency domain has to be characterized by the two-frequency CSD. We define cross-spectrally pure nonstationary fields as such that not only the condition (2.53) has to be fulfilled, but also the two-frequency complex degrees of spectral coherence are equal at all three points $\mathbf{r}_1$, $\mathbf{r}_2$, and $\mathbf{R}$, so that we can write

$$\mu(\mathbf{R}, \mathbf{R}; \omega_1, \omega_2) = \mu(\mathbf{r}_1, \mathbf{r}_1; \omega_1, \omega_2) = \mu(\mathbf{r}_2, \mathbf{r}_2; \omega_1, \omega_2). \tag{2.55}$$

On inserting from Eq. (2.51) into the definition (2.10), we find that the two-frequency CSD at point $\mathbf{R}$ is given by

$$\begin{aligned} W(\mathbf{R}, \mathbf{R}; \omega_1, \omega_2) = & \\ & + W(\mathbf{r}_1, \mathbf{r}_2; \omega_1, \omega_2) \exp(-i\omega_2\tau) + W(\mathbf{r}_2, \mathbf{r}_1; \omega_1, \omega_2) \exp(i\omega_1\tau) \\ & + W(\mathbf{r}_1, \mathbf{r}_1; \omega_1, \omega_2) + W(\mathbf{r}_2, \mathbf{r}_2; \omega_1, \omega_2) \exp[i(\omega_1 - \omega_2)\tau], \end{aligned} \tag{2.56}$$

and the spectral density at that point is

$$S(\mathbf{R}; \omega) = S(\mathbf{r}_1; \omega) + S(\mathbf{r}_1; \omega) + 2\Re[W(\mathbf{r}_1, \mathbf{r}_2; \omega, \omega) \exp(-i\omega\tau)],$$

where we have used the Hermitian property $W(\mathbf{r}_2, \mathbf{r}_1; \omega, \omega) = W^*(\mathbf{r}_1, \mathbf{r}_2; \omega, \omega)$ of the CSD and $\Re$ denotes the real part. Let us first consider the condition (2.53) and choose the spectral densities at the points $\mathbf{r}_1$ and $\mathbf{r}_2$ so that they are related by $S(\mathbf{r}_2; \omega) = C_{12} S(\mathbf{r}_1; \omega)$, where C_{12} is a proportionality constant.

Making use of the definition (2.18), we may cast Eq. (2.57) into the form

$$S(\mathbf{R}; \omega) = S(\mathbf{r}_1; \omega) \left\{ 1 + C_{12} + 2\sqrt{C_{12}} \, |\mu(\mathbf{r}_1, \mathbf{r}_2; \omega, \omega)| \cos[\Phi(\mathbf{r}_1, \mathbf{r}_2; \omega, \omega) - \omega\tau] \right\}, \tag{2.57}$$

where $\Phi(\mathbf{r}_1, \mathbf{r}_2; \omega, \omega)$ is the phase of $\mu(\mathbf{r}_1, \mathbf{r}_2; \omega, \omega)$. This equation shows that even if the phase of the correlation function is flat, the interference features spectral fringes when $\tau \neq 0$ and the equalities (2.53) would no longer hold. Therefore, the cross-spectral purity of nonstationary light is meaningful only in the zero-time-delay region. This is due to spectral correlations of nonstationary light, which is in stark contrast to stationary light that never exhibits spectral interference effects. As a result, Eq. (2.56) can be simplified to

$$\begin{aligned} W(\mathbf{R}, \mathbf{R}; \omega_1, \omega_2) = & W(\mathbf{r}_1, \mathbf{r}_2; \omega_1, \omega_2) + W(\mathbf{r}_2, \mathbf{r}_1; \omega_1, \omega_2) \\ & + W(\mathbf{r}_1, \mathbf{r}_1; \omega_1, \omega_2) + W(\mathbf{r}_2, \mathbf{r}_2; \omega_1, \omega_2), \end{aligned} \tag{2.58}$$

so that the spectral density at the observation plane becomes

$$S(\mathbf{R}; \omega) = S(\mathbf{r}_1; \omega) \left\{ 1 + C_{12} + 2\sqrt{C_{12}} \Re[\mu(\mathbf{r}_1, \mathbf{r}_2; \omega, \omega)] \right\}. \tag{2.59}$$

Upon noting that $W(\mathbf{r}_2, \mathbf{r}_2; \omega_1, \omega_2) = C_{12} W(\mathbf{r}_1, \mathbf{r}_1; \omega_1, \omega_2)$, we may express the complex degree of spectral coherence at point $\mathbf{R}$ in the form

$$\mu(\mathbf{R}, \mathbf{R}; \omega_1, \omega_2) = \mu(\mathbf{r}_1, \mathbf{r}_1; \omega_1, \omega_2) \times \frac{1 + C_{12} + \left[W(\mathbf{r}_1, \mathbf{r}_2; \omega_1, \omega_2) + W(\mathbf{r}_2, \mathbf{r}_1; \omega_1, \omega_2)\right] / W(\mathbf{r}_1, \mathbf{r}_1; \omega_1, \omega_2)}{1 + C_{12} + 2\sqrt{C_{12}} \Re\left[\mu(\mathbf{r}_1, \mathbf{r}_2; \omega, \omega)\right]}. \tag{2.60}$$

For the first equality in Eq. (2.55) to hold the field must fulfill

$$\frac{W(\mathbf{r}_1, \mathbf{r}_2; \omega_1, \omega_2) + W(\mathbf{r}_2, \mathbf{r}_1; \omega_1, \omega_2)}{W(\mathbf{r}_1, \mathbf{r}_1; \omega_1, \omega_2)} = 2\sqrt{C_{12}} \Re\left[\mu(\mathbf{r}_1, \mathbf{r}_2; \omega, \omega)\right]. \tag{2.61}$$

However, we are at an impasse: the left-hand side of this equation is generally complex-valued and depends on two frequency coordinates, whereas the strictly real-valued right-hand side depends only on one frequency.

It is conceivable that this relation can be fulfilled at some special points for certain correlation functions, but we are interested in the case where the field accross the whole wavefront is cross-spectrally pure. Therefore, we assume that the CSD is of the separable form

$$W(\mathbf{r}_1, \mathbf{r}_2; \omega_1, \omega_2) = W_\mathrm{s}(\mathbf{r}_1, \mathbf{r}_2) W_\mathrm{f}(\omega_1, \omega_2), \tag{2.62}$$

in which case the left-hand side of Eq. (2.61) reduces precisely to the right-hand side. The spectral density for a cross-spectrally pure field is then given by

$$S(\mathbf{r}; \omega) = W_\mathrm{s}(\mathbf{r}, \mathbf{r}) W_\mathrm{f}(\omega, \omega) = S_\mathrm{s}(\mathbf{r}) S_\mathrm{f}(\omega). \tag{2.63}$$

Equations (2.61) and (2.62) demonstrate that nonstationary light is cross-spectrally pure if the two-point, two-frequency CSD separates into a product of a purely space-domain and a purely frequency-domain correlation function. It also follows that the complex degree of spectral coherence can be cast into the form

$$\mu(\mathbf{r}_1, \mathbf{r}_2; \omega_1, \omega_2) = \mu_\mathrm{s}(\mathbf{r}_1, \mathbf{r}_2) \mu_\mathrm{f}(\omega_1, \omega_2), \tag{2.64}$$

where the spatial correlation factor

$$\mu_\mathrm{s}(\mathbf{r}_1, \mathbf{r}_2) = \frac{W_\mathrm{s}(\mathbf{r}_1, \mathbf{r}_2)}{\sqrt{S_\mathrm{s}(\mathbf{r}_1) S_\mathrm{s}(\mathbf{r}_2)}} \tag{2.65}$$

is independent of frequency, and the spectral correlation factor

$$\mu_\mathrm{f}(\omega_1, \omega_2) = \frac{W_\mathrm{f}(\omega_1, \omega_2)}{\sqrt{S_\mathrm{f}(\omega_1) S_\mathrm{f}(\omega_2)}} \tag{2.66}$$

is in turn independent of spatial position. Equation (2.64) is actually the space-frequency domain reduction formula for cross-spectrally pure nonstationary fields, sharing some similarity with the space-time domain formula of Eq. (2.54) in the stationary case.

In view of the Wiener–Khintchine relationship between the CSD and MCF, combining Eqs. (2.13) and (2.62) immediately implies a separability condition for the MCF, as in

$$\Gamma(\mathbf{r}_1, \mathbf{r}_2; t_1, t_2) = \Gamma_\mathrm{s}(\mathbf{r}_1, \mathbf{r}_2) \Gamma_\mathrm{t}(t_1, t_2), \tag{2.67}$$

where $\Gamma_\mathrm{s}(\mathbf{r}_1, \mathbf{r}_2) = W_\mathrm{s}(\mathbf{r}_1, \mathbf{r}_2)$. The temporal intensity of a cross-spectrally pure field is therefore

$$I(\mathbf{r}; t) = \Gamma_\mathrm{s}(\mathbf{r}, \mathbf{r})\Gamma_\mathrm{t}(t, t) = I_r(\mathbf{r})I_\mathrm{t}(t), \tag{2.68}$$

and the spatial distribution of such a field is not dependent on time or frequency, and thus $I_r(\mathbf{r}) = S_r(\mathbf{r})$. The two-point, two-time complex degree of coherence, defined in Eq. (2.17), therefore also factors into the form

$$\gamma(\mathbf{r}_1, \mathbf{r}_2; t_1, t_2) = \gamma_\mathrm{s}(\mathbf{r}_1, \mathbf{r}_2)\gamma_\mathrm{t}(t_1, t_2). \tag{2.69}$$

Here the spatial correlation factor is time independent, and fulfills $\mu_\mathrm{s}(\mathbf{r}_1, \mathbf{r}_2) = \gamma_\mathrm{s}(\mathbf{r}_1, \mathbf{r}_2)$, whereas the temporal correlation factor is

$$\gamma_\mathrm{t}(t_1, t_2) = \frac{\Gamma_\mathrm{t}(t_1, t_2)}{\sqrt{I_\mathrm{t}(t_1)I_\mathrm{t}(t_2)}}. \tag{2.70}$$

The space-time domain reduction formula for nonstationary fields in Eq. (2.69) is a direct counterpart of the reduction formula (2.54) for stationary fields.

2.3.3 Propagation of light from cross-spectrally pure sources

In Mandel's original paper [66], it was found that cross-spectral purity is approximately preserved throughout the half-space $z > 0$, when stationary fields are considered. In paper **I**, we showed that this is not the case anymore for cross-spectrally pure nonstationary fields, which we will consider next. Let us take a spectral electric field that is known at the plane $z = 0$, where the transverse coordinate is denoted by $\boldsymbol{\rho} = (x, y)$. We can consider its propagation into the positive half-space $z > 0$ with the well-known angular spectrum representation, which states that the field at an arbitrary point $\mathbf{r} = (x, y, z)$ is given by

$$E(\mathbf{r}; \omega) = \int_{-\infty}^{\infty} E(\boldsymbol{\kappa}; \omega) \exp\left(ik_z z\right) \exp\left(i\boldsymbol{\kappa} \cdot \boldsymbol{\rho}\right) \mathrm{d}^2\kappa. \tag{2.71}$$

Here the longitudinal component of the wave vector is given by $k_z = \sqrt{k^2 - \kappa^2}$, where $k = |\mathbf{k}|$, $\mathbf{k}$ being the wave vector in free space, and $\kappa = |\boldsymbol{\kappa}|$. Additionally, the angular spectrum is given by

$$E(\boldsymbol{\kappa}; \omega) = \frac{1}{(2\pi)^2} \int_{-\infty}^{\infty} E(\boldsymbol{\rho}; \omega) \exp\left(-i\boldsymbol{\kappa} \cdot \boldsymbol{\rho}\right) \mathrm{d}^2\rho. \tag{2.72}$$

The correlation function can be propagated simply by inserting from Eq. (2.71) into Eq. (2.10), which yields the expression

$$\begin{aligned} W(\mathbf{r}_1, \mathbf{r}_2; \omega_1, \omega_2) = \iint_{-\infty}^{\infty} & T(\boldsymbol{\kappa}_1, \boldsymbol{\kappa}_2; \omega_1, \omega_2) \exp\left[-i\left(k_{z1}^* z_1 - k_{z2} z_2\right)\right] \\ & \times \exp\left[-i\left(\boldsymbol{\kappa}_1 \cdot \boldsymbol{\rho}_1 - \boldsymbol{\kappa}_2 \cdot \boldsymbol{\rho}_2\right)\right] \mathrm{d}^2\kappa_1 \mathrm{d}^2\kappa_2, \end{aligned} \tag{2.73}$$

where we now have two longitudinal angular frequency components $k_{zj} = \sqrt{k_j^2 - \kappa_j^2}$, with $j = 1, 2$ and the spectral domain ACF is defined as

$$\begin{aligned} T(\boldsymbol{\kappa}_1, \boldsymbol{\kappa}_2; \omega_1, \omega_2) = & \frac{1}{(2\pi)^4} \iint_{-\infty}^{\infty} W(\boldsymbol{\rho}_1, \boldsymbol{\rho}_2; \omega_1, \omega_2) \\ & \times \exp\left[i\left(\boldsymbol{\kappa}_1 \cdot \boldsymbol{\rho}_1 - \boldsymbol{\kappa}_2 \cdot \boldsymbol{\rho}_2\right)\right] \mathrm{d}^2\rho_1 \mathrm{d}^2\rho_2. \end{aligned} \tag{2.74}$$

We now take a field that is cross-spectrally pure at the initial plane, which has a CSD that can therefore be expressed as a product $W_\mathrm{s}(\boldsymbol{\rho}_1, \boldsymbol{\rho}_2) W_\mathrm{f}(\omega_1, \omega_2)$. Then, in view of Eq. (2.74), the ACF is also separable to $T_\mathrm{k}(\boldsymbol{\kappa}_1, \boldsymbol{\kappa}_2)$ and $W_\mathrm{f}(\omega_1, \omega_2)$, which means that it is also obviously cross-spectrally pure.

However, if we insert this into Eq. (2.73), we see that the cross-spectral purity is immediately broken when propagating beyond the initial plane, since the magnitude of the wave vector is dependent on frequency $k = \omega/c$. The same conclusion is true also if paraxial propagation is considered by approximating

$$k_{zj} \approx k_j - \frac{\kappa_j^2}{2k_j}, \tag{2.75}$$

which would lead to the Fresnel propagation formula for nonstationary fields. However, if a narrow-band field with a spectrum concentrated around some central frequency $\omega = \omega_0$ is considered, we can approximate

$$k_{zj} \approx \sqrt{k_0^2 - \kappa_j^2}. \tag{2.76}$$

This case is equivalent to the one considered by Mandel, which approximately preserves cross-spectral purity upon propagation. However, this condition is strictly speaking never fulfilled for pulsed light, and the problem becomes larger the shorter the pulses are. Especially in the case of ultrashort pulses, one needs to consider their spatiotemporal properties.

3 Partially coherent field models

As we have seen in the earlier sections, there are a multitude of tools to theoretically characterize the coherence properties of nonstationary fields, and partial coherence is to be expected from realistic sources [6,31,84]. Not only is it important to characterize the correlation properties of nonstationary fields, but it is also of utmost importance to understand that fields with certain correlation functions can exhibit remarkable phenomena; effects which cannot be reproduced with completely coherent fields. Most commonly these correlation-induced effects have been examined in the spatial domain, where a wide range of different properties have been theoretically predicted and experimentally demonstrated. Usually, they are related to the reshaping of the spatial intensity distribution, via self-focusing [85–87], self-splitting [88,89], and even self-steering [90]. The intensity ditribution may take on a completely new form, such as a flat-topped, arrayed, or cusped distribution, or it may even rotate [91–98]. Partially coherent fields have also been found to produce lower levels of scintillation in atmospheric propagation [36,42,99], and spatial correlations can even be used to increase the resolution of imaging systems [53,54].

There is no particular reason why such effects would not be possible in the temporal domain as well. Indeed, it has been theoretically proven that pulses can temporally self-focus [100], self-split [101], or change shape [102], all within the domain of linear optics. Unfortunately, experimental investigations of these effects are scarce, for the lack of methods to measure and produce desired temporal correlations. We shall show in chapters 4 and 5 schemes that can be used to realize a wide range of different types of spatial and temporal correlations, which are necessary for future experimental demonstrations of a large variety of effects. In this chapter, we will first consider a strictly realistic model for spatiotemporally coupled pulsed beams. Afterwards, we concentrate on the formalism of some mathematically simpler fields, which show interesting correlation-induced effects. Covering all of the known correlation-induced phenomena would be beside the point, and we shall therefore concentrate on a few selected effects. After considering spatiotemporal coupling effects, we will assume cross-spectral purity for the simple model fields in this chapter and consider only either temporal or spatial properties at a time.

3.1 SPATIOTEMPORAL COUPLING

Coupling between spatial and temporal domains can manifest as a consequence of the frequency dependence of resonator modes, which is often ignored. However, when we have a resonator with several locked modes, the resulting pulsed beam is no longer separable to spatial and temporal contributions, i.e., it is not cross-spectrally pure. Such fields can be studied if their mode distribution is known, in which case we can theoretically examine them by starting from the coherent-mode representation, as was done in paper **II**. This representation is essentially a superposition of coherent fields, a somewhat similar approach as the genuine representation depicted in section 2.2.2, and it will be the starting point for our examination.

3.1.1 Space-frequency domain formulation

A realistic laser has a resonator that is usually fabricated with spherical mirrors. If the cavity is stable, it supports Hermite-Gaussian (HG) lasing modes, where the number of supported modes depends on the cavity parameters [103–105]. The HG modes are defined under the paraxial approximation as having the space-frequency representation of the form

$$\psi_m(x;\omega) = g(\omega)\frac{(2/\pi)^{1/4}}{\sqrt{2^m m! w_0(\omega)}} H_m\left[\frac{\sqrt{2}x}{w_0(\omega)}\right]\exp\left[-\frac{x^2}{w_0^2(\omega)}\right], \tag{3.1}$$

where H_m is the Hermite polynomial of order m. Since the HG modes are separable in cartesian coordinates, it is sufficient to consider one-dimensional representations along the x-axis. Additionally, the width of the beam waist varies with frequency according to the expression

$$w_0(\omega) = \sqrt{\frac{\omega_0}{\omega}} w_0, \tag{3.2}$$

where we take $w_0 = w(\omega_0)$ as the beam width at a reference frequency ω_0, which may be chosen as the peak or mean frequency of the spectral weight function $g(\omega)$. Additionally, the spectral weight is normalized such that $\int_0^\infty g(\omega)\mathrm{d}\omega = 1$. These choices define a set of eigenfunctions, which satisfy the orthonormality condition

$$\int_D \int_0^\infty \psi_m^*(x;\omega)\psi_n(x;\omega)\mathrm{d}\omega\mathrm{d}x = \delta_{mn}, \tag{3.3}$$

where δ_{mn} is the Kronecker delta. Therefore, these Hermite-Gaussian modes are coherent modes in the sense as they have been defined for nonstationary fields [106,107]. If more than one of these modes are present in a field, we can express the field as a coherent-mode superposition

$$W(x_1,x_2;\omega_1,\omega_2) = \sum_{m=0}^{\infty} c_m \psi_m^*(x_1;\omega_1)\psi_m(x_2;\omega_2), \tag{3.4}$$

which represents a valid correlation function [106]. We choose the weights c_m as [108]

$$c_m = w_0\sqrt{\frac{2\pi}{\beta}}\frac{1}{1+1/\beta}\left(\frac{1-\beta}{1+\beta}\right)^m, \tag{3.5}$$

which are frequency independent. Here, the parameter β is related to the spatial coherence properties of the field in a way that will become apparent below, and we assume that the different frequency components are completely correlated. We will see later that the coupling between spatial and temporal domains will nonetheless cause a decrease in the temporal coherence.

Upon inserting from Eqs. (3.1), (3.2), and (3.5) into Eq. (2.10), we can evaluate the summation and normalize the resulting CSD with the spectral density. This yields the spectral domain degree of coherence and spectral density of the form

$$\mu(x_1,x_2;\omega_1,\omega_2) = \exp\left[-\frac{\left(\sqrt{\omega_1}x_1 - \sqrt{\omega_2}x_2\right)^2}{2\omega_0\sigma^2}\right]\exp\left[i\varphi(\omega_1,\omega_2)\right], \tag{3.6}$$

$$S(x;\omega) = \sqrt{\frac{\omega}{\omega_0}}\,|g(\omega)|^2 \exp\left(-\frac{\omega}{\omega_0}\frac{2x^2}{w^2}\right), \tag{3.7}$$

respectively, and we have introduced the parameters

$$\sigma = \frac{\sqrt{\beta}}{\sqrt{1-\beta^2}} w_0, \tag{3.8}$$

$$w = \frac{w_0}{\sqrt{\beta}}, \tag{3.9}$$

which describe the spatial coherence width of the field at the plane of the waist for $\omega = \omega_0$ and the width of the waist, respectively. The phase term φ depends on the phase of the weight function $\varphi(\omega_1, \omega_2) = \arg[g(\omega_2)] - \arg[g(\omega_1)]$. It is clear that the weight function $g(\omega)$ is closely linked to the power spectrum of the field, which we need to fix before we move to the temporal domain.

3.1.2 Propagation of coupled fields

Fields that are spatiotemporally coupled – such as the one described here – are notorious for the mathematical difficulty related to their propagation. Even in the paraxial approximation, propagating a coupled field requires one to evaluate a six-fold integration over a tensor equation [81]. Therefore, it is worthwhile to consider simpler methods for achieving the same result. Noting that propagating a single mode described by Eq. (3.1) is a rather simple operation, since it is governed by Gaussian beam propagation. We shall therefore consider the paraxial free-space propagation of the HG modes, which is described by the function

$$\begin{aligned}\psi_m(x,z;\omega) = g(\omega)\frac{(2/\pi)^{1/4}\exp\left[i\phi(z;\omega)\right]}{\sqrt{2^m m! w_0(z;\omega)}} H_m\left[\frac{\sqrt{2}x}{w_0(z;\omega)}\right] \\ \times \exp\left[-\frac{x^2}{w_0^2(z;\omega)}\right]\exp\left[i\frac{\omega}{c}\frac{x^2}{2R(z)}\right],\end{aligned} \tag{3.10}$$

where c is the speed of light, z is the propagation distance, and the quantities

$$w_0(z;\omega) = \sqrt{\frac{\omega_0}{\omega}} w_0(z), \tag{3.11}$$

$$w_0(z) = w_0\left(1 + \frac{z^2}{z_\mathrm{R}^2}\right)^{1/2}, \tag{3.12}$$

$$R(z) = z + \frac{z_\mathrm{R}^2}{z}, \tag{3.13}$$

$$\phi(z;\omega) = \frac{\omega}{c} z - \left(m + \frac{1}{2}\right)\arctan\left(\frac{z}{z_\mathrm{R}}\right), \tag{3.14}$$

$$z_{\mathrm{R}} = \frac{\omega w_0^2(\omega)}{2c} = \frac{\omega_0 w_0^2}{2c}, \tag{3.15}$$

are the usual Gaussian-beam propagation parameters. Beams that consist of these HG modes are called isodiffracting, and their defining property is that the waist of the beam is frequency dependent in a manner that causes the Rayleigh range, z_{R}, to be the same at all frequencies.

Propagating all of the modes and then computing the correlation function yields the propagated space-frequency degree of coherence and spectral density of the form

$$|\mu(x_1, x_2, z; \omega_1, \omega_2)| = \exp\left[-\frac{\left(\sqrt{\omega_1}x_1 - \sqrt{\omega_2}x_2\right)^2}{2\omega_0\sigma^2(z)}\right], \tag{3.16}$$

$$S(x, z; \omega) = \sqrt{\frac{\omega}{\omega_0}}\,|g(\omega)|^2\,\frac{w}{w(z)}\exp\left[-\frac{\omega}{\omega_0}\frac{2x^2}{w^2(z)}\right], \tag{3.17}$$

respectively, where we have left the phase terms out for brevity, and defined the parameters

$$\sigma(z) = \sigma\frac{w(z)}{w}, \tag{3.18}$$

$$w(z) = w\left(1 + \frac{z^2}{z_{\mathrm{R}}^2}\right)^{1/2} = \frac{w_0(z)}{\sqrt{\beta}}. \tag{3.19}$$

Clearly, whenever the field can be expressed as a superposition of modes that can be propagated as Gaussian beams, it is the preferred method. If no modal decomposition is known, then the mathematical difficulty increases considerably.

3.1.3 Transformation to space-time domain

Having successfully propagated the space-frequency domain field, we can use the Wiener–Khintchine theorem to transform it to the space-time domain. Prior to this, we need to fix the spectral weight function $g(\omega)$. It is advantageous to use the power-exponential form, defined by

$$\left(\frac{\omega}{\omega_0}\right)^{1/4} g(\omega) = \frac{1}{\sqrt{\Gamma(2n)}}\left(2n\frac{\omega}{\omega_0}\right)^n \exp\left(-n\frac{\omega}{\omega_0}\right), \tag{3.20}$$

where n is a real and positive constant that controls the width of the spectrum and $\Gamma(2n)$ is the familiar gamma function. For simplicity, we assume a flat spectral phase, and thus the weight function remains real valued. We prefer the power-exponential distribution because it contains no negative frequencies, and is therefore a physically plausible broadband spectrum. A Gaussian spectral weight might seem mathematically more desirable, but it is prone to computational artifacts. The choice of power-exponential spectrum leaves us with great freedom over the spectral bandwidth, and it corresponds closely to the actual spectrum produced by titanium-doped sapphire lasers.

We can use Eqs. (3.16) and (3.17), together with Eq. (2.18), to obtain the CSD of the propagated field. Afterwards, we can transform the expression to the temporal domain with the use of Eq. (2.13), as in

$$\begin{aligned}\Gamma(x_1,x_2,z;t_1,t_2) = \frac{w}{w(z)}\iint_0^\infty \left(\frac{\omega_1}{\omega_0}\frac{\omega_2}{\omega_0}\right)^{1/4} g^*(\omega_1)g(\omega_2) \\ \times \exp\left[-\frac{\omega_1 x_1^2+\omega_2 x_2^2}{\omega_0 w^2(z)}\right]\exp\left[-\frac{\left(\sqrt{\omega_1}x_1-\sqrt{\omega_2}x_2\right)^2}{2\omega_0\sigma^2(z)}\right] \\ \times \exp\left\{i\left[\omega_1 t_1-\omega_2 t_2-(\omega_1-\omega_2)\frac{z}{c}\right]\right\} \\ \times \exp\left[-i\frac{\omega_1 x_1^2-\omega_2 x_2^2}{2cR(z)}\right]\mathrm{d}\omega_1\mathrm{d}\omega_2. \end{aligned} \tag{3.21}$$

In the space-frequency domain, the expression for the field was remarkably simple. Unfortunately, this is not the case in the space-time domain, and the final result for the spatiotemporal field is obtained by inserting from Eq. (3.20) into Eq. (3.21) and evaluating the integrals. The integral can be solved analytically, and it is best to present the final result as a sum of three terms

$$\Gamma(x_1,x_2,z;t_1,t_2) = \sum_{j=1}^{3}\Gamma_j(x_1,x_2,z;t_1,t_2), \tag{3.22}$$

which is due to the considerable length of each contribution. Explicitly, writing out the three components, we have

$$\begin{aligned}\Gamma_1(x_1,x_2,z;t_1,t_2) = (2h)^{2h}\omega_0^2\frac{\Gamma^2(n+1)}{\Gamma(2h)}\frac{w}{w(z)}T_n^{-(n+1)}(x_1,x_2,z;t_1,t_2) \\ \times {}_2F_1\left[n+1,n+1;\frac{1}{2};\frac{x_1^2x_2^2}{4\sigma^4(z)T_n(x_1,x_2,z;t_1,t_2)}\right], \end{aligned} \tag{3.23}$$

$$\begin{aligned}\Gamma_2(x_1,x_2,z;t_1,t_2) = -(2h)^{2h}\omega_0^2\frac{\Gamma^2(n+3/2)}{(n+1)^2\Gamma(2h)}\frac{w}{w(z)}T_n^{-(n+3/2)}(x_1,x_2,z;t_1,t_2) \\ \times {}_2F_1\left[n+\frac{3}{2},n+\frac{3}{2};-\frac{1}{2};\frac{x_1^2x_2^2}{4\sigma^4(z)T_n(x_1,x_2,z;t_1,t_2)}\right] \\ \times \left[\frac{\sigma^2(z)}{x_1x_2}T_n(x_1,x_2,z;t_1,t_2)-\frac{x_1x_2}{4\sigma^2(z)}\right], \end{aligned} \tag{3.24}$$

$$\begin{aligned}\Gamma_3(x_1,x_2,z;t_1,t_2) = (2h)^{2h}\omega_0^2\frac{\Gamma^2(n+3/2)}{(n+1)^2\Gamma(2h)}\frac{w}{w(z)}T_n^{-(n+3/2)}(x_1,x_2,z;t_1,t_2) \\ \times {}_2F_1\left[n+\frac{3}{2},n+\frac{3}{2};\frac{1}{2};\frac{x_1^2x_2^2}{4\sigma^4(z)T_n(x_1,x_2,z;t_1,t_2)}\right] \\ \times \left[\frac{\sigma^2(z)}{x_1x_2}T_n(x_1,x_2,z;t_1,t_2)-\left(n+\frac{3}{2}\right)\frac{x_1x_2}{\sigma^2(z)}\right], \end{aligned} \tag{3.25}$$

where ${}_2F_1(a,b;c;z)$ is the Gauss hypergeometric function, and we have employed an auxiliary function T_n, which is defined as

$$T_n(x_1,x_2,z;t_1,t_2) = \left[T^*(x_1,z;t_1)+n\right]\left[T(x_2,z;t_2)+n\right] \tag{3.26}$$

with

$$T(x,z;t) = \left[\frac{1}{w^2(z)}+\frac{1}{2\sigma^2(z)}\right]x^2 + i\omega_0\left[t'-\frac{x^2}{2cR(z)}\right]. \tag{3.27}$$

Here $t' = t - z/c$ is the time measured in the moving reference frame of the pulse. We can perform a quick analysis on the pulses we have formulated by considering the on-axis field. This is done by setting $x_1 = x_2 = 0$, which causes all of the hypergeometric functions in the MCF to equal unity and $\Gamma_2 + \Gamma_3 = 0$. Under these conditions, the axial MCF takes on the remarkably simple form

$$\Gamma(0,0,z;t_1,t_2) = (2h)^{2h}\omega_0^2\frac{\Gamma^2(n+1)}{\Gamma(2h)}\frac{w}{w(z)}T_n(0,0,z;t_1,t_2)^{-(n+1)}, \tag{3.28}$$

and the axial intensity is given by

$$I(0,z;t) = (2h)^{2h}\omega_0^2\frac{\Gamma^2(n+1)}{\Gamma(2h)}\frac{w}{w(z)}T_n(0,0,z;t,t)^{-(n+1)}, \tag{3.29}$$

so that we can write the on-axis complex degree of temporal coherence as

$$\gamma(0,0,z;t_1,t_2) = \frac{\left[\left(n^2+\omega_0^2t_1'^2\right)\left(n^2+\omega_0^2t_2'^2\right)\right]^{(n+1)/2}}{\left[n^2+\omega_0^2t_1't_2'+ih\omega_0\left(t_2'-t_1'\right)\right]^{n+1}}. \tag{3.30}$$

We immediately notice that $|\gamma(0,0,z;t_1,t_2)| = 1$, for all values of w, σ, and n. Hence, the on-axis field is temporally completely coherent with any set of parameters we choose to use. It needs to be noted that this is no longer true if we move away from the center of the beam.

The axial intensity distribution is symmetric with respect to time, which is to be expected given that we assumed a flat spectral phase. The full width at half-maximum of the pulse is found with

$$t'_{\mathrm{FWHM}} = T_0\frac{n}{\pi}\sqrt{2^{1/(n+1)}-1}, \tag{3.31}$$

where $T_0 = 2\pi/\omega_0$ is the duration of a single optical cycle at the carrier frequency. Now it is easily found that we are in the single-cycle regime when $n \sim 15$. Increasing n yields longer pulses and decreasing it will produce pulses that are shorter than a single optical cycle. The notion of sub-cycle pulses may seem counter-intuitive, since the shortest event one can imagine for an oscillating signal is a single cycle. But there is no physical or mathematical reason why a pulse cannot be shorter than a single cycle of its own carrier wave [9–15]. Such short pulses usually suffer from stability issues, since in this region the relative phase between the carrier and envelope makes a large difference in the overall pulse shape. This phase is usually quantified with the term carrier-envelope phase (CEP), which signifies the change in the relative phase between the carrier and envelope per one resonator round trip. The CEP accumulates if the group and phase velocities of the pulse train are not equal, and one of the greatest challenges in modern ultrashort pulse research is the stabilization of such pulses.

3.1.4 Isodiffracting pulses

Looking at the expression for the time-domain pulses introduced in Eqs. (3.22)–(3.25), we see that this is not a particularly transparent result. Indeed, these expressions are a good example of a solution to a specific problem, which is too complicated for one to sketch or even imagine. Therefore, we turn to illustrating the main characteristics of the field defined by the aforementioned equations as a function of selected parameters. For convenience, we shall use dimensionless quantities, defined by normalizing to some relevant scale. The transverse spatial coordinates x_1 and x_2 are normalized to the modal scale parameter w_0, the longitudinal spatial coordinate z to the Rayleigh range z_R, and the temporal coordinates to the optical cycle T_0. This allows us to examine the results on a general level, and we are not tied to some specific situation. The spectral width is controlled by varying the parameter n and the state of spatial coherence is controlled by the choice of β.

The question that immediately comes to mind is how does the spatiotemporal coupling manifest itself in these pulses? Figure 3.1 illustrates the normalized spatiotemporal intensity profiles at the initial plane. We consider pulses that have a low degree of spatial coherence with $\beta = 0.1$ and varying spectral bandwidths.

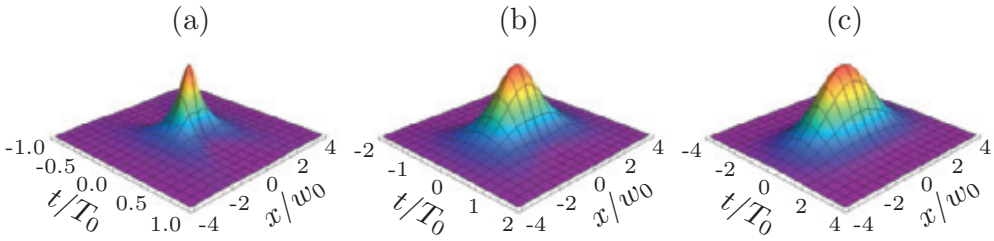

Figure 3.1: Spatiotemporal intensity profiles $I(x,0;t)$ for $\beta = 0.1$. (a) Sub-cycle pulse with $n = 1$, (b) single-cycle pulse with $n = 15$, and (c) two-cycle pulse with $n = 50$ (from paper **II**).

From Fig. 3.1 it is quite clear that coupling effects reduce with increasing n, and nearly vanish above the single-cycle regime. It was also found that coupling becomes stronger with decreasing coherence, which makes sense since less coherent pulses have more spatial modes in them. We demonstrate this, and the propagation of such pulses, in Fig. 3.2 below.

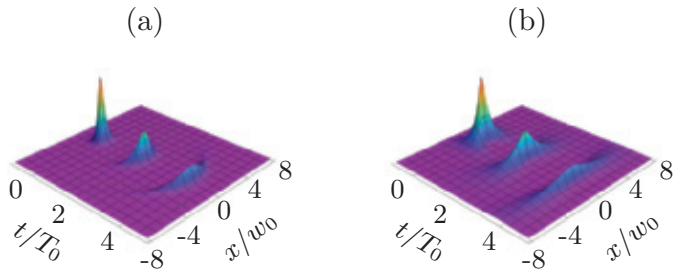

Figure 3.2: Spatiotemporal intensity profiles $I(x,z;t)$ for pulses with $n = 1$ at different propagation distances $z/z_R = 0, 2, 4$. (a) $\beta = 1$ and (b) $\beta = 0.1$ (from paper **II**).

The spatiotemporal intensities $I(x,z;t)$ have been plotted at different propagation distances $z_q = qz_R$ that are multiples of the Rayleigh range z_R. For clarity and compactness, we draw the pulses centered at the temporal instants $t_q = qT_0$. The pulses with low spatial coherence approach plane waves very quickly, which is a common feature of low coherence beams. This also makes the coupling more apparent, and spatiotemporal effects can be observed in Fig. 3.2, since the pulse profiles feature side lobes, with temporal lengths greater than the axial pulse duration. This temporal widening when moving off-axis warrants a closer inspection from the coherence point of view. Let us first consider the spatial coherence properties of the pulses. Figure 3.3 illustrates the absolute value of the time-domain complex degree of spatial coherence

$$\gamma(x_1, x_2, 0; 0, 0) = \frac{\Gamma(x_1, x_2, 0; 0, 0)}{\sqrt{I(x_1, 0; 0) I(x_2, 0; 0)}} \tag{3.32}$$

for the pulses at the initial plane.

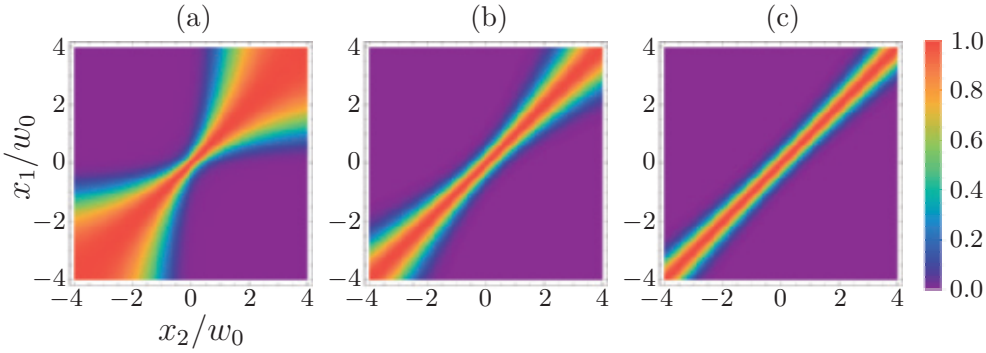

Figure 3.3: Absolute value of the complex degree of spatial coherence, $|\gamma(x_1, x_2, 0; 0, 0)|$, for $\beta = 0.1$. (a) Sub-cycle pulse with $n = 1$, (b) single-cycle pulse with $n = 15$, and (c) two-cycle pulse with $n = 50$ (from paper **II**).

It is plain to see that for small values of n, the pulses do not obey the Schell model in the spatial domain, since the correlation functions depend on both x_1 and x_2, and not only on their difference. That is, the width of the degree of spatial coherence in the anti-diagonal direction is shortest near the center of the pulse and increases along the direction of the average spatial coordinate $\bar{x} = \frac{1}{2}(x_1 + x_2)$. This is highly prominent for sub-cycle pulses, but diminishes rapidly in the few-cycle regime.

Recalling Eq. (3.30), we know that the field along the optical axis is fully temporally coherent regardless of the choice of variables. However, the degree of temporal coherence depends on both β and n when moving off-axis. Figure 3.4 illustrates the absolute value of the two-time complex degree of temporal coherence

$$\gamma(w_0, w_0, 0; t_1, t_2) = \frac{\Gamma(w_0, w_0, 0; t_1, t_2)}{\sqrt{I(w_0, 0; t_1) I(w_0, 0; t_2)}} \tag{3.33}$$

for the pulse at the initial plane, and transverse distance $x_1 = x_2 = w_0$ from the optical axis for $\beta = 0.1$. The temporal degrees of coherence have some clear differences and similarities with the spatial degrees of coherence that were shown earlier.

The greatest difference is that the spatial coherence area increases with larger bandwidth, whereas the temporal coherence decreases. The two domains also have a clear similarity, since they both depart from the Schell model with small n, and reduce back with decreasing bandwidth.

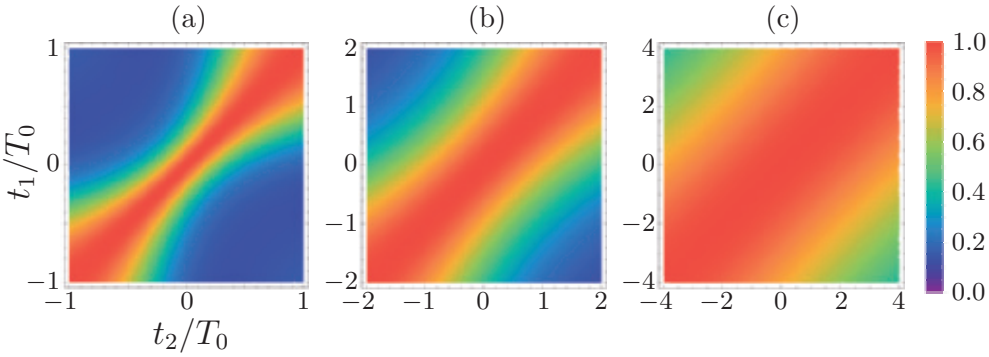

Figure 3.4: Absolute value of the complex degree of temporal coherence, $|\gamma(w_0, w_0, 0; t_1, t_2)|$, at an off-axis spatial position $x_1 = x_2 = w_0$ and for $\beta = 0.1$. (a) Sub-cycle pulse with $n = 1$, (b) single-cycle pulse with $n = 15$, and (c) two-cycle pulse with $n = 50$ (from paper **II**).

From these two figures, we come to understand the nature of the spatiotemporal coupling. Evidently, when we approach the coupling regime, the spatial and temporal coherence properties mix. The temporal coherence decreases and spatial coherence increases, so the coupling affects all properties of the pulse, not just the spatiotemporal intensity profile. We can employ the overall degree of temporal coherence as a function of spatial position, defined as

$$[\bar{\gamma}(x,z)]^2 = \frac{\iint_{-\infty}^{\infty} I(x,z;t_1) I(x,z;t_2) \, |\gamma(x,x,z,t_1,t_2)|^2 \, \mathrm{d}t_1 \mathrm{d}t_2}{\iint_{-\infty}^{\infty} I(x,z;t_1) I(x,z;t_2) \mathrm{d}t_1 \mathrm{d}t_2}, \tag{3.34}$$

to conveniently characterize the position dependent temporal coherence. Figure 3.5 illustrates this quantity for pulses with different bandwidths at the initial plane.

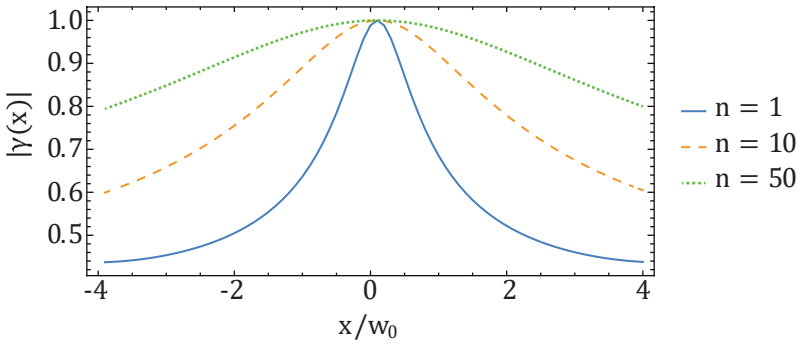

Figure 3.5: Overall degree of temporal coherence at the initial plane, scanned over the x-axis for $n = 1$, $n = 15$, and $n = 50$ (from paper **II**).

We see that the temporal coherence of the pulses decreases substantially when moving away from the optical axis, and the effect is most striking for sub-cycle pulses. As was mentioned earlier, the physical origin for the spatiotemporal coupling can be traced back to the frequency dependence of the spatial modes. In view of Eq. (3.2), the low-frequency components have a larger spatial extent than the high-frequency components, and thus the beam profile becomes essentially redshifted when one moves away from the optical axis. This implies that while the field is clearly not cross-spectrally pure, the spatiotemporal coupling effects are prominent only below the few-cycle pulse regime. Thus, it is well justified to ignore spatiotemporal effects when the considered pulses are generated in a stable cavity and they are relatively long.

3.2 SELF-FOURIER TRANSFORMING BEAMS

When a beam of light propagates, it generally experiences some sort of evolution, due to diffraction and the spatiotemporal properties it has at the initial plane. Fields that do not change upon appreciable propagation are called diffraction free [43], or propagation invariant [44, 45]. However, such properties are generally confined to some propagation length; after a large enough distance they will also change considerably and experience diffraction, a property which is outlined in Fig. 3.6 for a Bessel beam. Such a beam can be produced, for example, with a refractive axicon, which refracts the light so that the beam overlaps with itself and produces an interference pattern. If the axicon is chosen properly (cone angle and field size), the pattern can be rather long and this is what we call a Bessel beam. Of course, this is just one example of a propagation invariant beam, and there exists a large variety of diffraction free fields [44, 46].

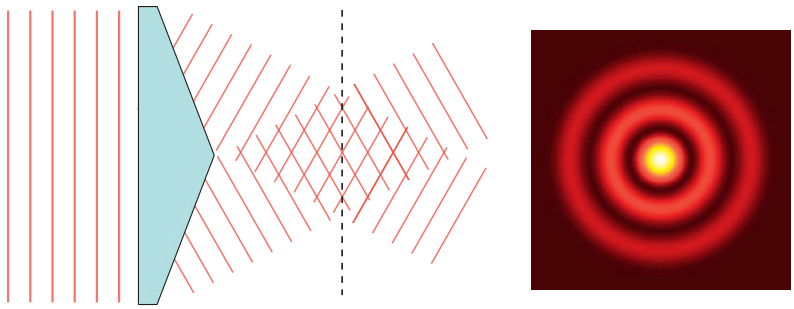

Figure 3.6: Depiction of a Bessel beam produced with a refractive axicon and the cross-sectional intensity distribution taken along the dashed line.

Whereas propagation invariant beams are defined only within a certain volume of space, it could be of interest to have beams that change only in scale, so that all of their other properties remain the same after any propagation length. We defined a class of beams which we termed self-Fourier transforming in paper **III** and examined the propagation of one such beam in paper **IV**. The defining property of these fields is that the correlation functions retain their mathematical forms in Fourier transformations over the transverse plane. In other words, $W(\boldsymbol{\rho}_1, \boldsymbol{\rho}_2)$ has the same functional form as $T(\boldsymbol{\kappa}_1, \boldsymbol{\kappa}_2)$.

Let us begin by recalling the propagation integrals of Eqs. (2.73) and (2.74), and write them in the form

$$W(\mathbf{r}_1,\mathbf{r}_2) = \iint_{-\infty}^{\infty}\iint_{-\infty}^{\infty} W(\boldsymbol{\rho}_1',\boldsymbol{\rho}_2')\exp\left[-i\left(k_{z1}^{*}z_1 - k_{z2}z_2\right)\right] \times \exp\left\{-i\left[\boldsymbol{\kappa}_1\cdot(\boldsymbol{\rho}_1-\boldsymbol{\rho}_1') - \boldsymbol{\kappa}_2\cdot(\boldsymbol{\rho}_2-\boldsymbol{\rho}_2')\right]\right\}\mathrm{d}^2\kappa_1\mathrm{d}^2\kappa_2\mathrm{d}^2\rho_1\mathrm{d}^2\rho_2, \quad (3.35)$$

where $\mathbf{r}_j = (\boldsymbol{\rho}_j, z_j)$, with $j = 1,2$. We are interested in the spatial coherence properties of the beam at transverse planes located at a distance z from the initial plane. By setting $z_1 = z_2 = z$ and considering paraxial propagation, we can integrate over $\boldsymbol{\kappa}_1$ and $\boldsymbol{\kappa}_2$ to find the Fresnel propagation formula for partially coherent light [31],

$$W(\boldsymbol{\rho}_1,\boldsymbol{\rho}_2,z) = \left(\frac{k}{2\pi z}\right)^2 \iint_{-\infty}^{\infty} W(\boldsymbol{\rho}_1',\boldsymbol{\rho}_2') \times \exp\left[-ik\frac{(\boldsymbol{\rho}_1-\boldsymbol{\rho}_1')^2 - (\boldsymbol{\rho}_2-\boldsymbol{\rho}_2')^2}{2z}\right]\mathrm{d}^2\rho_1'\mathrm{d}^2\rho_2'. \quad (3.36)$$

Further, considering propagation to the far zone, we can approximate

$$W(\boldsymbol{\rho}_1,\boldsymbol{\rho}_2,z) \approx \left(\frac{k}{2\pi z}\right)^2 \exp\left(-ik\frac{\rho_1^2-\rho_2^2}{2z}\right) \times \iint_{-\infty}^{\infty} W(\boldsymbol{\rho}_1',\boldsymbol{\rho}_2')\exp\left[-ik\frac{\boldsymbol{\rho}_1\boldsymbol{\rho}_1' - \boldsymbol{\rho}_2\boldsymbol{\rho}_2'}{z}\right]\mathrm{d}^2\boldsymbol{\rho}_1'\mathrm{d}^2\boldsymbol{\rho}_2', \quad (3.37)$$

which corresponds to the Fraunhofer diffraction formula for partially coherent light and where $\rho = |\boldsymbol{\rho}|$. A well-known property of light is that in the far field, the field distribution is essentially defined by the Fourier transform of the initial plane field, as can be seen from Eq. (3.37). But, since the self-Fourier transforming beams preserve their functional forms in these transformations, their properties do not evolve after propagating to the far field and they change only in scale. However, the properties of self-Fourier transforming beams in the Fresnel zone require further investigation. The model field we examined in paper **IV** did not retain the shape of its spatial density, but it is not clear whether this is a general feature of these types of fields, or just a characteristic of that particular field.

Probably the simplest experimentally feasible self-Fourier transforming field is a monochromatic Gaussian beam, although it is a somewhat trivial example. This is due to the properties of Gaussian distribution, which retains its mathematical form in Fourier transformation. There are some other special functions – such as the hyperbolic secant or sine with a squared argument – that have this property, but finding nontrivial self-Fourier transforming beams would be tedious if one just relies on these special cases. Therefore, it is necessary to look at the mathematical properties of the Fourier transform and see whether some general condition exists. Suppose that we have an arbitrary function $f(x)$, which has the Fourier transform $F(x)$, and we define a composite function $g(x) = f(x) + F(x)$. Due to linearity of the Fourier transform, any composite function of this type retains its form upon Fourier transformation, and this knowledge can also be utilized to construct optical beams.

Accordingly, we can define a field that is the superposition of two electric fields with the forms of each others' Fourier transforms, that is

$$E(\boldsymbol{\rho}) = E_{\mathrm{f}}(\boldsymbol{\rho}) + E_{\mathrm{F}}(\boldsymbol{\rho}), \quad (3.38)$$

where $E_{\mathrm{F}}(\boldsymbol{\rho})$ is the Fourier transform of $E_{\mathrm{f}}(\boldsymbol{\rho})$. Then we can write the CSD of the total field as

$$\begin{aligned} W(\boldsymbol{\rho}_1,\boldsymbol{\rho}_2) =& \left\langle \left[E_{\mathrm{f}}^*(\boldsymbol{\rho}_1)+E_{\mathrm{F}}^*(\boldsymbol{\rho}_1)\right]\left[E_{\mathrm{f}}(\boldsymbol{\rho}_2)+E_{\mathrm{F}}(\boldsymbol{\rho}_2)\right]\right\rangle \\ =& W_{\mathrm{f}}(\boldsymbol{\rho}_1,\boldsymbol{\rho}_2)+W_{\mathrm{F}}(\boldsymbol{\rho}_1,\boldsymbol{\rho}_2)+2\left\langle E_{\mathrm{f}}^*(\boldsymbol{\rho}_1)E_{\mathrm{F}}(\boldsymbol{\rho}_2)\right\rangle, \end{aligned} \tag{3.39}$$

which is a superposition of the individual correlation functions, plus a term responsible for cross-correlation. If the fields are mutually uncorrelated, then the last term will tend to zero, and their incoherent superposition becomes

$$W(\boldsymbol{\rho}_1,\boldsymbol{\rho}_2) = W_{\mathrm{f}}(\boldsymbol{\rho}_1,\boldsymbol{\rho}_2)+W_{\mathrm{F}}(\boldsymbol{\rho}_1,\boldsymbol{\rho}_2), \tag{3.40}$$

which is the CSD of a self-Fourier transforming beam. If we take the coherent but mutually uncorrelated elementary fields $e_{\mathrm{f},m}(\boldsymbol{\rho})$ and $e_{\mathrm{F},m}(\boldsymbol{\rho})$, and weigh them with a function c_m, we get a coherent mode representation for self-Fourier transforming beams

$$W(\boldsymbol{\rho}_1,\boldsymbol{\rho}_2) = \sum_m c_m\left[e_{f,m}^*(\boldsymbol{\rho}_1)e_{f,m}(\boldsymbol{\rho}_2)+e_{F,m}^*(\boldsymbol{\rho}_1)e_{F,m}(\boldsymbol{\rho}_2)\right]. \tag{3.41}$$

All fields that obey this representation are self-Fourier transforming, although the inverse may not be true. Indeed, it is also possible to construct a beam with a correlation function that is self-Fourier transforming by considering the product of two distinct functions, for example, the product of a Gaussian and a hyperbolic sine function [109]. In such a case an alternative treatment would be necessary.

3.3 SPATIAL SELF-FOCUSING

One of the most well-known correlation-induced effects is the spatial self-focusing of certain types of beams [85–87]. As the name suggests, such beams will focus on their own after some propagation distance, and it is one of the properties of nonuniformly correlated beams [85], although this property is also shared by other correlation functions, as we showed in paper **V**. Consequently, this effect has nothing to do with the self-focusing encountered in nonlinear optics, and correlation-induced self-focusing actually does not require a medium, i.e., it occurs even in free space propagation.

Let us continue ignoring the temporal dependence for simplicity, and recall the genuine representation outlined in section 2.2.2, so that we can write

$$\Gamma(\boldsymbol{\rho}_1,\boldsymbol{\rho}_2) = \int_{-\infty}^{\infty} p(v)H^*(\boldsymbol{\rho}_1,v)H(\boldsymbol{\rho}_2,v)\mathrm{d}v. \tag{3.42}$$

For mathematical simplicity, we take the kernel H to be a Gaussian function, such that

$$H(\boldsymbol{\rho},v) = \exp\left(-\frac{\rho^2}{2w_0^2}\right)\exp\left(-iv\rho^2\right), \tag{3.43}$$

where $\rho = |\boldsymbol{\rho}|$, and v is a parameter that determines the curvature of the spatial phase term, with the dimension $1/m^2$. Inserting this into Eq. (3.42) yields an MCF

of the form

$$\Gamma(\boldsymbol{\rho}_1,\boldsymbol{\rho}_2) = \exp\left(-\frac{\rho_1^2+\rho_2^2}{2w_0^2}\right)\gamma(\boldsymbol{\rho}_1,\boldsymbol{\rho}_2), \tag{3.44}$$

where the complex degree of spatial coherence, $\gamma(\boldsymbol{\rho}_1,\boldsymbol{\rho}_2)$, is yet again completely determined by the weight function $p(v)$, which is of the Fourier form

$$\gamma(\boldsymbol{\rho}_1,\boldsymbol{\rho}_2) = \int_{-\infty}^{\infty} p(v)\exp\left[-iv(\rho_2^2-\rho_1^2)\right]\mathrm{d}v. \tag{3.45}$$

The choice of weight function is obviously very important and it can change the correlation function dramatically. For example, if the weight function is also a Gaussian, then the resulting field will be nonuniformly correlated [85,100]. On the other hand, if it is described by the rectangular function, then the resulting field will be circularly correlated [110]. In fact, since the relationship between the correlation function and weight function is Fourier like, there is no difficulty in coming up with practically an unlimited amount of different types of coherence functions, all of which share the self-focusing property. The only real difference between these sources – apart from the form of the coherence function – is the shape of the focal spot. Thus, it can be interpreted that all other correlation-induced effects that redistribute the spatial intensity are contained in the self-focusing phenomenon.

Having established the general formulation for self-focusing sources, we now turn to examining the propagation properties of the field. Using the generalized Fresnel diffraction integral within paraxial approximation introduced in Eq. (3.36), the propagation of partially coherent beams through free space can be characterized with

$$\begin{aligned}\Gamma(\boldsymbol{\rho}_1,\boldsymbol{\rho}_2,z) = \left(\frac{k}{2\pi z}\right)^2 &\iint_{-\infty}^{\infty}\Gamma(\boldsymbol{\rho}_1',\boldsymbol{\rho}_2') \\ &\times\exp\left[-ik\frac{(\boldsymbol{\rho}_1-\boldsymbol{\rho}_1')^2-(\boldsymbol{\rho}_2-\boldsymbol{\rho}_2')^2}{2z}\right]\mathrm{d}^2\boldsymbol{\rho}_1'\mathrm{d}^2\boldsymbol{\rho}_2',\end{aligned} \tag{3.46}$$

in the space-time domain. Inserting from Eq. (3.42), we get

$$\begin{aligned}\Gamma(\boldsymbol{\rho}_1,\boldsymbol{\rho}_2,z) = \left(\frac{k}{2\pi z}\right)^2 &\int_{-\infty}^{\infty}p(v)\iint_{-\infty}^{\infty}H^*(\boldsymbol{\rho}_1',v)H(\boldsymbol{\rho}_2',v) \\ &\times\exp\left[-ik\frac{\left(\boldsymbol{\rho}_1-\boldsymbol{\rho}_1'\right)^2-\left(\boldsymbol{\rho}_2-\boldsymbol{\rho}_2'\right)^2}{2z}\right]\mathrm{d}^2\boldsymbol{\rho}_1'\mathrm{d}^2\boldsymbol{\rho}_2'\mathrm{d}v,\end{aligned} \tag{3.47}$$

further substituting Eq. (3.43) into Eq. (3.47) and by calculating the double integral, we obtain the propagated modes

$$\begin{aligned}H^*(\bar{\boldsymbol{\rho}}-\Delta\boldsymbol{\rho}/2,v,z)H(\bar{\boldsymbol{\rho}}+\Delta\boldsymbol{\rho}/2,v,z) = \frac{w_0^2}{w^2(v,z)}&\exp\left[-\frac{\bar{\rho}^2}{w^2(v,z)}\right] \\ &\times\exp\left\{-\frac{\Delta\rho^2}{4w^2(v,z)}-\bar{\rho}\Delta\rho\left[\sqrt{\frac{1}{w^2(v,z)}-\frac{z_R^2}{w_0^2z^2}}-i\frac{2k}{z}\right]\right\},\end{aligned} \tag{3.48}$$

where we have introduced the spatial mean and difference coordinates, $\bar{\boldsymbol{\rho}} = (\boldsymbol{\rho}_1 + \boldsymbol{\rho}_2)/2$ and $\Delta\boldsymbol{\rho} = \boldsymbol{\rho}_2 - \boldsymbol{\rho}_1$. Additionally, the widths of the propagated modes can be found with

$$w(v,z) = w_0 \left[\left(1 - \frac{vz}{k}\right)^2 + \frac{z^2}{z_R^2} \right]^{1/2}, \tag{3.49}$$

where have made use of the Rayleigh range $z_R = w_0^2 k/2$. These expressions differ from the usual Gaussian beam propagation only by the parameter v; if we choose $v = 0$, then these expressions reduce to the usual formulas. Examination of the extra factors shows that each mode gains its minimum width at the distance

$$z_{\min} = \frac{k}{v}. \tag{3.50}$$

The value for the waist of a single mode at this distance is then $w(z_{\min}) = (vw_0)^{-1}$, and the width of the whole beam can be found by integrating over all possible modes, which does not have an analytical expression. Although the remaining integral over v cannot be computed directly, we can numerically evaluate the field at any transverse plane z.

3.3.1 Focal spot engineering

It was noted early on that physically the spatial self-focusing of certain beams is due to the field being an incoherent superposition of coherent contributions with different propagation properties [85]. Accordingly, Eq. (3.48) can be interpreted to define a partially coherent field, constructed by incoherently superposing the elementary fields H, with the corresponding weights $p(v)$. Each elementary field then focuses to a point with a width given by Eq. (3.49), and a longitudinal position by Eq. (3.50). Hence, by choosing the weight function appropriately, in addition to producing different types of correlations, it is also possible to engineer the shape of the field at the focal plane. It is even possible to introduce beam steering into the equations, by replacing ρ in Eq. (3.43) with $\rho - \rho_0(v)$. This would cause each of the modes to focus at a different transverse position, but we shall not discuss such effects here.

If we set $\boldsymbol{\rho}_1 = \boldsymbol{\rho}_2 = \boldsymbol{\rho}$ in Eq. (3.48), we obtain the intensities of the individual modes

$$I(\boldsymbol{\rho},v,z) = |H(\boldsymbol{\rho},v,z)|^2 = \frac{w_0^2}{w^2(v,z)} \exp\left[-\frac{\rho^2}{w^2(v,z)} \right], \tag{3.51}$$

and we can find the total intensity $I(\boldsymbol{\rho},z)$ simply with

$$I(\boldsymbol{\rho},z) = \int_{-\infty}^{\infty} p(v) I(\boldsymbol{\rho},v,z) \mathrm{d}v, \tag{3.52}$$

in accordance with Eq. (3.48). It is possible to choose the weight from a wide class of functions; in particular, if we choose it to be of the Gaussian form, with

$$p(v) = \frac{\sigma^2}{\sqrt{\pi}} \exp\left(-\sigma^4 v^2\right), \tag{3.53}$$

and evaluate the integral in Eq. (3.45), we end up at the well-known nonuniformly correlated field [85]

$$\gamma(\boldsymbol{\rho}_1, \boldsymbol{\rho}_2) = \exp\left[-\frac{(\rho_2^2 - \rho_1^2)^2}{4\sigma^4}\right], \tag{3.54}$$

where σ is a spatial coherence parameter. According to Eq. (3.52), a nonuniformly correlated field consists of normally distributed modes with different focal distances, centered around $v = 0$.

If instead of a Gaussian weight function we choose a rectangular one, as in

$$p(v) = \sigma^2 \mathrm{rect}\left(\sigma^2 v^2\right), \tag{3.55}$$

then the coherence function becomes circularly correlated [110]

$$\gamma(\boldsymbol{\rho}_1, \boldsymbol{\rho}_2) = \mathrm{sinc}\left(\frac{\rho_2^2 - \rho_1^2}{2\pi\sigma^2}\right), \tag{3.56}$$

where $\mathrm{sinc}(x) = \sin \pi x / \pi x$. Now the modes that do focus have more weight than in the nonuniformly correlated beam, but the rectangular function has smaller bandwidth than the Gaussian function, indicating that it does not focus as strongly.

These two fields represent some of the well-known examples that feature self-focusing. It is not difficult to come up with new correlation functions that produce much more complex intensity distributions upon propagation. Let us, for example, write the weight function in the form of a finite delta comb

$$p(v) = \sum_{n=1}^{N} \delta(v - \kappa n), \tag{3.57}$$

where κ is an arbitrary real number, which defines the spacing of the comb. With this weight, the degree of coherence becomes

$$\gamma(\boldsymbol{\rho}_1, \boldsymbol{\rho}_2) = \exp\left[i\kappa(\rho_2^2 - \rho_1^2)\right] \frac{1 - \exp\left[i\kappa N(\rho_2^2 - \rho_1^2)\right]}{1 - \exp\left[i\kappa(\rho_2^2 - \rho_1^2)\right]}, \tag{3.58}$$

which we call a comb-correlation. If the comb spacing is chosen properly, it is possible to produce $N - 1$ isolated focal points along the propagation direction, or to elongate the depth of focus as is shown in Fig. 3.7 below.

The weight and correlation functions we have considered here are relatively simple examples of how one can engineer the focal intensity. Obviously, any physically realizable distribution can be used as the weight function, thus producing a wide range of different types of correlations and focusing properties. Additional freedom in focal spot design can be achieved if we allow the weight function to contain position dependent phase factors. Then it becomes possible to distribute the intensity also along the transverse plane, inducing spatial self-splitting, among other things. Because of these properties, it is justified to say that models with self-splitting can contain all of the correlation-induced effects that redistribute the spatial intensity distribution.

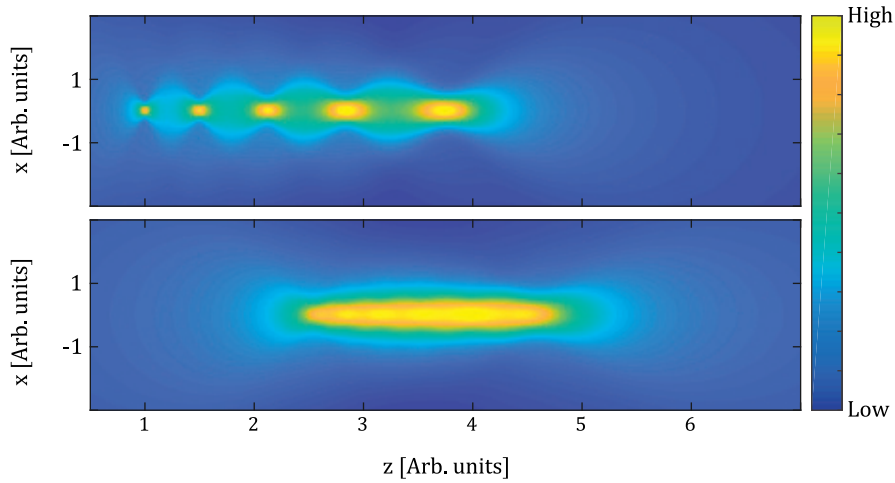

Figure 3.7: Intensity distributions of comb correlated fields propagated through free space. The parameters were chosen to get isolated (upper) and elongated (lower) focal spots.

3.4 TEMPORAL SELF-SPLITTING

The fact that correlation-induced phenomena also occur in the temporal domain comes naturally from space-time duality; whatever effects there are in the spatial domain, they usually have time domain pairs [111–115]. So let us now make a transition to the temporal domain, and demonstrate some basic properties of temporal self-splitting. We start by establishing the physical interpretation behind this correlation-induced effect and then introduce some self-splitting model pulses, which we outlined in paper **VI**.

Propagation of the mutual coherence function through dispersive media can be investigated with the generalized Collins formula in the temporal domain [116,117]

$$\Gamma\left(t_1,t_2,z\right)=\frac{\omega_0}{2\pi B}\exp\left[-\frac{i\omega_0 D}{2B}\left(t_1^2-t_2^2\right)\right]\times\iint_{-\infty}^{\infty}\Gamma_0\left(\tau_1,\tau_2\right)\exp\left[-\frac{i\omega_0 A}{2B}\left(\tau_1^2-\tau_2^2\right)\right]\exp\left[\frac{i\omega_0}{B}\left(\tau_1 t_1-\tau_2 t_2\right)\right]\mathrm{d}\tau_1\mathrm{d}\tau_2, \tag{3.59}$$

where A, B, C, and D are the elements of an arbitrary temporal transfer matrix (C being absent) and $\Gamma_0\left(\tau_1,\tau_2\right)$ is the MCF at $z=0$. We take the time coordinate as being measured in the reference frame of the moving pulse. The generalized Collins formula works up to second order dispersion, since no temporal transfer matrices exist for higher order effects.

It is well-known that when propagating through a dispersive medium, coherent pulses transform in the temporal far field to a form that is functionally identical with their power spectra. The same can be found to be true for temporal $2F$ systems as well. We can show that the same result applies to partially coherent pulses, by

evaluating the temporal intensity using Eq. (3.59) by setting $t_1 = t_2 = t$

$$I(t,z) = \frac{\omega_0}{2\pi B}\iint_{-\infty}^{\infty}\Gamma_0(\tau_1,\tau_2)\exp\left[-\frac{i\omega_0}{2B}A\left(\tau_1^2-\tau_2^2\right)+\frac{i\omega_0 t}{B}(\tau_1-\tau_2)\right]\mathrm{d}\tau_1\mathrm{d}\tau_2. \tag{3.60}$$

If the pulses propagate through dispersive media to the temporal far field, the first exponential term will tend towards zero. On the other hand, for a temporal $2F$ system the first exponential term inside the integral is zero, since $A = 0$. In either case, the above equation can be written as

$$I(t,z) = \frac{\omega_0}{2\pi B}\iint_{-\infty}^{\infty}\Gamma_0(\tau_1,\tau_2)\exp\left[\frac{i\omega_0 t}{B}(\tau_1-\tau_2)\right]\mathrm{d}\tau_1\mathrm{d}\tau_2, \tag{3.61}$$

which bears a striking resemblance to another quantity. Applying the Wiener–Khintchine theorem of Eq. (2.14) to the correlation functions at the initial plane, and setting $\omega_1 = \omega_2 = \omega$, we find that spectral density is given by

$$S(\omega) = \frac{1}{(2\pi)^2}\iint_{-\infty}^{\infty}\Gamma_0(t_1,t_2)\exp\left[-i\omega(t_1-t_2)\right]\mathrm{d}t_1\mathrm{d}t_2. \tag{3.62}$$

Comparing these two expressions it is clear that the spectral density at the initial plane and the far field or Fourier-plane temporal intensity share the same functional form, irrespective of the degree of coherence. From these considerations it is clear how one can construct temporally self-splitting pulses: one only needs to shape the spectral density to whatever desired form and then compress the pulse. A transform limited pulse can be produced by having a flat spectral phase, and upon propagation it will acquire a phase which causes it to unravel and take on the shape of the spectral density.

We can again define an almost unlimited number of self-splitting pulses, but we will describe here only two that have distinct properties. It is possible to use the genuine representation to find a weight function and kernel that will produce an MCF of the form

$$\Gamma(t_1,t_2) = L_n\left(\frac{\Delta t^2}{T_c^2}\right)\exp\left(-\frac{t_1^2+t_2^2}{T_0^2}\right)\exp\left(-\frac{\Delta t^2}{2T_c^2}\right)\exp\left(-i\omega_0\Delta t\right), \tag{3.63}$$

where L_n is the Laguerre polynomial of order n, and the MCF reduces to the GSM case when $n = 0$. The mean intensity for this type of field is a Gaussian function

$$I(t) = \exp\left(-\frac{2t^2}{T_0^2}\right), \tag{3.64}$$

and by normalizing we find that the complex degree of temporal coherence is of the form

$$\gamma(\Delta t) = L_n\left(\frac{\Delta t^2}{T_c^2}\right)\exp\left(-\frac{\Delta t^2}{2T_c^2}\right)\exp\left(-i\omega_0\Delta t\right). \tag{3.65}$$

A field which obeys this correlation function is a Laguerre-Gaussian correlated Schell-model (LGCSM) pulse, and its spectral density is

$$S(\omega) = \frac{T_0}{2\pi 2^n n!\Omega_0}\exp\left(-\frac{2\omega^2}{\Omega_0^2}\right)\sum_{k=0}^{n}\frac{2^k k!}{\left(1+\Omega_c^2/\Omega_0^2\right)^{n-k}}\binom{n}{k}^2 H_{2(n-k)}\left(\frac{\sqrt{2}\omega}{\Omega_0}\right). \tag{3.66}$$

Now it is quite obvious from Eq. (3.66) that the spectral density is no longer of the simple Gaussian form, while the initial pulse shape is. Thus, due to Eq. (3.61), we can expect that if such pulses are propagated to the temporal far field, the pulse shape will experience changes.

Another type of self-splitting pulses is the Hermite-Gaussian correlated Schell-model (HGCSM), which we define in a similar way. We again take the mean intensity as being of the Gaussian form of Eq. (3.64), but assume that the complex degree of temporal coherence is determined by the function

$$\gamma(\Delta t) = \frac{H_{2n}\left(\Delta t/\sqrt{2}T_\mathrm{c}\right)}{H_{2n}(0)} \exp\left(-\frac{\Delta t^2}{2T_\mathrm{c}^2}\right) \exp\left(-i\omega_0 \Delta t\right). \tag{3.67}$$

These choices define the class of HGCSM pulse trains, and we can again see that the degree of temporal coherence reduces to that of conventional GSM pulses for $n = 0$. The correlation function introduced here also corresponds to a non-negative definite kernel – as it should – and by employing the usual tools it is simple to find that the spectral density of this source is given by

$$S(\omega) = \frac{(-1)^n}{2\pi} \frac{T_0}{\Omega_0} \frac{2^{-n}\beta^{2n}}{(2n-1)!!} \exp\left(-\frac{2\varpi^2}{\Omega_0^2}\right) H_{2n}\left(\frac{i\sqrt{2}\varpi}{\Omega_\mathrm{c}}\right). \tag{3.68}$$

And yet again, it is obvious that the spectral density is not of the Gaussian form anymore.

3.4.1 Propagation to the temporal far field

The actual behavior of these sources is revealed only after they are propagated, which can be done analytically. One interesting propagation distance is the temporal far field, which is defined similarly as its spatial counter part [118, 119], that is, the propagation length is much greater than the Rayleigh range of the beam. A typical feature of a spatial field that has entered the far-zone, is that it propagates with no change in its form. A corresponding phenomenon also happens in the temporal domain, as we will see. Let us start with the LGCSM pulses; on substituting from Eq. (3.63) into Eq. (3.59) and changing to the mean and average coordinates allows us to cast the equations into a solvable form, and the integration yields the following propagation formula

$$\begin{aligned}\Gamma\left(t_1, t_2, z\right) =& \frac{\omega_0 T_0}{2\sqrt{2}B} \exp\left[-\frac{i\omega_0 D}{2B}(t_1^2 - t_2^2)\right] \exp\left[-\frac{T_0^2\omega_0^2}{8B^2}(t_1 - t_2)^2\right] \\ &\times \exp\left[-\frac{d^2(t_1, t_2)}{4c}\right] \sum_{q=0}^{n} \binom{n}{q} \frac{1}{q!\,(2T_\mathrm{c})^{2q}\, c^{q+1/2}} H_{2q}\left[\frac{d(t_1, t_2)}{2\sqrt{c}}\right],\end{aligned} \tag{3.69}$$

where we have reverted back to the absolute coordinates and employed the shorthand notations

$$c = \frac{1}{2T_0^2} + \frac{1}{2T_\mathrm{c}^2} + \frac{T_0^2}{8}\left(\frac{A\omega_0}{B}\right)^2, \tag{3.70}$$

$$d(t_1, t_2) = \frac{\omega_0}{2B}(t_2 + t_1) + iT_0^2 \frac{A\omega_0^2}{4B^2}(t_2 - t_1). \tag{3.71}$$

Expression (3.69) gives the MCF at the output plane of an arbitrary temporal optical system that can be expressed with the use of ABCD matrix formalism.

In the present case, we are mainly interested in studying the evolution of the temporal intensity profile upon propagation through a linearly dispersive medium, such as an optical fiber. For this type of system the ABCD matrix is of the form [116, 117]

$$\begin{pmatrix} A & B \\ C & D \end{pmatrix} = \begin{pmatrix} 1 & \omega_0 \beta_2 z \\ 0 & 1 \end{pmatrix}, \tag{3.72}$$

and β_2 is the group velocity dispersion coefficient. Substituting the values from Eq. (3.72) into Eq. (3.69), and setting $t_1 = t_2 = t$, the mean intensity after an arbitrary propagation distance is given by

$$I(t,z) = \frac{T_0}{2\sqrt{2}\beta_2 z} \exp\left[-\frac{2t^2}{T^2(z)}\right] \sum_{q=0}^{n} \binom{n}{q} \frac{1}{q!(2T_c)^{2q}[c(z)]^{q+1/2}} H_{2q}\left[\frac{\sqrt{2}t}{T(z)}\right], \tag{3.73}$$

where

$$T(z) = T_0 \left(1 + \frac{z^2}{z_T^2}\right)^{1/2}, \tag{3.74}$$

$$c(z) = \frac{1}{2T_0^2\beta^2}\left(1 + \frac{z_T^2}{z^2}\right), \tag{3.75}$$

and

$$z_T = z_G \beta = \frac{T_0^2}{2\beta_2}\left(1 + \frac{T_0^2}{T_c^2}\right)^{-1/2} \tag{3.76}$$

is the temporal Rayleigh range of the pulsed beam. The Rayleigh range z_T we employ reduces to the usual temporal Rayleigh range $z_G = T_0^2/2\beta_2$ that is encountered for coherent Gaussian pulses in the coherent limit of $\beta \to 1$.

Carrying out the same procedures for the HGCSM pulses defined by Eq. (3.67), we get an MCF of the form

$$\begin{aligned} \Gamma(t_1,t_2,z) = {} & \frac{\omega_0 T_0}{2\sqrt{2c}B} \exp\left[-\frac{i\omega_0 D}{2B}\left(t_1^2 - t_2^2\right)\right] \frac{(-1)^n 2^{-n}}{(2n-1)!!} \\ & \times \exp\left[-\frac{T_0^2\omega_0^2}{8B^2}(t_1 - t_2)^2\right] \exp\left[-\frac{d^2(t_1,t_2)}{4c}\right] \left(\frac{1}{2T_c^2}\right)^n \\ & \times \left(2T_c^2 - \frac{1}{c}\right)^n H_{2n}\left[-\frac{id(t_1,t_2)}{2c\sqrt{2T_c^2 - 1/c}}\right], \end{aligned} \tag{3.77}$$

and the average intensity of such pulses propagted through a linearly dispersive medium is then given by

$$\begin{aligned} I(t,z) = {} & \frac{(-1)^n 2^{-n}}{(2n-1)!!} \frac{T_0}{T(z)} \exp\left[-\frac{2t^2}{T^2(z)}\right] H_{2n}\left[-\frac{i\sqrt{2}t}{T_c(z)}\right] \\ & \times \left[1 - \left(1 + \frac{T_c^2}{T_0^2}\right)^{-1}\left(1 + \frac{z_T^2}{z^2}\right)^{-1}\right]^n, \end{aligned} \tag{3.78}$$

where

$$T_c(z) = T_c \left[\left(1 + z^2/z_T^2\right) \left(1 + z_G^2/z^2\right) \right]^{1/2}. \tag{3.79}$$

A more in-depth investigation of the propagation properties of fields with these correlation properties is warranted. In Fig. 3.8, we show how the LGCSM and HGCSM pulses evolve upon propagation through a linearly dispersive medium.

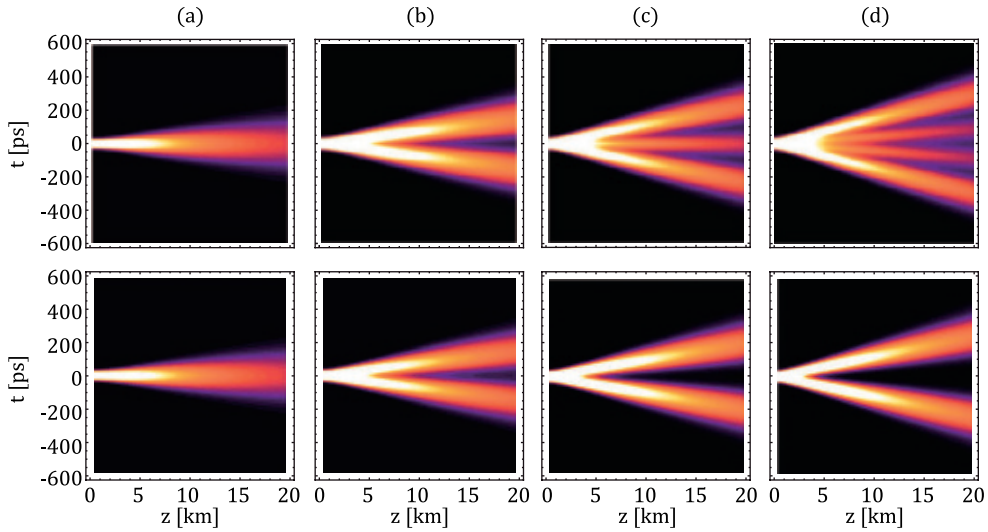

Figure 3.8: Pulse evolution upon propagation in a linearly dispersive medium. Upper row: LGCSM, lower row: HGCSM, with (a) $n = 0$, (b) $n = 1$, (c) $n = 2$, and (d) $n = 3$.

For these simulations, we have chosen the length of the initial pulse to be $T_0 = 30$ ps and the group velocity dispersion as $\beta_2 = 50$ ps^{2}km^{-1}, which are close to typical values found in optical telecommunication. In addition to these parameters, we set the temporal coherence time of the pulses to be $T_c = 10$ ps, thus they are fairly incoherent. The plots extend to the temporal far zone, $z \gg z_T$, where $z_T = 2.85$ km with the chosen parameters.

It is clear that the order n plays an important role in the self-splitting properties of these model pulses, since a single Gaussian pulse at the initial plane evolves to $n + 1$ sub-pulses for the LGCSM case. On the other hand, the HGCSM pulse always produces two sub-pulses, but their separation increases with increasing n. When $n = 0$, both models reduce to GSM pulses that do not split upon propagation. Similarly to the spatial correlation-induced effects, temporal phenomena can also be engineered widely. For example, it is rather easy to envision a type of pulse that confines itself when propagated to the far zone. Looking at Eqs. (3.61) and (3.62), we can simply take a pulse with a single-lobed spectrum and give it some spectral phase that produces a multiply-peaked temporal pulse. This will lead to pulses that have a self-confining property, i.e., the inverse of the pulses considered here.

4 Measurement of nonstationary light

The complete characterization of pulsed fields is a long-standing problem, and some of the schemes found in the stationary case have been used to measure the correlation properties of nonstationary fields [120–122]. However, the assumption of stationarity is not valid for pulsed sources and this affects a wide range of experiments as well. The most limiting factor in measuring pulsed light is that there are no detectors that are fast enough, and we always end up integrating over time. Some measurement schemes have been introduced to overcome this problem with interferometric and self-referencing techniques [8, 16, 17]. However, there are still some types of light, which we cannot measure directly even with modern methods.

4.1 SPATIAL DOMAIN

This section will outline some of the major concepts behind spatial coherence measurements and how they can be applied to pulsed sources. The nature of nonstationary sources has to be taken into account even in the spatial domain, which may complicate some of the experiments. Some alternative methods are then examined, which were introduced in papers **VII**, **VIII**, as well as **IX**, and their applicability for measuring pulsed sources is established. In coherence research, spatial coherence is probably the most intuitive domain for experiments, and as such, several methods have been established for probing the spatial properties of light [104, 123–140]. The development of several different types of methods comes in response to the ever increasing arsenal of available sources [141–150]. In fact, spatial coherence is a somewhat special case, since it manifests itself whenever two light beams interact. For example, if a light beam is split into two and the copies partially overlap, then the overlapping region contains an interference pattern, which has the form of the spatial coherence function. Therefore, spatial coherence can be measured with any spatially shearing or folding interferometer, as long as there is no dispersion and the time delay between the two beams is zero. The overlapping region contains a single slice of the correlation function, and by scanning the beams over each other it is possible to extract full knowledge of the complex degree of spatial coherence.

When people consider spatial coherence, they are mostly interested in stationary fields. As such, theoretical formulations for spatially partially coherent model fields usually do not have any mention of the temporal dependence. However, it is entirely possible that spatial coherence is also a function of time, even for stationary fields. A situation like that could very well be constructed by periodically modulating a beam of light with some optical element, such as a rotating ground glass plate. In the case of the CSD, it is customary not to ignore the spectral dependence, since different wavelengths can have different spatial coherence properties, which implies cross-spectral impurity. In fact, it is simple to construct a field that is completely spatially coherent in the frequency domain, but becomes partially coherent upon transformation to the temporal domain.

4.1.1 Young's interferometer

The double-slit experiment, or Young's interferometer [151,152], is probably the first device which was used to measure spatial coherence. The concept behind its operation is very simple and the results are intuitive, so it has been examined extremely thoroughly in several settings. As such, it has become the standard tool for spatial coherence measurements. Although it has been around for more than 200 years, there are still some misconceptions on its usage. The biggest problem is that it is not enough to do a single measurement with Young's interferometer, if you want to completely characterize the spatial coherence of a light source. The interferometer works by sampling the incident radiation with two small slits or pinholes at two different spatial coordinates, and superposing the samples at an observation plane, as is depicted in Fig. 4.1. Thus, the measurement has to be repeated over all possible spatial coordinate pairs, which requires one to move the apertures.

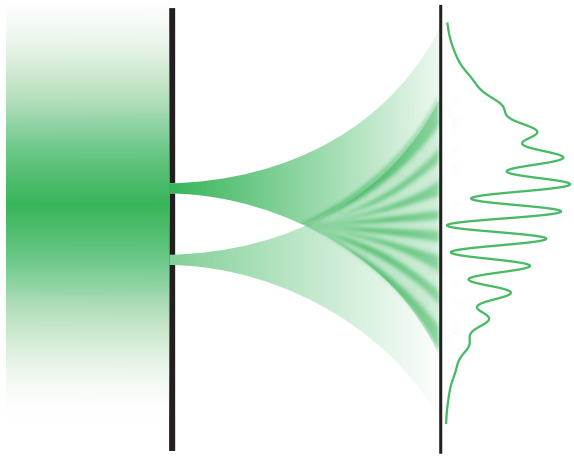

Figure 4.1: Basic principle of Young's interferometer: light - incident from the left - is sampled with two pinholes, and the resulting interference pattern is recorded at some observation plane.

Over the recent years, several modified versions of Young's interferometer have been introduced, which allow for a measurement over all coordinates accross the whole wavefront [104, 123–129]. Irrespective of the exact scheme, the mathematical form of the spectral interference pattern in Young's interferometer is given by

$$S(\mathbf{R};\omega) = |K_1|^2 S(\mathbf{r}_1;\omega) + |K_2|^2 S(\mathbf{r}_2;\omega) + 2|K_1||K_2|\sqrt{S(\mathbf{r}_1;\omega)S(\mathbf{r}_2;\omega)}\,\Re\left\{\mu(\mathbf{r}_1,\mathbf{r}_2;\omega,\omega)\exp\left(-i\omega\tau\right)\right\}, \qquad (4.1)$$

where the coefficients K_j are weakly frequency dependent factors [31] and $\tau = (R_1 - R_2)/c$ is the time difference between the paths R_1 and R_2, measured from the slits to a point at the detector plane. Two conclusions can be drawn from this: i) to measure wide bandwidth fields, the interferometer has to be paired with a spectrometer to resolve the different frequencies, and ii) there is a position dependent time delay at the observation plane, and thus temporal coherence is mixed into the measurement. Due to the limitations of Young's interferometer in coherence measurement, it is necessary to explore some alternative methods.

4.1.2 Grating interferometer

The grating interferometer is a type of zero time delay, z-scanning spatial coherence measurement device, which was first presented in paper **VII**, and refined in paper **VIII**. The interferometer overcomes some of the limitations of Young's interferometer, and its operation principle is illustrated in Fig 4.2. We consider only the x-component of the incident field, $E_0(x;\omega)$, which is normal to a grating with a period d. The field is split into two diffraction orders $m = 1$ and $m = -1$, which propagate towards directions $\theta_{\pm 1}(\omega)$ given by the grating equation.

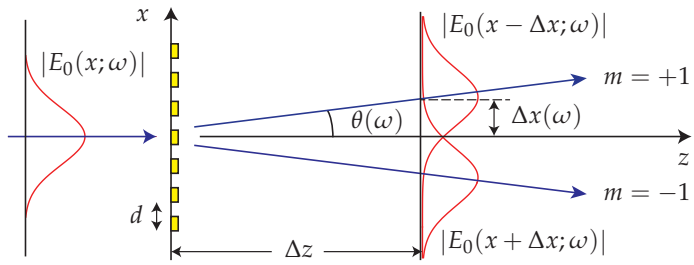

Figure 4.2: Basic principle of a grating interferometer. Here the incident field is split into two copies which are sheared upon propagation. The actual number of diffraction orders depends on the grating profile (from paper **VII**).

We can calculate the shear between the diffracted fields at a distance of Δz behind the grating, with

$$\Delta x(\omega) = \Delta z \tan\theta(\omega) = \Delta z \tan\left[\arcsin\left(\frac{2\pi c}{\omega d}\right)\right] \approx \frac{2\pi c \Delta z}{\omega d}, \tag{4.2}$$

where the last form applies in the paraxial approximation. Assuming that the propagation distance is short and the beam width is large enough to neglect diffractive spreading, the total field at a distance Δz may be expressed as

$$\begin{aligned} E(x,\Delta z;\omega) = {} & T_{+1}(\omega) E_0(x-\Delta x;\omega) \exp\left[i\left(k_x x + k_z \Delta z\right)\right] \\ & + T_{-1}(\omega) E_0(x+\Delta x;\omega) \exp\left[i\left(-k_x x + k_z \Delta z\right)\right], \end{aligned} \tag{4.3}$$

where $k_x = 2\pi/d$, $k_z = \sqrt{(\omega/c)^2 - k_x^2}$, and $T_{\pm 1}(\omega)$ are the complex amplitudes of orders $m = \pm 1$, and we have dropped the explicit frequency dependence of Δx for brevity of notation. Ideally, we would like to employ a phase grating with a sinusoidal profile, since it produces only the two desired orders with equal powers. But, because they are difficult to fabricate, a simpler alternative is to use symmetric binary phase gratings and blocking elements for the unnecessary orders.

The efficiency and the period of the gratings are critical parameters when designing the device. Obviously, the efficiency determines how dim sources one can measure, and if sinusoidal gratings can be fabricated, the overall efficiency can reach 50 % in the double grating configuration. Although, such a grating could be used on its own for coherence measurements, raising the maximum efficiency to 100 %, and thus potentially allowing spatial coherence measurements even for single photon sources. The period of the gratings is equally important, as it dictates the length of the device. It is possible to minimize the footprint of the setup by employing simple trigonometry and the grating equation.

To find out what the device actually measures, we turn to the correlation functions introduced in chapter 2. The spectral density of the interference pattern is given by

$$S(x, \Delta x; \omega) = \langle |E(x, \Delta x; \omega)|^2 \rangle, \tag{4.4}$$

and inserting from Eq. (4.3) yields the expression

$$\begin{aligned} S(x, \Delta x; \omega) = \eta(\omega) \big[& S_0(x - \Delta x; \omega) + S_0(x + \Delta x; \omega) \\ & + W_0(x - \Delta x, x + \Delta x; \omega) \exp(-i4\pi x/d) \\ & + W_0^*(x - \Delta x, x + \Delta x; \omega) \exp(i4\pi x/d) \big]. \end{aligned} \tag{4.5}$$

Making use of the definition of the complex degree of spectral coherence in Eq. (2.18), we find that

$$\begin{aligned} & S(x, \Delta x; \omega) = \\ & \eta(\omega) \Big[S_0(x - \Delta x; \omega) + S_0(x + \Delta x; \omega) + 2\sqrt{S_0(x - \Delta x; \omega) S_0(x + \Delta x; \omega)} \\ & \times |\mu_0(x - \Delta x, x + \Delta x; \omega)| \times \cos\{\arg[\mu_0(x - \Delta x, x + \Delta x; \omega)] - 4\pi x/d\} \Big], \end{aligned} \tag{4.6}$$

which is an interference pattern with a constant spatial period d, given that the phase of the complex degree of coherence is flat. If the argument of $\mu_0(x - \Delta x, x + \Delta x; \omega)$ is not constant, then the period of the interference fringes can vary from spot to spot.

The spectral interference pattern of Eq. (4.6) can be observed if an imaging spectrometer is used as a detector. This way, one can image the interference pattern onto the plane of a two-dimensional array detector so that spatial resolution is in the x direction, and the y-axis resolves the spectral components. By measuring the spectral density $S(x; \omega)$ from both arms of the interferometer together with the visibility

$$V(x, \Delta x; \omega) = \frac{2\sqrt{S_0(x - \Delta x; \omega) S_0(x + \Delta x; \omega)}}{S_0(x - \Delta x; \omega) + S_0(x + \Delta x; \omega)} |\mu_0(x - \Delta x, x + \Delta x; \omega)| \tag{4.7}$$

of the interference fringes at the desired frequency ω, one can determine the absolute value of the complex degree of spectral coherence, $|\mu_0(x - \Delta x, x + \Delta x; \omega)|$. Additionally, the phase of this quantity can be obtained from the positions of the interference fringes.

If the employed detector is not an imaging spectrograph but a square-law array detector, such as a CCD, one measures the intensity distribution of the interference pattern, i.e., the frequency-integrated spectral density

$$I(x, \Delta x) = \int_0^\infty S(x, \Delta x; \omega) \mathrm{d}\omega. \tag{4.8}$$

Inserting from Eq. (4.5), we obtain

$$\begin{aligned} I(x, \Delta x) = & \int_0^\infty \eta(\omega) \left[S_0(x - \Delta x; \omega) + S_0(x + \Delta x; \omega) \right] \mathrm{d}\omega \\ & + \exp(-i4\pi x/d) \int_0^\infty \eta(\omega) W_0(x - \Delta x, x + \Delta x; \omega) \mathrm{d}\omega \\ & + \exp(i4\pi x/d) \int_0^\infty \eta(\omega) W_0^*(x - \Delta x, x + \Delta x; \omega) \mathrm{d}\omega. \end{aligned} \tag{4.9}$$

Since Δx depends on both Δz and ω according to Eq. (4.2), there is no precise general connection between the interference pattern of Eq. (4.9) and $\gamma_0(x_1, x_2; 0)$, even if $\eta(\omega)$ is independent of ω. From this chain of reasoning, it is clear that narrowband sources can be measured with a simple CCD detector, but for larger bandwidths one requires an imaging spectrometer to resolve the interference pattern spectrally. To ensure that the measurements are all done at the same z plane, one should move the gratings and keep the detector stationary, which also removes most of the alignment issues. This configuration is depicted in Fig. 4.3, which we used in paper **VIII** to measure the light from an unstable and exotic source, the wood laser [153].

This light source is produced by combining transparent wood – a relatively new material [154–156] that has found use in optical physics [157,158] – with a laser dye. When the wood sample is pumped in the absorption region of the dye, the fibers act as miniature resonators, and the output is essentially an incoherent superposition of coherent fields, with a quasi-random weight function. This causes the output of the laser to be relatively bright and spatially partially coherent. Unlike a random laser, the wood laser features some degree of order, which is due to the structure of the wood [159]. Because of these properties, we called this type of sources as quasi-random lasers. This source type not restricted only to wood templates, and it is entirely possible to produce different types of them by growing semiconductor pillars [160–162], for example.

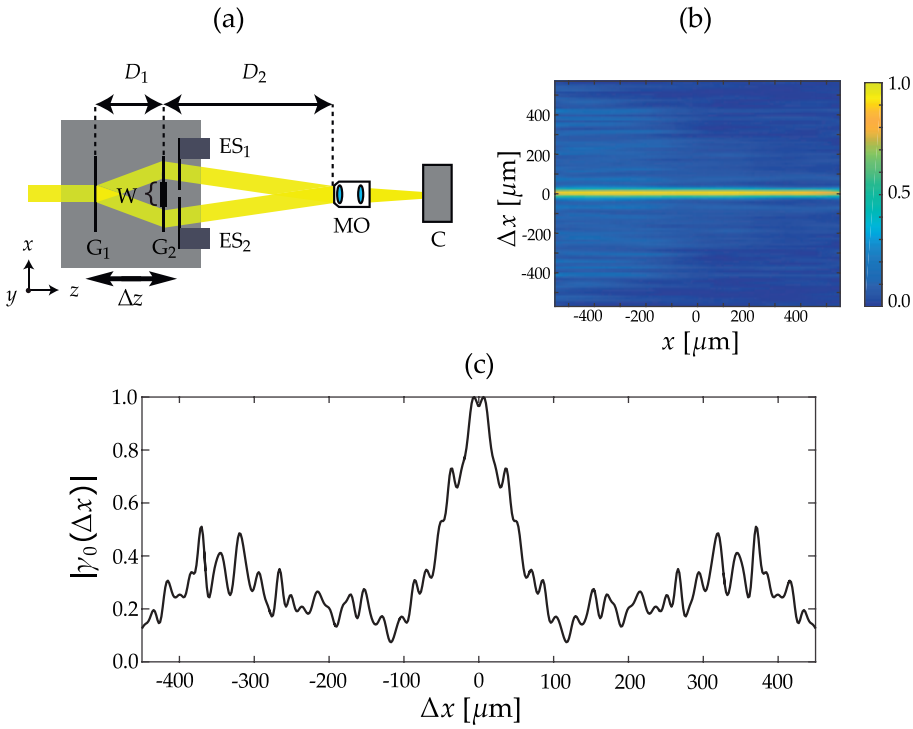

Figure 4.3: Measurement results from wood laser experiments. (a) Configuration with z-scanned gratings, (b) absolute value of spatial degree of coherence for the light emitted from the wood laser and (c) a cross-section from (b), in the Δx direction, at $x = -200$ μm.

The grating interferometer is a spatial coherence measurement device that overcomes some of the main issues in Young's interferometer, that is, the efficiency and time delay problems. But it requires specially fabricated gratings and the use of an imaging spectrometer if one wishes to measure broadband light. One may also employ a device that has similar advantages as the grating interferometer, but which can be constructed from components that every optical laboratory has on the shelf. Moreover, this class of devices – to be discussed below – does not require the use of an imaging spectrograph to correctly measure large bandwidth sources, thus reducing the complexity of the device.

4.1.3 Wavefront folding interferometer

The wavefront folding interferometer (WFI) is historically speaking one of the most notable spatial coherence measurement devices [130–132]. It features high efficiency and simple design, but it has not risen to the level of Young's interferometer in popularity, mainly due to the fact that it can only measure Schell-model sources in its traditional form. However, it is possible to extend the operational capabilities of the WFI so that it can measure general non-Schell model sources, as we did in paper **IX**. In the following, we shall use the same notation as before for the incident light, and consider field components along both x- and y-axes.

A standard WFI configuration splits the incident beam into two, which are folded in x and y directions by prisms and recombined at the detection plane. The prisms are slightly tilted to produce interference fringes and the optical paths are made equal by z-scanning one of the arms. When the center of the input beam is aligned to the edges of the two prisms, as in Fig. 4.4(a), the WFI measures spatial coherence between two symmetrically located transverse points, but as a function of their separation only. This is the usual configuration for a WFI, where the device is limited to spatial coherence measurements of Schell-model fields. A shear of $(\Delta x, \Delta y)$ between the optical axes of the incident field $E_0(x, y; \omega)$ and the interferometer – as shown in Fig. 4.4(b) – leads to interference between fields at the coordinates (x, y') and (x', y), where $x' = -x + 2\Delta x$ and $y' = -y + 2\Delta y$ are the folded and sheared transverse coordinates.

Let us take the prism P1 as being tilted to an angle α_x in the x direction and P2 to α_y in the y direction. Further, if P2 is assumed to be shifted in the z direction by an amount Δz from the equal-path position, the spectral field at point $(x_\mathrm{d}, y_\mathrm{d})$ on the detector can be written in the form

$$E(x_\mathrm{d},y_\mathrm{d};\omega) = \frac{1}{2}\left\{E_0(x,y';\omega)\exp\left[iC_x(\omega)x\right] + E_0(x',y;\omega)\exp\left[-iC_y(\omega)y\right]\exp\left[i\phi(\omega)\right]\right\}, \tag{4.10}$$

where $\phi(\omega) = 2\Delta z\omega/c$, $C_x(\omega) = 2\sin\alpha_x\omega/c$, and $C_y(\omega) = 2\sin\alpha_y\omega/c$. Then, by employing the definitions in Eqs. (2.10) and (2.18), as well as the Hermiticity of the CSD, the spectral density at the detector can be written as

$$S(x_\mathrm{d},y_\mathrm{d};\omega) = \frac{1}{4}\left[S_0(x,y';\omega) + S_0(x',y;\omega)\right] + \frac{1}{2}\sqrt{S_0(x,y';\omega)S_0(x',y;\omega)}\left|\mu_0(x,y',x',y;\omega)\right| \times \cos\left\{\arg\left[\mu_0(x,y',x',y;\omega)\right] - C_x(\omega)x - C_y(\omega)y + \phi(\omega)\right\}. \tag{4.11}$$

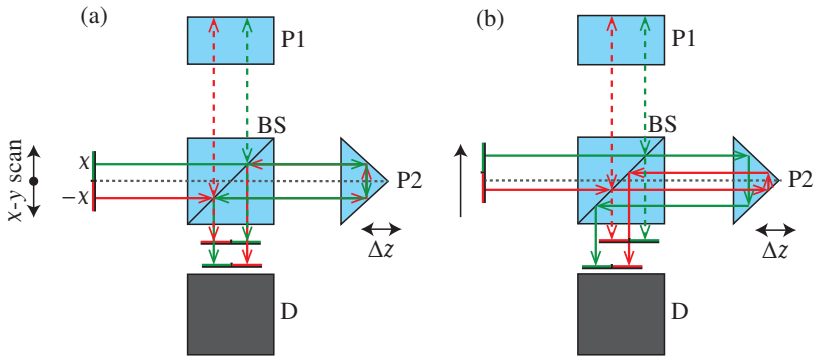

Figure 4.4: Basic configuration for a laterally scanning WFI. The input is split by beamsplitter BS and retroreflected by prisms P1 and P2 towards the imaging system D. In (a) the beam is centered on the prism edge, whereas in (b) it has been shifted along the x-axis. Dashed lines show paths through P1 and solid ones through P2 (from paper **IX**).

It is noteworthy that at the output of the interferometer, the field is specular, i.e. it fulfills $W(x_1, y_1, x_2, y_2) = W(-x_1, -y_1, x_2, y_2)$, which makes the WFI an attractive device also for generating specular and antispecular beams [163, 164], as long as the obstruction by the prism edges is dealt with. The visibility of the interference fringes around point $(x_\mathrm{d}, y_\mathrm{d})$ is given by

$$V(x_\mathrm{d}, y_\mathrm{d}; \omega) = \frac{2\sqrt{S_0(x, y'; \omega) S_0(x', y; \omega)}}{S_0(x, y'; \omega) + S_0(x', y; \omega)} \left| \mu_0(x, y', x', y; \omega) \right|, \tag{4.12}$$

and thus, it is possible to find information on the correlations from the interference pattern.

If the detector unit D in Fig. 4.4 is not an imaging spectrograph but a combination of an imaging system and a square-law array detector, the WFI measures the time-integrated intensity, which is equal to

$$I(x_\mathrm{d}, y_\mathrm{d}) = \int_0^\infty S(x_\mathrm{d}, y_\mathrm{d}; \omega) \mathrm{d}\omega. \tag{4.13}$$

On inserting from Eq. (4.11) and integrating, we get

$$\begin{aligned} I(x_\mathrm{d}, y_\mathrm{d}) = \frac{1}{4} \left[I_0(x, y') + I_0(x', y) \right] + \frac{1}{2} \sqrt{I_0(x, y') I_0(x', y)} \left| \gamma_0 \left(x, y', x', y; \tau - \tau_0 \right) \right| \\ \times \cos \left\{ \arg \left[\gamma_0 \left(x, y', x', y; \tau - \tau_0 \right) \right] - \omega_0 \left(\tau - \tau_0 \right) \right\}, \end{aligned} \tag{4.14}$$

where

$$\tau = 2 \left(x \sin \alpha_x + y \sin \alpha_y \right) / c \tag{4.15}$$

is a position-dependent time delay due to the tilted wavefronts and $\tau_0 = 2\Delta z / c$ is the time delay caused by the optical path length difference. Expression (4.14) represents an interference pattern where the fringe visibility is given by

$$V(x_\mathrm{d}, y_\mathrm{d}; \omega) = \frac{2\sqrt{I_0(x, y') I_0(x', y)}}{I_0(x, y') + I_0(x', y)} \left| \gamma_0(x, y', x', y; \tau - \tau_0) \right|. \tag{4.16}$$

Because of τ in Eq. (4.14), the WFI mixes spatial and temporal coherence to some extent. In order to measure broadband fields correctly, it is necessary to compensate for the path length difference at each measurement point $(x_\mathrm{d}, y_\mathrm{d})$ by adjusting τ_0 accordingly.

A novel configuration of the WFI, which we introduced in paper **IX**, is to employ two beam splitters and three mirrors, depicted in Fig. 4.5(a). The device was used to measure the spatial degree of coherence for a multimode laser diode (Thorlabs L808P500MM), and the absolute value is shown in Fig. 4.5(b), while in Fig. 4.5(c) is the corresponding phase. The amplitude and phase of the complex degree of coherence can be extracted with simple Fourier signal processing: take the normalized interference pattern, Fourier transform it and remove negative frequencies. Then inverse Fourier transform to obtain the complex valued degree of coherence.

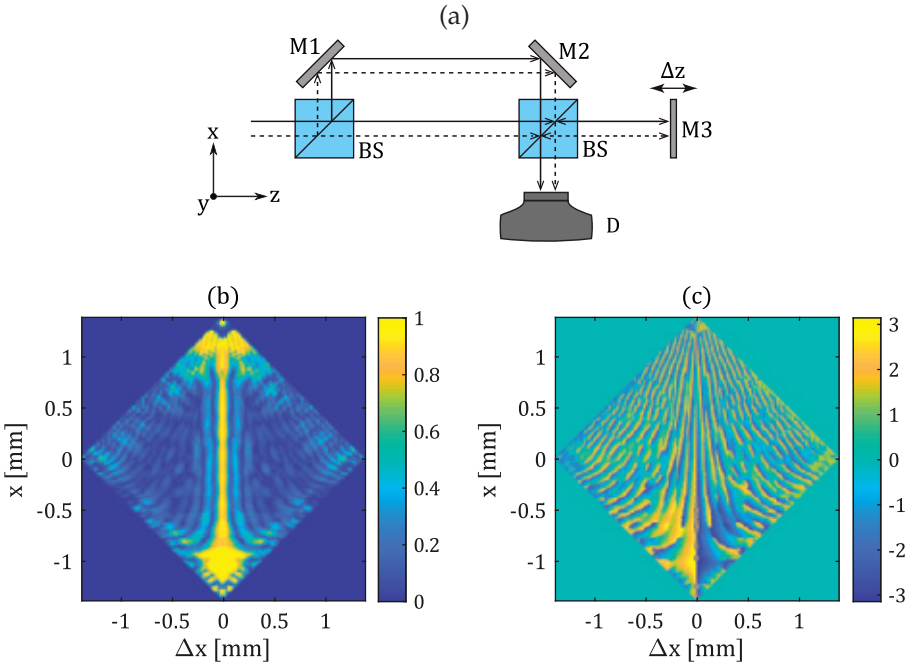

Figure 4.5: Results of experiments done with the WFI on a laser diode. (a) The employed setup, (b) the absolute value of the complex degree of coherence, $|\gamma_0(x, x'; 0)|$, and (c) the corresponding phase.

By shearing the optical axes of the input beam and the interferometer in the x direction, it is possible to measure the coherence of the field between arbitrary points along the plane. This setup offers two major advantages: first, there is no central obstruction like the edge of a prism, and second, the setup is nearly polarization insensitive. With two retroreflecting glass prisms, the visibility of the interference fringes may drop dramatically for certain input polarization states. This is because the polarization of the input light rotates when it experiences total internal reflection between the glass-air interface, and since the two prisms are oriented perpendicularly with respect to each other, they rotate the polarization to opposite directions. If the difference in the refractive indices at the reflection boundary is suitable (~ 0.515), the visibility will go to zero, no matter what the input degree of coherence is.

4.2 SPECTRAL DOMAIN

Spectral domain coherence is an important subject in nonstationary theory. Unlike in the stationary case, correlations between different frequencies are allowed, which results in fields that have nonconstant temporal properties. To characterize the spectral correlation properties, we employ the CSD and note that it is intimately linked to the MCF via the Wiener–Khintchine theorem. Indeed, one cannot consider spectral correlations independently from temporal properties, since they define and shape each other. However, in this section we again assume cross-spectral purity, and ignore spatial properties.

As much as we would like to measure the CSD directly to find out the complete spectral correlation properties of a source, it is not a simple problem. Whereas spectral density is straightforward to measure, there exists no direct method to quantify the spectral phase. It may seem easy enough from the definition in Eq. (2.10), but it needs to be noted that whenever two waves with different frequencies are superposed, the resulting sum wave will feature beating, i.e., modulation that has the same frequency as the difference between the two interfering frequencies. To measure a pulsed source, one would require a detector that is capable of resolving signals on the order of $10^{14} - 10^{15}$ Hz, whereas fastest modern semiconductor detectors are capable of going only up to 10^{12} Hz. Since direct measurement is not possible, it is necessary to device methods, which indirectly probe the spectral coherence properties of a wide range of different sources, as outlined in paper **X**.

4.2.1 Field autocorrelation

We will start from the MCF and CSD in average and difference coordinates that were defined in Eqs. (2.21) and (2.22) and ignore the spatial dependence altogether. Then the correlation functions will be of the form

$$\Gamma(\bar{t}, \Delta t) = \langle E^*(\bar{t} - \Delta t/2) E(\bar{t} + \Delta t/2) \rangle, \tag{4.17}$$

$$W(\bar{\omega}, \Delta\omega) = \langle E^*(\bar{\omega} - \Delta\omega/2) E(\bar{\omega} + \Delta\omega/2) \rangle. \tag{4.18}$$

Casting the correlation functions in this form is highly advantageous when we are concerned with experimental settings, since realistic detectors will always integrate over average time. The simplest experimental device for probing coherence is the variable delay Michelson interferometer, depicted in Fig. 4.6, and it has been widely employed to measure the coherence length in the context of stationary light.

The device measures the field autocorrelation, $A(\Delta t)$, of the time domain electric field, $E(t)$, as in

$$A(\Delta t) = \int_{-\infty}^{\infty} E^*(\bar{t} - \Delta t/2) E(\bar{t} + \Delta t/2) \mathrm{d}\bar{t}. \tag{4.19}$$

The temporal domain pulses have the corresponding spectral representations, $E(\omega)$, so that replacing the time domain pulses with their Fourier transforms and applying some simple mathematical operations, one obtains the expression

$$A(\Delta t) = \int_{0}^{\infty} |E(\omega)|^2 \exp(-i\omega t) \mathrm{d}\omega, \tag{4.20}$$

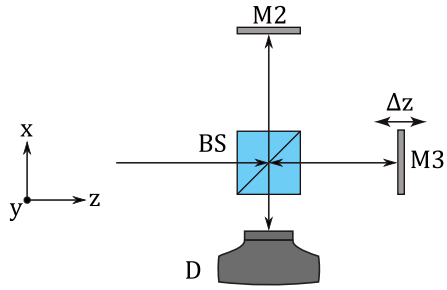

Figure 4.6: Traditional variable delay Michelson interferometer.

that is, the autocorrelation of a single pulse is the Fourier transform of its spectral power content.This result is the well-known autocorrelation theorem, and it has profound consequences in Michelson interferometry. One might think intuitively that the field autocorrelation is somehow related to the temporal pulse shape or length, but this is generally not the case. The autocorrelation theorem of Eq. (4.20) holds for any spectral phase, and it is therefore insensitive to changes in the pulse shape caused by spectral phase variations. In fact, temporally integrating field interferometric techniques do not yield any direct time domain information, but rather, one may gain information only on the spectrum of the pulse. This is in contrast to the widely employed intensity autocorrelation, which generally contains information on the pulse length [8].

There is one situation where the field autocorrelation does yield an estimate of the pulse length: when a pulse is generated by amplitude modulating a stationary signal. This is because modulation in the temporal domain results in the modulation of the spectrum, such that

$$A(\Delta t) = \int_0^\infty |E_0(\omega) * H(\omega)|^2 \exp(-i\omega t)\mathrm{d}\omega, \tag{4.21}$$

where $E_0(\omega)$ is the initial spectral field, $H(\omega)$ is the Fourier transform of the temporal window function $h(t)$, and the asterisk denotes convolution. If the spectral field is much narrower than the spectral window function and $H(\omega)$ is strictly real, then the temporal pulse is approximately $h(t)$. But the autocorrelation theorem states that if the modulated pulse attains spectral phase, the field autocorrelation cannot detect any change in the pulse length. Thus, there is no way of ensuring whether the pulse length really is equal to the width of $h(t)$, or if it has some other value.

If a detector that is faster than the repetition rate of the laser is employed, then it is possible to measure the autocorrelation for each pulse separately, like in Eq. (4.19). A slower detector would see an ensemble average over the single-shot autocorrelation traces, which is equal to

$$\langle A(\Delta t)\rangle = \int_0^\infty \langle |E(\omega)|^2\rangle \exp(-i\omega t)\mathrm{d}\omega = \int_0^\infty S(\omega)\exp(-i\omega t)\mathrm{d}\omega, \tag{4.22}$$

meaning that such measurement contains information only on the mean power spectrum of the source. Comparing Eqs. (4.17), (4.19), and (4.22), it is evident that the field autocorrelation is equal to the time integrated MCF. Thus,

$$\langle A(\Delta t)\rangle = \int_{-\infty}^\infty \Gamma(\bar{t}, \Delta t)\mathrm{d}\bar{t} = \Gamma^{(\mathrm{int})}(\Delta t), \tag{4.23}$$

indicating that with an autocorrelation we can measure the coherence correctly only for sources that are of the Schell-model type [165]. However, there is no way to know what type of source is being measured with these techniques.

4.2.2 Field cross-correlation

There is another linear correlation measurement that is experimentally feasible, and which contains information on coherence, as established in paper **X**. We take two different time domain pulses, $E_i(t)$ and $E_j(t)$, where $i \neq j$. These can be consequent pulses from the same source, or probe and signal from different sources. Interfering them results in the field cross-correlation,

$$X(\Delta t) = \int_{-\infty}^{\infty} E_i^*(\bar{t} - \Delta t/2) E_j(\bar{t} + \Delta t/2) \mathrm{d}t. \tag{4.24}$$

Doing the same operations as in the case of autocorrelation, we find that the field cross-correlation is the Fourier transform of the product of the spectral fields,

$$X(\Delta t) = \int_{0}^{\infty} E_i^*(\omega) E_j(\omega) \exp(-i\omega t) \mathrm{d}\omega. \tag{4.25}$$

Clearly, if there is a known and highly coherent probe pulse and an unknown signal, then we can very simply find the unknown pulse with inversion of Eq. (4.25). This technique is essentially spectral interferometry without a spectrometer and one can use it to completely characterize arbitrary pulses. However, the technique is limited since it requires one to find a stable and well-known probe pulse in the right wavelength region and somehow synchronize its repetition rate with the unknown pulse laser. Because of this, it is desirable to look at what information can be extracted if E_i and E_j are subsequent pulses derived from the same source. Single-shot measurements do not contain a lot of information in this case, since both signals are unknown, but if we take the ensemble average of the cross-correlation, we can quantify some of the correlation properties.

The imaginary part of the term $\langle E_i^*(\omega) E_j(\omega) \rangle$ will always tend towards zero for sufficiently many pulses, since completely coherent pulses cancel each other, and incoherent signals will average out over a large ensemble. If a source produces N different pulse realizations, then there will be an overall of $N^2 - N$ possible pairs from that group. If we perform the measurement over all possible pairs, then we can write the ensemble averaged cross-correlation with only the real contribution, as in

$$\langle X(\Delta t) \rangle = \frac{1}{N^2 - N} \int_0^{\infty} \sum_{i \neq j}^{N} \left[E_i^*(\omega) E_j(\omega) + E_i(\omega) E_j^*(\omega) \right] \exp(-i\omega t) \mathrm{d}\omega, \tag{4.26}$$

where we have written the ensemble average explicitly. It is straightforward to see that this is equivalent to

$$\begin{aligned} \langle X(\Delta t) \rangle = \frac{1}{N^2 - N} \int_0^{\infty} \Bigg[& \left| \sum_{i \neq j}^{N} E_i(\omega) + E_j(\omega) \right|^2 \\ & - \sum_{i \neq j}^{N} |E_i(\omega)|^2 - \sum_{i \neq j}^{N} |E_j(\omega)|^2 \Bigg] \exp(-i\omega t) \mathrm{d}\omega, \end{aligned} \tag{4.27}$$

when the squares are completed. Now the summations go through all possible pulses and we can rewrite the cross-correlation with n as

$$\langle X(\Delta t)\rangle = \frac{1}{N^2-N}\int_0^\infty \left[\left|\sum_{n=1}^{N} E_n(\omega)\right|^2 - \sum_{n=1}^{N}|E_n(\omega)|^2\right]\exp(-i\omega t)\mathrm{d}\omega, \tag{4.28}$$

which we can further write using the bracket notation so that

$$\langle X(\Delta t)\rangle = \frac{1}{N^2-N}\int_0^\infty \left[N^2|\langle E(\omega)\rangle|^2 - N\langle|E(\omega)|^2\rangle\right]\exp(-i\omega t)\mathrm{d}\omega. \tag{4.29}$$

By doing this measurement over a large ensemble of pulses, only the squared terms will be significant and we can approximate

$$\langle X(\Delta t)\rangle \approx \int_0^\infty S_{\mathrm{qc}}(\omega)\exp(-i\omega t)\mathrm{d}\omega, \tag{4.30}$$

where $S_{\mathrm{qc}}(\omega) = |\langle E(\omega)\rangle|^2$ is the quasi-coherent part of the spectrum. This is effectively the same result as the Dudley-Coen degree of coherence measured with a modified Michelson interferometer [166, 167]. But here the spectral resolution is introduced through a temporal cross-correlation, rather than an imaging spectrometer, greatly simplifying the setup. Some possible configurations are shown in Fig. 4.7, first for subsequent pulses from the same train and then for pulses generated from different sources.

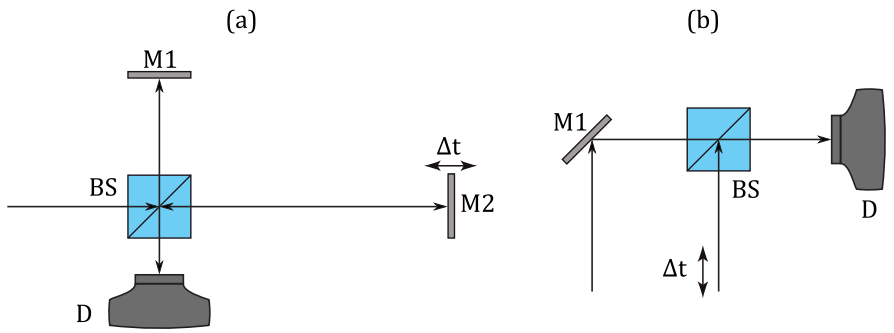

Figure 4.7: Cross-correlation setups for (a) measuring consecutive pulses from the same source, and (b) for signal–probe measurements.

4.2.3 Spectral phase interferometry for direct electric field reconstruction

In a way similar to spatial coherence measurements, it is possible to introduce a shear between the interfering fields in the spectral domain. This allows the measurement of the whole correlation function, but accomplishing a large enough shear is not a simple task. For small bandwidth pulses, it is possible – at least in principle – to attain a large enough spectral shear with acousto-optic devices. When measuring ultrashort pulses, the power spectrum is so wide that nonlinear methods are required. Probably the most notable spectrally shearing measurement scheme is the spectral phase interferometry for direct electric field reconstruction (SPIDER) [8,17].

The concept behind SPIDER is shown in Fig. 4.8: two pulses separated by a time delay τ are sum-frequency mixed with an orthogonally polarized and massively chirped pulse, and the spectral interference pattern is recorded with a spectrometer. The chirped pulse is used to accomplish the spectral shear, since the frequencies in the pulse separate temporally when the chirp is large enough and the temporal separation τ determines the fringe spacing in the resulting spectral interference pattern.

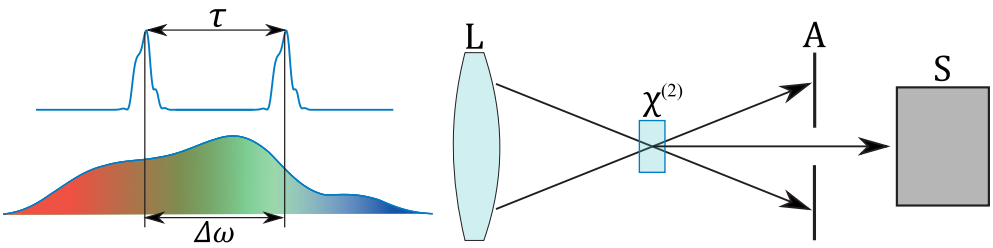

Figure 4.8: Basic configuration for a SPIDER apparatus. A pulse pair is inserted into a second order nonlinear crystal together with a orthogonally polarized and massively chirped pulse, where all three pulses are derived from the same initial pulse. The nonlinear crystal is cut for sum-frequency generation, and the upconverted pulse pair is measured with a spectrometer.

Obviously, this is just one variation of SPIDER, though it may be the most common one. Any device that mixes a pulse with a spectral slice of itself in a sum-frequency generating crystal and then measures the spectral interference between two upconverted pulses can be considered to be in the same family of experimental methods. SPIDER is often considered to be a temporal domain measurement, since the end goal is to find the shape of the temporal pulse. But it is in fact more appropriate to consider it as a frequency domain method, since it measures the spectral interference pattern at the detector, which is given by

$$S(\bar{\omega}, \Delta\omega) = \langle |E_{\mathrm{u}}(\bar{\omega} - \Delta\omega/2) + E_{\mathrm{u}}(\bar{\omega} + \Delta\omega/2) \exp(-i\bar{\omega}\tau)|^2 \rangle \tag{4.31}$$

where the subscript u denotes the upconverted pulse obtained via sum frequency generation. Following the conventions in the earlier sections, we can write the spectral fringe pattern in the form

$$\begin{aligned} S(\bar{\omega}, \Delta\omega) = {} & S_{\mathrm{u}}(\bar{\omega} - \Delta\omega/2) + S_{\mathrm{u}}(\bar{\omega} + \Delta\omega/2) \\ & + 2\sqrt{S_{\mathrm{u}}(\bar{\omega} - \Delta\omega/2) S_{\mathrm{u}}(\bar{\omega} + \Delta\omega/2)}\, \Re\{\mu_{\mathrm{u}}(\bar{\omega}, \Delta\omega) \exp(-i\bar{\omega}\tau)\}, \end{aligned} \tag{4.32}$$

from where we see that the SPIDER apparatus measures a slice from the spectral correlation function μ_{u} along the ω direction at a fixed spectral shear $\Delta\omega$. One slice is enough to find the spectral phase [168–170], as long as the spectral shear is sufficiently larger than zero. If $\Delta\omega = 0$, then the phase terms exactly cancel out and the measurement yields only the spectral density. Even at moderate spectral shear, the high frequency phase components wash out for partially coherent pulses, and the method yields an erroneous result for the pulse length [171]. However, when a pulse train does feature partial coherence, SPIDER can measure the complete correlation function for the upconverted pulse by shearing the frequency over the

whole power spectrum. This is an advantage in the measurement setup that has not been utilized before, either experimentally, or theoretically.

It is possible to recover the spectral degree of coherence for the original pulse train by considering the properties of the upconverted pulse. Sum-frequency generation is governed by the nonlinear polarization

$$P^{NL}(\mathbf{r};t) = 2\epsilon_0\chi^{(2)}E_1(\mathbf{r};t)\exp(-i\omega_1 t)E_2(\mathbf{r};t)\exp(-i\omega_2 t), \tag{4.33}$$

where the frequencies ω_1 and ω_2 are now the carrier frequencies of the fields $E_1(t)$ and $E_2(t)$, respectively. Additionally, ϵ_0 is the permittivity of free space and $\chi^{(2)}$ is the second order nonlinear susceptibility. The polarization acts as a source term in the nonlinear wave equation

$$\nabla^2 E_{\mathrm{u}}(\mathbf{r};t) - \frac{n^2(\omega)}{c^2}\frac{\partial^2}{\partial t^2}E_{\mathrm{u}}(\mathbf{r};t) = \frac{1}{\epsilon_0 c^2}\frac{\partial^2}{\partial t^2}P^{NL}(\mathbf{r};t) \tag{4.34}$$

where $n(\omega)$ is the frequency dependent refractive index and we assume that light propagates to the positive half-space $z > 0$. By inserting Eq. (4.33) into the wave equation it is possible to find the upconverted field. We can use a few good approximations to vastly simplify this problem: first of all, for the nonlinear material, we assume that its nonlinearity is weak and that the crystal is thin with low dispersion. Second, we assume that the slowly varying envelope approximation holds, i.e., the pulse to be characterized is longer than a few optical cycles. These approximations break down when the pulse is very short and intense, but they are well justified in the majority of experimental situations. Under these conditions, the nonlinear wave equation can be cast into the form [16]

$$\frac{\partial}{\partial z}E_{\mathrm{u}}(\mathbf{r};t) = -i\frac{(\omega_1+\omega_2)^2}{2\epsilon_0 c^2 k}P^{NL}(\mathbf{r};t), \tag{4.35}$$

which has a correspondinly simple solution

$$E_{\mathrm{u}}(\mathbf{r};t) = -i\frac{z(\omega_1+\omega_2)^2}{2\epsilon_0 c^2 k}P^{NL}(\mathbf{r};t), \tag{4.36}$$

where we have not considered the phase-matching condition, since it affects only the amplitude of the signal. Thus, if we ignore the spatial dependence and some constants in front of the equation, the upconverted field is given by

$$E_{\mathrm{u}}(t) = E_1(t)E_2(t)\exp\left(-i\omega_{\mathrm{u}}t\right), \tag{4.37}$$

where $\omega_{\mathrm{u}} = \omega_1 + \omega_2$ is the carrier frequency of the upconverted pulse. By Fourier transforming to the spectral domain, we find that

$$E_{\mathrm{u}}(\omega+\omega_{\mathrm{u}}) = E_1(\omega+\omega_{\mathrm{u}}) * E_2(\omega+\omega_{\mathrm{u}}), \tag{4.38}$$

where the asterisk denotes a convolution between the input spectral fields.

In SPIDER, the pulse to be measured, $E_0(t)$, is mixed with a massively chirped copy of itself. The chirp must be large enough to separate the frequencies so that when sampling the pulse with a temporal window of the same width as the original pulse, the chirped pulse will have an approximately constant intensity and phase. In other words, the parts of the chirped pulse that are sum-frequency mixed with

the original pulses have an essentially constant complex amplitude of either $E_0(\omega_0 + \Delta\omega/2)$ or $E_0(\omega_0 - \Delta\omega/2)$, where ω_0 is the center frequency of the spectrum and $\Delta\omega$ is the spectral shear. Then the frequency domain representation of the upconverted pulses simply becomes

$$E_{\mathrm{u}}(\bar{\omega} + \Delta\omega/2) = E_0(\omega_0 + \Delta\omega/2)E_0(\bar{\omega} + \Delta\omega/2), \tag{4.39}$$

and

$$E_{\mathrm{u}}(\bar{\omega} - \Delta\omega/2) = E_0(\omega_0 - \Delta\omega/2)E_0(\bar{\omega} - \Delta\omega/2), \tag{4.40}$$

where we have ignored the carrier frequency for brevity. Then the CSD for the upconverted pulses is given by

$$W_{\mathrm{u}}(\bar{\omega}, \Delta\omega) = \langle C(\Delta\omega)E_0^*(\bar{\omega} + \Delta\omega/2)E_0(\bar{\omega} - \Delta\omega/2)\rangle, \tag{4.41}$$

where $C(\Delta\omega) = E_0^*(\omega_0 + \Delta\omega/2)E_0(\omega_0 - \Delta\omega/2)$ is just a complex number in an experimental interference pattern, since each measurement is done at a fixed $\Delta\omega$. If the pulse train is not completely coherent, $C(\Delta\omega)$ is a random variable, which uniformly shifts the spectral interference pattern from shot to shot, leading to a reduced visibility of fringes. Thus, it cannot be straightforwardly removed from the ensemble averaged CSD. However, by employing Fourier signal processing, it is possible to remove its contribution before averaging, and the original correlation function $W_0(\bar{\omega}, \Delta\omega)$ can be computed numerically from single-shot measurements. Therefore, SPIDER can be used to measure the spectral correlations of pulsed light correctly, whenever single-shot measurements are possible. Even if the repetition rate of the laser is too high for such experiments, Eq. (4.41) still yields a useful measure on the stability of the pulse train. Additionally, if we consider the correlation function along the $\Delta\omega$ direction at $\bar{\omega} = 0$, we find that

$$W_{\mathrm{u}}(0, \Delta\omega) = \langle [E_0^*(\omega_0 + \Delta\omega/2)E_0(\omega_0 - \Delta\omega/2)]^2\rangle, \tag{4.42}$$

which is a slice of a root-mean-square type spectral correlation function and it can be used to retrieve an estimate for the temporal pulse shape.

These considerations apply for self-referencing SPIDER devices; if instead of using the pulse itself to shear the spectra, we employ some tunable reference source, then we can write the upconverted CSD as

$$W_{\mathrm{u}}(\bar{\omega}, \Delta\omega) = W_R(\omega_0, \Delta\omega)W_0(\bar{\omega}, \Delta\omega), \tag{4.43}$$

where $W_R(\omega_0, \Delta\omega)$ is the CSD of the reference field. The spectral correlation functions can be factored in this way, since two independent sources are mutually uncorrelated, and we can normalize to obtain

$$\mu_{\mathrm{u}}(\bar{\omega}, \Delta\omega) = \mu_R(\omega_0, \Delta\omega)\mu_0(\bar{\omega}, \Delta\omega). \tag{4.44}$$

If the reference field is completely coherent, then the expression simply reduces to

$$\mu_{\mathrm{u}}(\bar{\omega}, \Delta\omega) = \mu_0(\bar{\omega}, \Delta\omega), \tag{4.45}$$

since $\mu_R(\omega_0, \Delta\omega) = 1$ at all possible coordinates. But even if the reference field is not completely coherent, it's possible to remove it, if it is known.

Since SPIDER can measure the spectral correlation function of the original pulse train correctly, it is highly desirable for the characterization of partially coherent pulsed fields. Although it has some constraints due to requiring a second order nonlinearity, it will probably evolve to a reliable method for measuring complex pulses, such as supercontinua [166,167,172–175].

4.3 TEMPORAL DOMAIN

Since linear interference measurements carried out in the time domain yield information on the spectral properties of the field, then doing similar type of measurements in the spectral domain should give us information on the time domain pulse. Indeed, it is simple to show that a spectral autocorrelation yields the time domain intensity, that is

$$\langle A(\Delta\omega)\rangle = \mathcal{F}\{I(t)\}, \tag{4.46}$$

Unfortunately – as was mentioned earlier – this quantity cannot be directly measured. Only when one has a suitable probe signal, it is possible to carry out spectral interferometry and gain information on the time domain pulse. But if the starting point is that we know nothing about the properties of the pulses we produce, then spectral interferometry will not work and we have to transition to higher order correlation measurements.

4.3.1 Intensity correlations

It was recognized early on in the development of pulsed lasers that linear interferometric measurements are not sufficient to find out the temporal characteristics of nonstationary sources. One of the first experimental schemes that could yield some information on the pulse length was the intensity autocorrelation [8,16]. Mathematically, we can represent this operation as

$$A_I(\Delta t) = \int_{-\infty}^{\infty} I(t-\Delta t/2)I(t+\Delta t/2)\mathrm{d}t. \tag{4.47}$$

However, unlike the field autocorrelation, Eq. (4.47) does not form a Fourier transform pair with any measurable quantity like the spectrum. Experimentally, the intensity autocorrelation is performed by rotating the polarization states in the two arms of a Michelson interferometer – to avoid interference fringes – and the pulses are then fed into a second harmonic generating crystal. The motivation for this setup is that since the nonlinear process is intensity dependent, the output from such an interferometer is the brightest when the two copies are perfectly overlapping, and decays with increasing time delay.

The intensity autocorrelation gates the pulse with itself, which makes it possible to find out the root-mean-square (rms) duration of the pulse, without any knowledge of the pulse shape. This is due to the properties of Fourier transform, which is clear when we consider the autocorrelation as a convolution of a function with itself. If we have a convolution of two functions of the form $h(t) = f(t) * g(t)$, then the rms widths of these functions are related by a pythagorean sum [16]

$$T_h^2 = T_f^2 + T_g^2. \tag{4.48}$$

Because we are now dealing with a convolution of a function with itself, $f(t) = g(t)$, then $T_f = T_g$ and the rms width of the pulse is simply

$$T_f = T_h/\sqrt{2}. \tag{4.49}$$

Therefore, it is possible to unambiguously determine the time window of the pulse length with a simple autocorrelation measurement. However, we are usually interested in the full width at half maximum (FWHM) of the pulse intensity instead

of the rms value. Unlike the rms width, one cannot reliably find out the FWHM for the pulse from an intensity autocorrelation trace, because some pulse shape has to be assumed. Worse yet, the pulse shape cannot be uniquely identified from the autocorrelation trace, since there are infinitely many pulses that produce the same autocorrelation.

An obvious improvement to this is to employ a cross-correlation, similarly to the previous section. If one has a coherent and known probe pulse, then we can write

$$X_I(\Delta t) = \int_{-\infty}^{\infty} I_i(t - \Delta t/2) I_j(t + \Delta t/2) \mathrm{d}t, \tag{4.50}$$

and finding out the pulse shape becomes a deconvolution problem. Interestingly, if the probe is much shorter than the signal, then we don't even need to know the probe pulse, just that it is much shorter than the signal. In this case we may approximate

$$X_I(\Delta t) \approx \int_{-\infty}^{\infty} \delta(t - \Delta t/2) I_j(t + \Delta t/2) \mathrm{d}t = I_j(\Delta t), \tag{4.51}$$

where $\delta(t)$ is the Dirac delta, and the measurement yields the signal pulse exactly. Thus, it is experimentally rather simple to find out the shape of an unknown pulse, if you have a much shorter pulse with which to probe it. It is also possible to be sure that your probe is shorter than the signal, by first measuring the intensity autocorrelations for both of them, which yields the rms pulse lengths. Although, if one wishes to measure the shape of the shortest pulse that can be produced, then this method will clearly fail. Attempts to overcome this limitation include the third-order autocorrelation, triple correlation, and interferometric autocorrelation, to name a few. Unfortunately, only the triple correlation has been shown to uniquely yield the pulse shape, and the method still suffers from experimental complexity and is very rarely used [16]. Better methods have since surfaced, some of which we will be focusing on next.

4.3.2 Frequency resolved optical gating

Frequency resolved optical gating (FROG) refers to a large family of experimental techniques that can be used to uniquely characterize a pulse [16]. They have evolved from conventional intensity correlation methods, by adding frequency resolution to the setup. One of the biggest advantages is that you can realize a self-referencing FROG, thus eliminating the need for a shorter probe pulse and allowing one to measure the shortest pulses that can be made. Conceptually the simplest type of this device is the second-harmonic generating (SHG) FROG. It is based on the intensity autocorrelation, where the output from the nonlinear crystal is analyzed with an imaging spectrograph. This allows one to increase the available information on the pulse enough to iteratively retrieve the pulse amplitude and phase. The interferogram one measures from a SHG FROG obeys the equation

$$I_{\mathrm{SHG}}(\Delta t, \omega) = \left| \int_{-\infty}^{\infty} E(t) E(t - \Delta t) \exp(-i\omega t) \mathrm{d}t \right|^2. \tag{4.52}$$

There are several different versions of this device, each of which relies on different combinations of referencing and nonlinear gating mechanisms. The FROG trace is

unique for a given pulse, which means that it is possible to retrieve the temporal pulse shape unambigiously, when there is no measurement error. It is notable that the interferogram is superficially similar to the Wigner distribution,

$$W(t,\omega) = \int_{-\infty}^{\infty} E^*(t)E(t-\Delta t)\exp(-i\omega\Delta t)\mathrm{d}\Delta t. \tag{4.53}$$

One of the well-known properties of the Wigner distribution is that its marginals yield expectation values; that is, integration over time gives the mean power spectrum and integration over frequency the average temporal pulse. Because of this similarity, one may be tempted to look at the marginals of the FROG interferogram to find these properties. Unfortunately, only the power spectrum can be retrieved from the marginals [176], and we are forced to use iterative methods if we wish to also find the temporal pulse shape.

A FROG retrieval algorithm generally works as outlined in the flow chart of Fig. 4.9(a): you start from a guess for the pulse length and spectrum, and mathematically construct an interferogram. Then, discard the amplitude of the resulting FROG trace and replace it with the experimentally measured one, while retaining the phase. Finally, invert the interferogram to find how the pulse and spectrum have changed and update your guess. In essence, what this algorithm retrieves is not the pulse, but the phase of the interferogram, which can be used to find the pulse. The convergence of this algorithm is a key issue, and for pulses with sufficiently low complexity (small time-bandwidth product), it is fairly reliable. Figure 4.9(b) depicts the convergence properties of the algorithm with a Venn diagram, showing that there are essentially two constraints that need to be fulfilled. The guess for the pulse properties is projected onto each of them so that the updated guess approaches the real pulse. The intersection between the two constraints contains the desired result, but it may also contain pulse shapes that do not correspond to the pulse we want to measure. The area under the intersection depends on the experimental details, such as the complexity of the pulse, resolution in time and frequency, as well as alignment errors. When there is no experimental error and the pulse has a low time-bandwidth product, the intersection shrinks so that it contains essentially only the desired result.

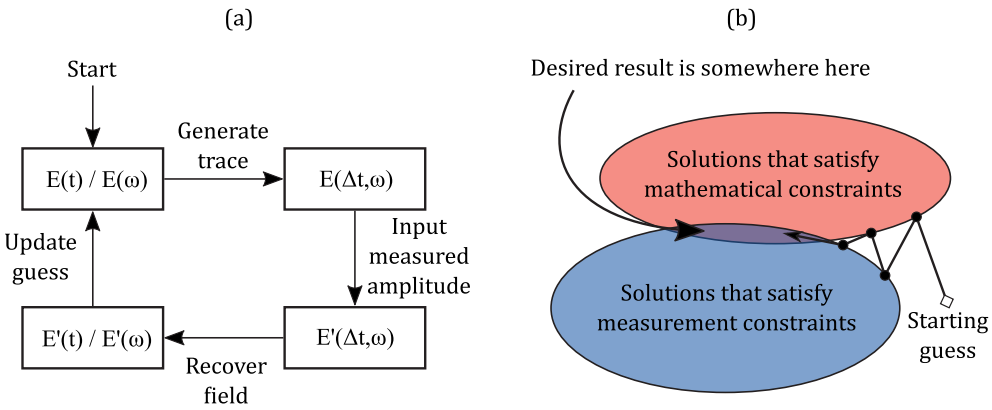

Figure 4.9: FROG retrieval procedure. (a) Flow chart of the basic process, and (b) diagram of the convergence properties.

One should use a FROG to measure pulses in a single-shot manner, and then construct the correlation functions from a large set of measured data. For high repetition rate lasers this is not always possible, and the ensemble averaged interferogram is then measured. If the train of pulses is completely coherent, the trace remains unchanged, since it is the same for all pulses. On the other hand, if the pulse train is partially coherent, the FROG trace becomes damped and it no longer corresponds to a unique pulse. Even in this case it is possible to develop a retrieval algorithm, which estimates the average pulse and the coherence properties of the pulse train [177].

Pulses generated by realistic sources often do not behave as nicely as we would like, and experimental inaccuracies are always present, causing the basic algorithm to fail. By including an additional constraint to the data, it is possible to improve the speed and reliability of the algorithm by several orders of magnitude. The simplest possible constraint one can measure in addition to the interferogram, is the power spectrum. It is straightforward to implement the measured spectrum into the improved algorithm, since it can be used to update the guess for the pulse. This leads to situation where all of the guesses are within the additional constraint data, otherwise the algorithm works exactly as before. A depiction of the improved algorithm and its convergence properties are given in Fig. 4.10 below, where the additional data constraints are marked with green.

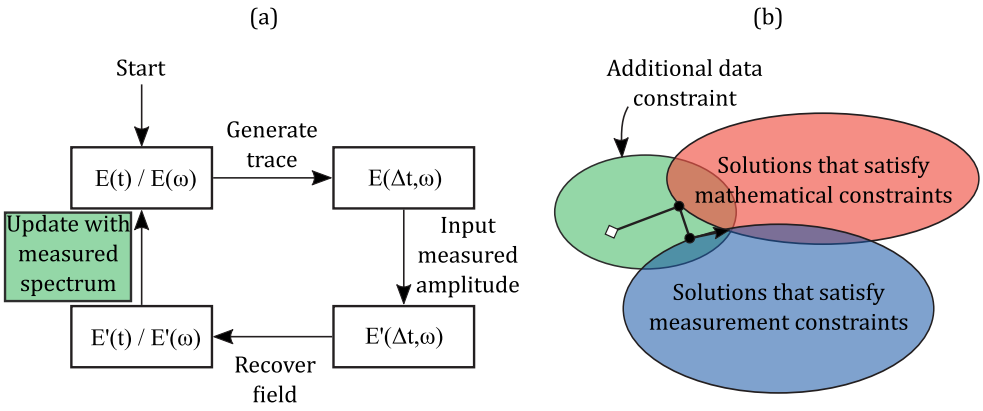

Figure 4.10: Same as Fig. 4.9, but for the improved algorithm. Here the green parts indicate additional constraints.

Ideally, the spectral density should be measured with the best attainable resolution, since some variations of FROG may struggle with spectral resolving power and thus the interferogram does not contain the best estimate for the spectral power distribution. Employing the improved algorithm allows for the retrieval of very complex pulses, and a simulated example of this can be found in Fig. 4.11. In this example, we have used the measured spectrum of a real titanium-doped sapphire laser, which was modulated with a complex spectral phase. Afterwards, the resulting interferogram was computed and 3 % of normally distributed additive noise was included to the interferogram. The noisy trace was used as the measured data and the improved algorithm was utilized to retrieve the temporal and spectral pulse properties.

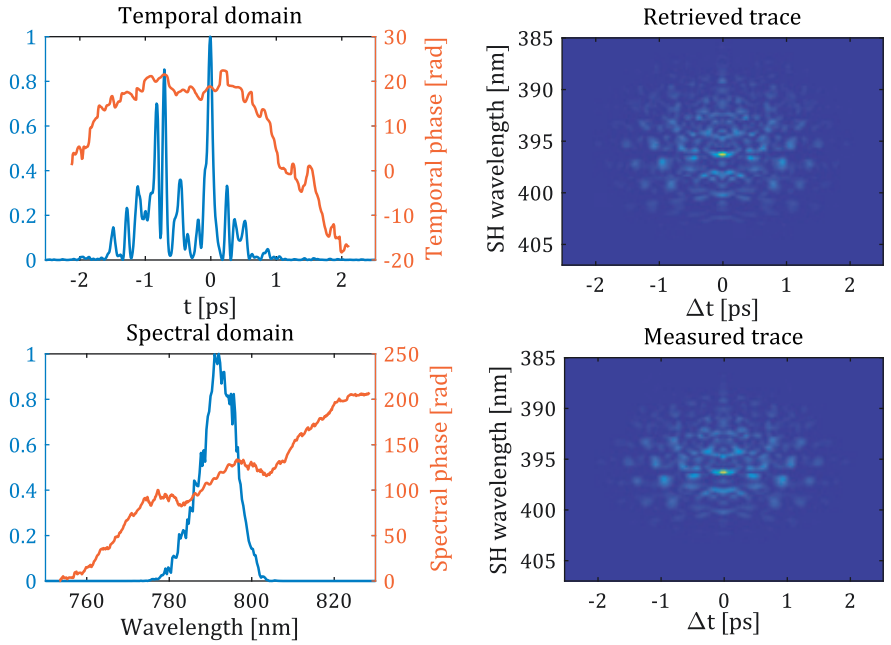

Figure 4.11: Simulated retrieval of a complex pulse. On the left are the retrieved temporal and spectral properties of the pulse and on the right the retrieved trace and the (simulated) measured FROG interferogram. The number of iterations is 37 and the rms error between the FROG traces is 0.0049, indicating a good convergence.

The retrieval was set to end automatically after the root-mean-square difference between the measured and retrieved traces was less than 0.5 %, which we quantified with

$$G^{(k)} = \sqrt{\frac{1}{N^2}\sum_{i,j=1}^{N}\left|I_{SHG}(\Delta t_i,\omega_j) - I_{SHG,k}(\Delta t_i,\omega_j)\right|^2}. \tag{4.54}$$

Here the summation stretches over the whole extent of the discretized time and frequency coordinates $(\Delta t_i, \omega_j)$, and the measured trace I_{SHG} is normalized to the same intensity as the k-th iteration of the retrieved trace $I_{SHG,k}$. The grid size for the interferogram was 512×512 pixels and the iteration started from a flat spectral phase. The improved algorithm converged to the correct result in 37 iteration cycles, whereas the original algorithm would not converge within any reasonable computation time. It is also notable that the employed power spectrum is relatively narrow, though it can support down to 120 fs FWHM pulses. The FROG trace is therefore narrow along the frequency axis with respect to its width along the time delay axis, which makes the pulse retrieval more challenging. Additionally, this example includes only phase changes, and even more complex pulses can be generated with spectral amplitude modulation.

5 Generation of model fields

As we have demonstrated, there exists a multitude of different types of partially coherent fields. They can be theoretically and numerically described, and it is possible to measure their properties. In fact, all of the properties of light are intimately tied to its coherence properties, and as such, coherence affects every aspect of light. Its propagation, measurement, imaging, and even the way it interacts with matter are all dictated by correlations. Due to this, partially coherent light has properties that cannot be reproduced with completely coherent light, and to access the benefits of partially correlated fields, we have to find ways to produce them.

It is sometimes said that coherence is a manifestation of determinism, that is, a completely coherent field is completely deterministic, whereas an incoherent field is not. However, it is simple to show that the inverse is not necessarily true, which can be seen already from the genuine representation discussed in section 2.2.2, or from the coherent mode representation. Choosing a deterministic kernel and weight function will lead to a deterministic field no matter what its coherence properties may be. Partial coherence is merely an indication that we do not know everything about the field, and whether we can know everything depends on determinism. If a partially coherent field would have to be partially deterministic, then we would have no way of generating those fields at will, since everything an experimenter does is always completely deterministic.

5.1 PARTIAL TEMPORAL COHERENCE

There exists several theoretical studies investigating the peculiar properties of temporal correlation-induced effects [100–102,178–180]. However, there are very few experimental works on the subject, due to the absence of suitable modulation schemes and the relatively new theoretical framework. While in the stationary case, the only way to control temporal coherence is to change the spectral power density, for non-stationary fields we can also engineer the spectral phase. This gives us an extra degree of freedom to produce partially coherent pulse trains, which we considered in paper **XI**. Some earlier schemes that allow control over temporal coherence do exist [181,182], but they are light inefficient and can be applied only in special cases.

It is also of interest to consider the repetition rate of the incident pulse train in comparison to the speed of possible modulation. It might seem that to produce truly partially coherent trains, one would need to modulate single pulses, which is not realistic when the repetition rate of the laser is high. However, it needs to be pointed out that the correlation functions of Eqs. (2.9) and (2.10) are defined an ensemble averages over the whole train of pulses. For truly partially correlated fields, the pulses contain no information on other realizations, and therefore their order does not matter. Thus, there are no limits on the modulation speed if the ensemble average is extended over all pulses in the train.

Generation of partially coherent pulse trains from a completely coherent one is a topic of considerable interest. Similarly, it would be highly desirable if the inverse was also possible, so that there would be some plausible way to increase the degree

of temporal coherence. In fact, there are ways to address this issue, as we outlined in paper **XII**, via temporal coherence filtering. We will show that these methods can be further expanded upon and their properties can be applied to stabilize pulses with very large bandwidths.

5.1.1 Time dependent spectral phase modulation

Spectral phase modulation can be realized with a multitude of different ways, such as spatial light modulators (SLM), acousto-optic deflectors (AOD), or deformable mirrors, to name a few. Each method has its pros and cons, but they all can be used to achieve the same thing: control over the pulse coherence properties. The principle of a coherence control setup is illustrated in Fig. 5.1. The devices we consider are essentially pulse shapers; if a pulse shaper is driven with a time varying signal, then the output produces time varying temporal profiles, and thus, temporal coherence is reduced. But the interesting feature in such devices is that the experimenter has complete control over the coherence properties and can produce almost any genuine correlation. In Fig. 5.1, the input field is dispersed by grating G_1 into its Fourier spectrum at the plane of the modulator, which imposes a spectral phase on the pulse train according to some time-dependent signal. The spectral components are subsequently recombined into a collimated output beam by lens L_2 and grating G_2.

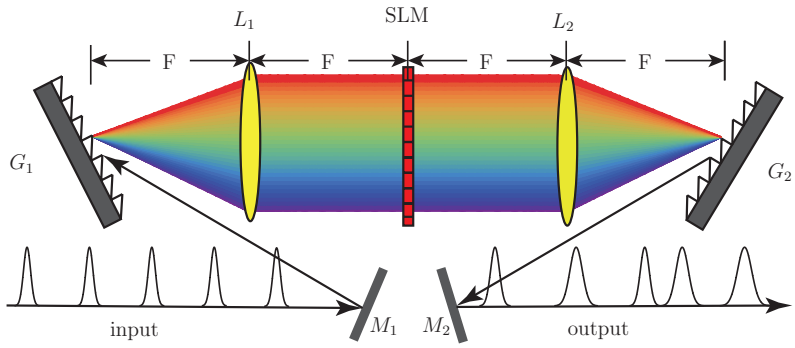

Figure 5.1: Passage of a pulsed beam through a pulse shaper. Here G_1 and G_2 are identical gratings, and L_1 and L_2 are achromatic lenses (from paper **XI**).

Phase modulation may be described with a complex spectral transmission function $t(\omega) = \exp[i\phi(\omega)]$, where the phase configuration $\phi(\omega)$ is suitably varied as a function of time. When a completely coherent incident pulse train is modulated, the output pulses have spectral representations $E_j(\omega) = t_j(\omega)E_0(\omega)$, where $t_j(\omega)$ can vary. The CSD function can then be written as

$$\begin{aligned} W(\omega_1,\omega_2) &= \langle E^*(\omega_1)E(\omega_2)\rangle \\ &= E_0^*(\omega_1)E_0(\omega_2)\langle \exp\{i[\phi(\omega_2)-\phi(\omega_1)]\}\rangle, \end{aligned} \tag{5.1}$$

where the final form naturally follows from the assumption that the input pulse train is fully coherent. If one can control the spectral phase $\phi(\omega)$, then it is simple to modulate coherence and attain a wide variety of different kinds of pulse trains. In particular, we can choose a linear phase profile $\phi(\omega) = \omega\tau$, where τ is a controlled

pseudorandom variable. The values of τ are weighted by a real, positive function $P(\tau)$ such that

$$\langle \exp(i\Delta\omega\tau)\rangle_\tau = \int_{-\infty}^{\infty} P(\tau)\exp(i\Delta\omega\tau)\mathrm{d}\tau, \tag{5.2}$$

where the subscript τ indicates averaging over all values of τ and $\int_{-\infty}^{\infty} P(\tau)\mathrm{d}\tau = 1$. In practice, the weight function $P(\tau)$ is a probability distribution and it is experimentally implemented by allocating each value of τ a time fraction proportional to $P(\tau)$. Inserting from (5.2) into (5.1) we obtain

$$W(\omega_1,\omega_2) = E_0^*(\omega_1)E_0(\omega_2)\int_{-\infty}^{\infty} P(\tau)\exp\left(i\Delta\omega\tau\right)\mathrm{d}\tau, \tag{5.3}$$

which is a Schell-model type correlation function. Since the spectral correlation function is essentially a product of the coherent input and modulation, then the MCF has to be of the form

$$\Gamma(t_1,t_2) = \int_{-\infty}^{\infty} P(\tau)E_0^*(t_1-\tau)E_0(t_2-\tau)\mathrm{d}\tau, \tag{5.4}$$

in accordance with the convolution theorem. The mean temporal intensity distribution of the pulse train is simply given by

$$I(t) = \int_{-\infty}^{\infty} P(\tau)I_0(t-\tau)\mathrm{d}\tau, \tag{5.5}$$

where $I_0(t)$ is the temporal intensity profile of the incident pulses. Now it is rather simple to control the coherence properties of the pulse train, just by changing the relative width of $P(\tau)$: if it is narrow compared to $I_0(t)$, the pulse train is quasi-coherent, and in the opposite limit the pulse train is quasi-stationary. The above formulation has a simple physical interpretation, since linear spectral phase corresponds to a shift in the temporal domain. Changing the spectral phase converts a strictly periodic input pulse train into a temporally jittered one, where the pulse arrival time varies according to the chosen weight function $P(\tau)$.

In addition to linear phase profiles it is possible to have higher order phase terms as well, which lead to further extensions of the range of desired pulse trains that can be realized. With higher order modulation, the CSD will no longer be of the Schell-model type and the MCF does not obey the elementary-pulse representation of Eq. (5.4). Nevertheless, the correlation functions in the frequency and time domains are still of mathematically genuine form. For instance, we can consider a quadratic phase profile

$$\phi(\omega) = \omega^2\tau/\Omega_\mathrm{c}, \tag{5.6}$$

with Gaussian incident pulses as well as a Gaussian weight function. This leads to a nonuniformly correlated pulse train [100] with a CSD of the form

$$W(\omega_1,\omega_2) = W_0\exp\left(-\frac{\omega_1^2+\omega_2^2}{\Omega^2}\right)\exp\left[-\frac{\left(\omega_1^2-\omega_2^2\right)^2}{2\Omega_\mathrm{c}^4}\right]. \tag{5.7}$$

Any other type of spectral phase modulation would also lead to modifications of the output pulses. However, linear modulation is already sufficient to realize several known model pulse trains. As a concrete example, if both the incident pulses and the weight function are Gaussian, we obtain a GSM pulse train [65]. Other choices of $P(\tau)$ lead to different model pulse trains, such as cosine-Gaussian, multi-Gaussian, and sinc Schell-model pulse trains [101,102,180].

5.1.2 Temporal coherence filtering

In the method described above, we started from completely coherent realizations and reduced their coherence. But it is possible, in principle, to increase the coherence of sources via filtering. This is commonly done in the spatial domain by employing a pinhole as a spatial coherence filter, but temporal and spectral domain analogs exist as well [181]. One way to achieve this is by employing Fabry–Pérot interferometers, with two distinct configurations: a very short, or a very long cavity.

Let us start from the short cavity, which we discussed in paper **XII**. When a single pulse is injected into a Fabry–Pérot interferometer, multiple reflections in the cavity modify the output to an exponentially decaying train of pulses, which is depicted in Fig. 5.2. If the cavity is shorter than the pulse length, then the output pulses will overlap, and different parts of the pulse will interfere with each other. This in turn can cause a significant increase in the coherence of the pulse train.

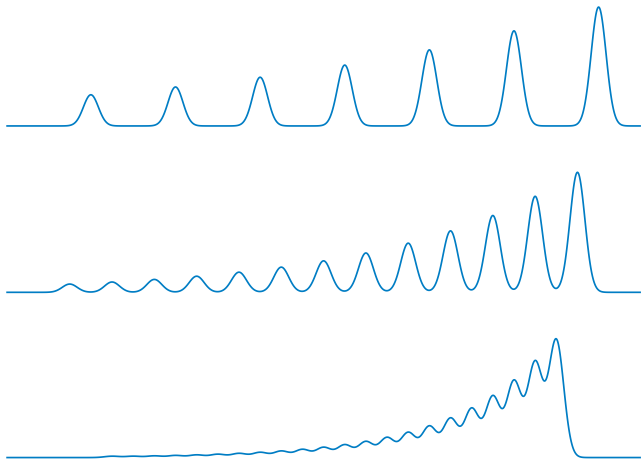

Figure 5.2: Outputs from Fabry–Pérot inteferometers of varying lengths, where the length of the cavity shrinks from up to down.

In the spectral domain, the interference between the overlapping pulses causes amplitude filtering and only a narrow part of the power spectrum is allowed to go through the device. This can be mathematically represented as

$$W(\omega_1, \omega_2) = H^*(\omega_1) H(\omega_2) W_0(\omega_1, \omega_2), \tag{5.8}$$

where $W_0(\omega_1, \omega_2)$ is the CSD of the input pulse train, and $H(\omega)$ is the spectral transmission function

$$H(\omega) = \frac{T}{1 - R \exp\left[i\rho(\omega)\right]} \tag{5.9}$$

T and $R = 1 - T$ being the transmittance and reflectance, respectively, and $\rho(\omega) = 2n(\omega) l\omega / c$ with l as the length of the cavity. Additionally, we are considering input light at normal incidence. The spectral density is then given by

$$S(\omega) = |H(\omega)|^2 S_0(\omega) \tag{5.10}$$

and the spectral degree of coherence takes on the form

$$\mu(\omega_1, \omega_2) = \frac{H^*(\omega_1)H(\omega_2)}{|H(\omega_1)||H(\omega_2)|}\mu_0(\omega_1, \omega_2), \tag{5.11}$$

indicating that a Fabry–Pérot interferometer modulates only the phase of the complex degree of spectral coherence. Using the Wiener–Khintchine theorem of Eq. (2.13), we find that the MCF is given by

$$\Gamma(t_1, t_2) = \int_{-\infty}^{t_1}\int_{-\infty}^{t_2} H^*(t_1 - t_1')H(t_2 - t_2')\Gamma_0(t_1', t_2')\mathrm{d}t_1'\mathrm{d}t_2', \tag{5.12}$$

and the upper limit in the integrals is due to causality. Although this integral does not have any general solution, it is possible to compute it for certain analytical examples, such as GSM pulses. But ultimately, the effect on coherence has to be verified with numerical models.

To this end, we employ a numerically generated supercontinuum ensemble, which closely corresponds to a real supercontinuum source [174, 183], and its properties are shown in Fig. 5.3.

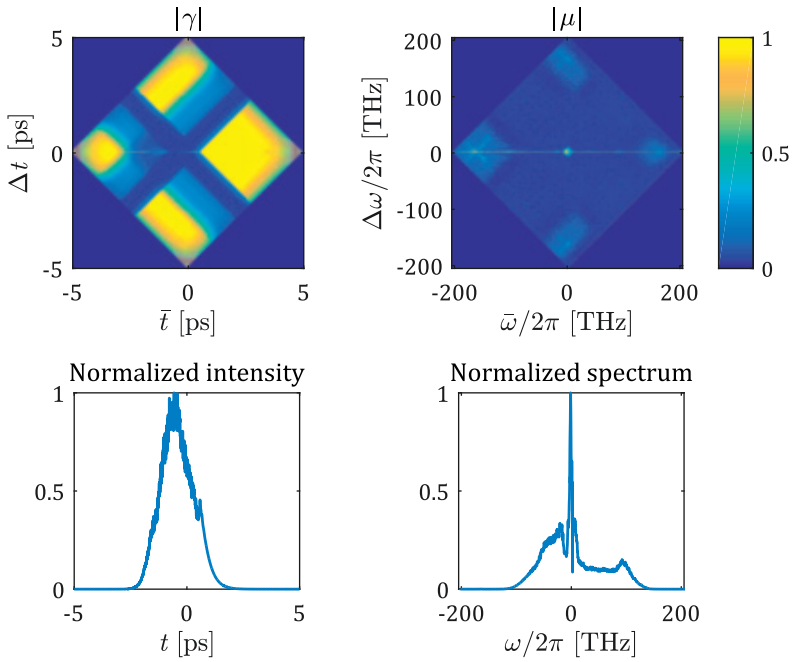

Figure 5.3: The properties of the input supercontinuum pulse train where the upper row features the correlation functions and lower row the mean temporal intensity and spectral density. The overall degree of coherence is 0.14.

The supercontinuum pulse ensemble corresponds to a situation where a pump pulse of 1 ps length and 1060 nm center frequency is injected to an anomalously dispersive photonic crystal fiber [183]. This choice results in a supercontinuum with a very low coherence, which nevertheless features a highly coherent portion in the spectral domain, centered around the pump wavelength. The overall degree of

coherence has been calculated with Eq. (2.19), and it was found to be 0.14 for this particular pulse train.

The properties of the chosen input pulse train make it a prime candidate for filtering with a very short Fabry–Pérot interferometer, since we can filter the spectrum around the most coherent part. The employed cavity has a length of 0.73 μm and mirror reflectivites of $R = 0.99$ at both ends of the cavity. Although the cavity is very short, it is at least in principle realizable with thin film stacks. As can be seen from Fig. 5.4 the gain in coherence is quite large, with an overall degree of coherence of 0.58. The simulations suggest that the coherence increases even when the spectral filtering is not centered around the most coherent portion of the spectral field, but in that case the increase in coherence is not as great.

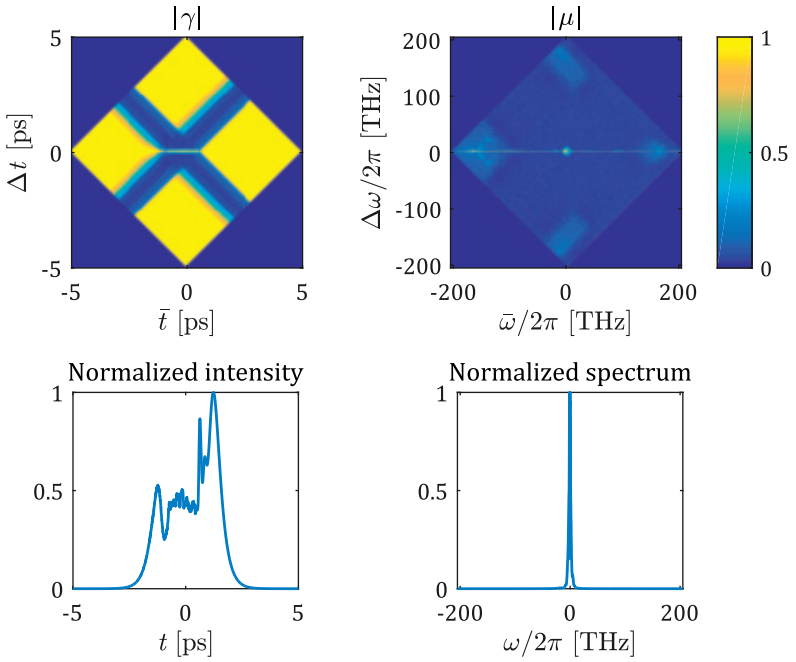

Figure 5.4: Same as Fig. 5.3, but for the output from a 0.73 μm long Fabry–Pérot interferometer. The overall degree of coherence is 0.58.

If, instead of a very short cavity, we have one where the cavity round trip time is on the order of repetition rate of the input pulse train, we get a rather different type of filtering. For very high repetition rates, a cavity like this is rather straightforward to accomplish, since a 1 GHz repetition rate laser would require just a $\sim$ 15 cm long cavity. In such a case, the intracavity field at the start of the Nth round trip is described by

$$E(t) = (1 - R) \sum_{n=0}^{N} R^{2n} E_n(t), \tag{5.13}$$

where we have assumed that the cavity round trip time is exactly equal to the pulse separation in the original pulse train. The time it takes for the pulse to traverse through the Fabry-Perót cavity can also be any multiple (or fraction) of the original

pulse separation, but in that case the cavity losses will increase due to additional reflections at the boundaries. In Fig. 5.5, we again employ the aforementioned supercontinuum ensemble, to inspect how the output field behaves. We employ similar reflectivity mirrors, and the cavity length corresponds to a single pulse separation.

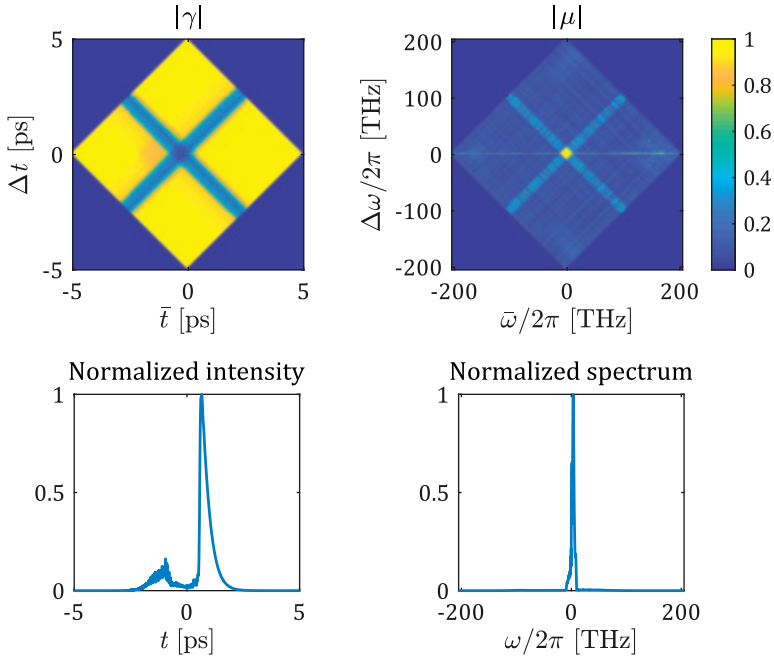

Figure 5.5: Same as Figs. 5.4, but for the output of a Fabry–Pérot interferometer with a length equal to the repetition rate. The overall degree of coherence is 0.93.

The overall degree of coherence is now 0.93, and the pulse train is nearly completely coherent. The dramatic increase in the degree of coherence has a simple physical explanation: if we inspect the limiting case, where $R^2 \to 1$, the intracavity field takes on the form

$$E(t) = \sum_{n=0}^{N} E_n(t), \tag{5.14}$$

meaning that different pulses from the original train are exactly superposed within the cavity. This leads to interference, where the parts of the pulse that remain constant from shot to shot add together and the randomly fluctuating parts average out. Therefore, it is clear that an external resonator can greatly affect the coherence of the pulse train, and it is possible to realize temporal coherence filtering.

5.2 ROTATING OPTICAL ELEMENTS

Modifying the coherence properties of electromagnetic fields can be achieved in multiple ways. Probably the most well-known case is the rotating ground glass diffuser [184–189], and even SLMs have been used to produce partial spatial coherence [190, 191]. Here, we will consider modulation methods that can produce

a wide variety of both spatial and temporal correlations: simple rotating optical elements, used to redirect beams and impose path length differences. When varied accordingly, they will produce fields with some of the properties discussed in earlier chapters. In particular, we will consider how to produce a certain kind of self-Fourier transforming beam introduced originally in paper **III**.

Although rotating optical elements provide a very simple way to produce different types of correlations, the range of possible modulations is as wide as the supply of elements. Diffusers can even have phase functions that are perfectly deterministic and ordered, but they still impose partial coherence on the incident light [192]. These elements modulate not only the spatial, but also the temporal coherence properties, and one is not confined to using only refractive optical elements. With suitable diffractive components, it would be possible to modulate also the polarization properties of incident light and get partially coherent and partially polarized beams.

5.2.1 Glass plates and wedges

Let us consider the geometries in Fig. 5.6. Here a completely coherent Gaussian beam propagates from the left towards a rotating glass plate or wedge. In the geometry of Fig. 5.6(a), the beam is deflected such that it draws a circle of radius r at the exit plane when the plate is rotated. In Fig. 5.6(b) the exit point of the principal ray is the same for all rotation angles of the wedge, but the angle with respect to the z-axis is β. In the final geometry of Fig. 5.6(c), the orientation of the wedge is reversed, producing the deflection angle β, and the beam also draws a circle of radius r at the exit plane.

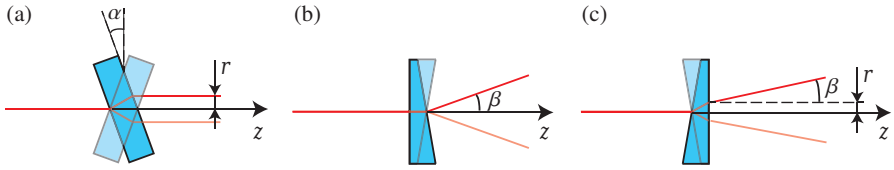

Figure 5.6: Mechanisms for producing Bessel-correlated beams. (a) Rotating glass plate tilted at an angle α, (b) rotating glass wedge with the front surface perpendicular to the propagation direction of the incident field, and (c) The same glass wedge, but with the back surface perpendicular to the propagation direction. The geometry after a 180 degree rotation is shown shaded (from paper **IV**).

For beams propagating through these optical elements it is convenient to model the spatial coherence properties of the field at the exit plane by using the shifted-elementary-beam theory [49, 193, 194], which expresses the CSD as

$$W(x_1, y_1, x_2, y_2) = \iint_{-\infty}^{\infty} p(x', y') e^*(x_1 - x', y_1 - y') e(x_2 - x', y_2 - y') \mathrm{d}x' \mathrm{d}y', \quad (5.15)$$

where $p(x', y')$ is the weight of elementary fields $e(x, y)$ centered around positions (x', y'). For brevity of notation, we drop the frequency dependence of all quantities. Starting from plane-parallel plates we take the weight function to be a delta ring of radius r,

$$p(\mathbf{r}', \phi) = \frac{1}{2\pi \mathbf{r}'} \delta(\mathbf{r}' - r), \quad (5.16)$$

where the ring radius depends on the inclination angle of the plate. Since the incident field is a Gaussian beam, the elementary field can be written in the form

$$e(x,y) = e_0 \exp\left(-\frac{x^2+y^2}{w_0^2}\right). \tag{5.17}$$

By evaluating the integral, we find that the field right after the rotating plate is

$$\begin{aligned} W(x_1,y_1,x_2,y_2) =& S_0 \exp\left(-\frac{x_1^2+x_2^2+y_1^2+y_2^2+2r^2}{w_0^2}\right) \\ &\times I_0\left[\frac{2r}{w_0^2}\sqrt{(x_1+x_2)^2+(y_1+y_2)^2}\right], \end{aligned} \tag{5.18}$$

where $S_0 = |e_0|^2$, and $I_0(x)$ denotes the modified Bessel function of the first kind and order zero. This is a type of Bessel correlated field, and it should not be confused with the propagation invariant Bessel beam. Figure 5.7 shows some measured spatial correlation functions, which were produced with a glass plate of varying tilt angles.

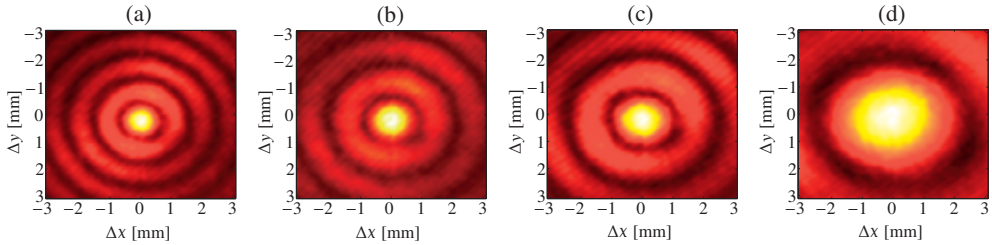

Figure 5.7: Experimentally measured Bessel correlations, produced with the geometry of Fig. 5.6(a). Tilt of the glass plate decreases to the right (from paper **IV**).

If we now turn to consider the geometry in Fig. 5.6(b), the field exiting the wedge can be modeled as before, but with a change of elementary contributions to

$$e(x,y,\phi) = e_0 \exp\left(-\frac{x^2+y^2}{w_0^2}\right) \exp\left[ik_0 \sin\beta\,(x\cos\phi + y\sin\phi)\right], \tag{5.19}$$

where ϕ is the azimuthal rotation angle of the wedge, and the weight function is the same delta function as before, except with $r = 0$. That is, all elementary field contributions arise from the same spot. Equation (5.19) describes a Gaussian beam propagating at an angle β with respect to the optical axis. If the speed of rotation is constant, all of the beams propagating towards different directions have an equal probability, and the resulting CSD is

$$W(x_1,y_1,x_2,y_2) = S_0 \exp\left(-\frac{x_1^2+x_2^2+y_1^2+y_2^2}{w_0^2}\right) J_0\left(k_0 \sin\beta\sqrt{\Delta x^2+\Delta y^2}\right), \tag{5.20}$$

which represents a Bessel-correlated Schell-model source [195–198] with a Gaussian spectral density. Additionally, we have employed the difference coordinates Δx and Δy for brevity of notation.

In the final geometry of Fig. 5.6(c), the elementary contributions are a mixture of the two earlier cases: they propagate towards angle β, and originate from a ring with radius r. The elementary contributions are therefore of the form

$$e(x,y,\phi) = e_0 \exp\left[-\frac{(x-r\cos\phi)^2+(y-r\sin\phi)^2}{w_0^2}\right] \times \exp\left\{ik_0 \sin\beta\left[(x-r\cos\phi)\cos\phi+(y-r\sin\phi)\sin\phi\right]\right\}. \quad (5.21)$$

On inserting this expression in Eq. (5.15) and integrating, we obtain

$$W(x_1,y_1,x_2,y_2) = S_0 \exp\left(-\frac{x_1^2+x_2^2+y_1^2+y_2^2+2r^2}{w_0^2}\right) J_0\left[a(x_1,y_1,x_2,y_2)\right] \quad (5.22)$$

with the auxiliary function

$$a(x_1,y_1,x_2,y_2) = \left[\left(k_0\sin\beta\,\Delta x - i\frac{4r}{w_0^2}\bar{x}\right)^2 + \left(k_0\sin\beta\,\Delta y - i\frac{4r}{w_0^2}\bar{y}\right)^2\right]^{1/2}, \quad (5.23)$$

where, again for brevity of notation, we have used the average coordinates $\bar{x}$ and $\bar{y}$. Equaiton (5.23) reveals that out of the three considered cases, this one is the most general. If we set $\beta = 0$ the expression reduces to Eq. (5.18), and on the other hand, if we set $r = 0$, we get Eq. (5.20).

5.2.2 Angular correlation properties

By inspecting the angular coherence properties of these three fields, we can gain insight to their propagation properties, and find some peculiar features. The angular correlation properties are linked to the spatial domain coherence functions via the Wiener–Khintchine theorem, as discussed in section 2.2.1. Let us consider the last geometry of Fig. 5.6 and note that the cases pertaining to Figs. 5.6(a) and 5.6(b) are special cases of this, attained by inserting either $\beta = 0$, or $r = 0$, in the final expression. The angular correlation function corresponding to Eq. (5.22) is therefore

$$T(k_{x1},k_{y1},k_{x2},k_{y2}) = T_0 \exp\left[-\frac{w_0^2}{4}\left(k_{x1}^2+k_{y1}^2+k_{x2}^2+k_{y2}^2+2k_0^2\sin^2\beta\right)\right] \times J_0\left[b(k_{x1},k_{y1},k_{x2},k_{y2})\right], \quad (5.24)$$

where $T_0 = S_0 w_0^4/16\pi^2$ and

$$b(k_{x1},k_{y1},k_{x2},k_{y2}) = \left[\left(r\Delta k_x - i2z_R\sin\beta\bar{k}_x\right)^2 + \left(r\Delta k_y - i2z_R\sin\beta\bar{k}_y\right)^2\right]^{1/2}. \quad (5.25)$$

In writing Eq. (5.25) we used the Rayleigh range $z_R = \frac{1}{2}k_0 w_0^2$, and introduced the center and difference spatial-frequency coordinates $\bar{k}_x = \frac{1}{2}(k_{x1}+k_{x2})$, $\bar{k}_y = \frac{1}{2}(k_{y1}+k_{y2})$ and $\Delta k_x = k_{x2}-k_{x1}$, $\Delta k_y = k_{y2}-k_{y1}$, respectively.

If we set $\beta = 0$ to consider the case of a rotating plane-parallel plate in Fig. 5.6(a), we find that the angular intensity takes the Gaussian form

$$T(k_{x1},k_{y1},k_{x2},k_{y2}) = T_0 \exp\left[-\frac{w_0^2}{2}\left(k_{x1}^2+k_{y1}^2+k_{x2}^2+k_{y2}^2\right)\right] J_0\left(r\sqrt{\Delta k_x^2+\Delta k_y^2}\right), \quad (5.26)$$

and the angular field produced in this case is of pure Bessel-correlated Schell-model form with a Gaussian intensity profile, which is complementary with the field produced by the rotating wedge in Fig. 5.6(b). On the other hand, setting $r = 0$ in Eq. (5.24) leads to the result

$$T(k_{x1}, k_{y1}, k_{x2}, k_{y2}) = T_0 \exp\left[-\frac{w_0^2}{4}\left(k_{x1}^2 + k_{y1}^2 + k_{x2}^2 + k_{y2}^2 + 2k_0^2 \sin^2\beta\right)\right] \times I_0\left(2z_R \sin\beta \sqrt{\bar{k}_x^2 + \bar{k}_y^2}\right), \tag{5.27}$$

which has a functional form similar to Eq. (5.18), showing that these two geometries form a Fourier tranform pair.

More importantly, the CSD defined in Eq. (5.22) has a striking resemblance with the ACF defined in Eq. (5.24). In fact, if we choose our parameters suitably, so that they fulfill the condtion

$$r = z_R \sin\beta, \tag{5.28}$$

then the correlation functions have identical functional forms in both spatial and angular domains. Fields of this type can be realized by choosing the thickness and the wedge angle in Fig. 5.6(c) appropriately, and they are an example of self-Fourier tranforming fields considered in section 3.2.

5.3 GENERATION OF CROSS-SPECTRALLY PURE FIELDS

Although cross-spectral purity is often implicitly assumed, it is difficult to identify non-trivial natural (or even man made) light fields that fulfill the conditions for cross-spectral purity in the stationary case, let alone in the nonstationary case. Trivial fields that are cross-spectrally pure include at least monochromatic fields and plane waves, although, strictly speaking these cannot be produced. In the stationary case, some efforts have been made to experimentally generate cross-spectrally pure fields [199]. Furthermore, by using achromatic Fourier transforming systems [33, 34, 200–203], it is also possible to generate cross-spectrally pure nonstationary fields from spatially incoherent sources, which we theoretically established in paper **I**.

5.3.1 Cross-spectrally pure stationary fields

Let us denote the transverse coordinates in the input and output planes of an optical system by $\boldsymbol{\rho}'$ and $\boldsymbol{\rho}$, respectively, and the impulse response of the system by $K(\boldsymbol{\rho}, \boldsymbol{\rho}'; \omega)$. Then, for stationary light, the CSD functions at the input and output planes are related by the integral expression

$$W(\boldsymbol{\rho}_1, \boldsymbol{\rho}_2; \omega) = \int_{-\infty}^{\infty} W(\boldsymbol{\rho}_1', \boldsymbol{\rho}_2'; \omega) K^*(\boldsymbol{\rho}_1, \boldsymbol{\rho}_1'; \omega) K(\boldsymbol{\rho}_2, \boldsymbol{\rho}_2'; \omega) \mathrm{d}^2\rho_1' \mathrm{d}^2\rho_2'. \tag{5.29}$$

We consider two types of systems that perform a spatial Fourier transform of the field at the input plane: conventional and achromatic Fourier processor. For a conventional Fourier transforming system that is realized with use of an achromatic lens of focal length F, the impulse response is given by

$$K(\boldsymbol{\rho}, \boldsymbol{\rho}'; \omega) = \frac{\omega}{i2\pi cF} \exp\left(-\frac{i\omega}{cF} \boldsymbol{\rho} \cdot \boldsymbol{\rho}'\right). \tag{5.30}$$

On the other hand, for an achromatic Fourier-transform system designed to operate around some wavelength $\lambda_0 = 2\pi c/\omega_0$, the impulse response is

$$K(\boldsymbol{\rho}, \boldsymbol{\rho}'; \omega) = \frac{\omega_0}{i2\pi cF} \exp\left(-\frac{i\omega_0}{cF}\boldsymbol{\rho}\cdot\boldsymbol{\rho}'\right), \tag{5.31}$$

which can be implemented in a number of ways via purely refractive or alternatively hybrid refractive-diffractive optical systems.

Let us take a field in the input plane that is spatially incoherent and which has a normalized spectrum that is independent on transverse position. Then the CSD at the input plane of the system is of the form

$$W(\boldsymbol{\rho}_1', \boldsymbol{\rho}_2'; \omega) = s(\omega) S(\boldsymbol{\rho}_1') \delta\left(\boldsymbol{\rho}'_1 - \boldsymbol{\rho}'_2\right), \tag{5.32}$$

which – according to the treatment in section 2.3 – is cross-spectrally pure, although in a somewhat trivial sense, since the field is spatially delta-correlated. If a conventional Fourier-transform system is employed, the CSD at the output plane is known to be

$$W(\boldsymbol{\rho}_1, \boldsymbol{\rho}_2; \omega) = \left(\frac{\omega}{cF}\right)^2 s(\omega) \tilde{S}\left(\frac{\omega}{cF}\Delta\boldsymbol{\rho}\right), \tag{5.33}$$

where $\Delta\boldsymbol{\rho} = \boldsymbol{\rho}_2 - \boldsymbol{\rho}_1$ and we have the Fourier-type relationship

$$\tilde{S}\left(\frac{\omega}{cF}\Delta\boldsymbol{\rho}\right) = \frac{1}{(2\pi)^2} \int_{-\infty}^{\infty} S(\boldsymbol{\rho}') \exp\left(-i\frac{\omega}{cF}\Delta\boldsymbol{\rho}\cdot\boldsymbol{\rho}'\right) \mathrm{d}^2\rho'. \tag{5.34}$$

Additionally, the complex degree of spatial coherence satisfies Wolf's scaling law, since it assumes the form [32]

$$\mu(\boldsymbol{\rho}_1, \boldsymbol{\rho}_2; \omega) = \frac{\tilde{S}\left(\omega\Delta\boldsymbol{\rho}/cF\right)}{\tilde{S}(0)}. \tag{5.35}$$

On the other hand, if instead of a conventional Fourier processor we use an achromatic Fourier transform system, the CSD at the output-plane has the form

$$W(\boldsymbol{\rho}_1, \boldsymbol{\rho}_2; \omega) = \left(\frac{\omega_0}{cF}\right)^2 s(\omega) \tilde{S}\left(\frac{\omega_0}{cF}\Delta\boldsymbol{\rho}\right), \tag{5.36}$$

which has the complex degree of coherence

$$\mu(\boldsymbol{\rho}_1, \boldsymbol{\rho}_2; \omega) = \frac{\tilde{S}\left(\omega_0\Delta\boldsymbol{\rho}/cF\right)}{\tilde{S}(0)} = \mu(\boldsymbol{\rho}_1, \boldsymbol{\rho}_2; \omega_0), \tag{5.37}$$

that is cross-spectrally pure around the time delay $\tau = \tau_0 = 0$. Hence, an achromatic Fourier-transform system provides simple means to generate cross-spectrally pure stationary fields from incoherent sources. It also seems that cross-spectrally pure fields form some type of duality relation with fields that satisfy Wolf's scaling law, which is a subject of future investigations.

5.3.2 Cross-spectrally pure nonstationary fields

Similarly to the stationary case, for nonstationary fields the relationship between the CSD functions at the input and output planes is given by

$$W(\boldsymbol{\rho}_1, \boldsymbol{\rho}_2; \omega_1, \omega_2) = \iint_{-\infty}^{\infty} W(\boldsymbol{\rho}'_1, \boldsymbol{\rho}'_2; \omega_1, \omega_2) K^*(\boldsymbol{\rho}_1, \boldsymbol{\rho}'_1; \omega_1) K(\boldsymbol{\rho}_2, \boldsymbol{\rho}'_2; \omega_2) \mathrm{d}^2\rho'_1 \mathrm{d}^2\rho'_2. \tag{5.38}$$

Let us assume that the CSD in the input plane is of the form

$$W(\mathbf{v}_1, \mathbf{v}_2; \omega_1, \omega_2) = \sqrt{s(\omega_1)s(\omega_2)}\mu(\boldsymbol{\rho}, \boldsymbol{\rho}; \omega_1, \omega_2)S(\mathbf{v}_1)\delta(\mathbf{v}_1 - \mathbf{v}_2). \tag{5.39}$$

Here again the normalized spectrum $s(\omega)$ of the field is taken to be independent of transverse position and the field is spatially incoherent. In addition to this, the spectral correlation function $\mu(\boldsymbol{\rho}, \boldsymbol{\rho}; \omega_1, \omega_2)$ is assumed to be position-independent. These assumptions hold, at least to a good approximation, if a spectrally partially coherent pulse train passes through a rotating diffuser, so that each individual pulse experiences a different roughness distribution.

The CSD at the output plane of a conventional Fourier-transform system is obtained by inserting from Eq. (5.39) into Eq. (5.38), resulting in the expression

$$\begin{aligned} W(\boldsymbol{\rho}_1, \boldsymbol{\rho}_2; \omega_1, \omega_2) = &\frac{\omega_1\omega_2}{(cF)^2}\sqrt{s(\omega_1)s(\omega_2)}\mu(\boldsymbol{\rho}, \boldsymbol{\rho}; \omega_1, \omega_2) \\ &\times \tilde{S}\left[(\omega_2\boldsymbol{\rho}_2 - \omega_1\boldsymbol{\rho}_1)/cF\right], \end{aligned} \tag{5.40}$$

which gives the complex degree of coherence

$$\mu(\boldsymbol{\rho}_1, \boldsymbol{\rho}_2; \omega_1, \omega_2) = \mu(\boldsymbol{\rho}, \boldsymbol{\rho}; \omega_1, \omega_2)\frac{\tilde{S}\left[(\omega_1\boldsymbol{\rho}_1 - \omega_2\boldsymbol{\rho}_2)/cF\right]}{\tilde{S}(0)}. \tag{5.41}$$

This result appears to be analogous to the stationary Wolf's scaling law – at least supreficially. Again, by switching to an achromatic Fourier-transform len, the CSD at the output plane becomes

$$W(\boldsymbol{\rho}_1, \boldsymbol{\rho}_2; \omega_1, \omega_2) = \left(\frac{\omega_0}{cF}\right)^2\sqrt{s(\omega_1)s(\omega_2)}\mu(\boldsymbol{\rho}, \boldsymbol{\rho}; \omega_1, \omega_2)\tilde{S}(\omega_0\Delta\boldsymbol{\rho}/cF), \tag{5.42}$$

which is of the separable form of form of Eq. (2.62) and thus cross-spectrally pure over the whole wavefront at the output plane. The normalized spectrum therefore remains equal to $s(\omega)$ at the output, and the complex degree of spectral coherence is of the form of Eq. (2.64), as in

$$\mu(\boldsymbol{\rho}_1, \boldsymbol{\rho}_2; \omega, \omega) = \frac{\tilde{S}(\omega_0\Delta\boldsymbol{\rho}/cF)}{\tilde{S}(0)}. \tag{5.43}$$

Starting from a spatially incoherent source, one can produce cross-spectrally pure field with relatively simple Fourier transforming systems. The generation of such fields is of interest whenever the spatial and temporal characteristics of light have to be separated, which is possible only when the field is cross-spectrally pure over the whole wavefront.

6 Conclusions

This thesis contains results from several theoretical and experimental works on nonstationary fields. Starting from the very basic notions of pulsed fields, the general form of correlation functions, their possible transformations, as well as their representation were discussed. The mathematical properties of the two-coordinate correlation functions were compared to the single coordinate case, and special attention was paid to fields which are cross-spectrally pure (paper **I**). Afterwards, the spatiotemporal properties of pulses were investigated in the case of stable laser cavities, where it was established that only very short pulses feature strong spatiotemporal coupling effects (paper **II**). Several spatial and temporal partially coherent models were investigated, some of which were known before hand (papers **III–VI**), while others are new. Then, the measurement of nonstationary light was considered in spatial, spectral and temporal domains (papers **VII–X**), and novel results were found in SPIDER and FROG measurement modalities. Finally, it was investigated how fields such as the ones discussed before could be generated (papers **XI** and **XII**), and some interesting new results on cross-spectral purity were found. Detailed accounts of the main findings and possible future prospects are given below.

6.1 SUMMARY OF THE MAIN RESULTS

Paper **I** examines the concept of cross-spectral purity in the context of nonstationary fields. In the stationary case, the defining property of cross-spectrally pure fields is that the normalized spectral density of the field is constant at two points accross the wavefront, as well as in their superposition. Light that fulfills this condition also obeys the reduction formula, which states that the spatial and temporal degrees of coherence are separable. In research of pulsed light, a condition similar to the reduction formula is often implicitly assumed, and the correlation function is written as a product of contributions from two distinct domains. We showed that for nonstationary fields the condition for cross-spectral purity is actually more stringent, requiring that not only the spectral density but also the cross-spectral density remains invariant at the three investigated points. Additionally, we showed that cross-spectral purity is retained upon propagation only when the field is quasi-monochromatic, and thus it is not preserved for pulsed fields. The study concludes with an investigation of methods that allow the production of cross-spectrally pure fields from spatially incoherent sources.

In paper **II**, we model the behavior of realistic pulsed beams, produced in stable laser cavities which support several frequency dependent modes. Such resonators generate fields that are partially coherent, as well as spatiotemporally coupled, and thus not cross-spectrally pure. By employing the coherent mode superposition, we found an analytical expression for the field at the initial plane in the space-frequency domain. The field was propagated to an arbitrary plane and transformed to the space-time domain, in order to inspect the spatiotemporal coupling phenomena. It was shown that these effects become most prominent below the few-cycle regime and away from the optical axis of the pulsed beam, whereas the axial field

remains completely coherent. Furthermore, we found that the spatiotemporal coupling mixes the coherence properties between space and time. In other words, although it was assumed that all of the frequencies are completely correlated, partial spatial coherence decreased the degree of coherence also in the time domain. Additionally, the two domains have an inverse relationship, since temporal domain coherence decreased with stronger coupling, while spatial coherence increased. These results give some clarity to when it is justified to assume cross-spectral purity and write the correlation functions in a separable form, and what are the possible spatiotemporal effects in coupled fields.

The experiments outlined in paper **III** were designed to measure some of the coherence properties of supercontinuum light generated in bulk media. The medium in this case was a plate of fused silica, which was pumped with femtosecond pulses to obtain a supercontinuum. The bulk generated supercontinuum was found to be almost completely spatially coherent, in contrast to some earlier investigations. One of the problems in these experiments was that the fused silica plate deteriorated rather quickly from being exposed to such intense pulses. To overcome this problem, we decided to place the plate into a rotating holder, which increased the lifetime of the bulk medium sufficiently. We also found that rotating the plate produced an unexpected modulation, and Bessel-type rings were observed in the spatial coherence function. We promptly identified that the physical situation mathematically corresponds to a shifted elementary beam theory, and we investigated the properties of fields generated by rotating glass slabs, as well as wedges. The modulation scheme introduced in this work is exceedingly simple, yet a very powerful tool to produce Bessel-correlated fields. In the process we also found a new class of fields that could retain their mathematical forms in Fourier-transformations, and dubbed them self-Fourier transforming beams.

This new class of fields demanded closer examination, which we carried out in paper **IV**. The work concentrated on the analysis of a specific self-Fourier transforming beam, namely the Bessel-correlated beam produced with a suitable glass wedge. It was found that the whole correlation function is invariant in the near- and far fields, but at intermediate distances the spatial intensity distribution may change, although the normalized degree of coherence remains unchanged. It is, as of now, still unclear whether this is a common feature of all self-Fourier transforming beams. In addition to theoretically deriving the propagation formulas, we carried out experiments which confirmed our results. In this thesis, the expressions for self-Fourier transforming beams were studied further and a coherent mode superposition model was derived for them. With this model, it is possible produce self-Fourier transforming beams at will, and it is not necessary to try to find mathematical functions which innately have this property. It remains to be seen what are the most general properties of this class of beams, and what are their potential applications.

Paper **V** theoretically investigated the propagation properties of a circularly correlated beam. These fields exhibit complete coherence along any circle that is concentric with the source center, whereas at different distances, the degree of coherence can attain a large variety of values. We found that this type of field is specular and self focusing, similarly to the more well-known nonuniformly correlated fields. The circularly correlated beam was then numerically propagated through free-space, as well as in oceanic turbulence, where it was found that highly turbulent media could disturb the self-focusing properties. Within this thesis, the correlation-induced focusing was analyzed further, and it was found that the focal point can be engineered

widely by employing different types of spatial correlation functions. Beams which focused multiple times upon propagation or produced an elongated focal spot were used as rudimentary examples of specifically engineered focal spots. Furthemore, it was established that by choosing the correlation properties of the field appropriately, it is possible to freely design the intensity distribution in three dimensional space. Temporal domain self-focusing was not investigated, although on grounds of space-time duality, such effects are also possible.

Correspondingly, in paper **VI**, we introduced some model fields which exhibit temporal self-splitting upon propagation through linear, normally dispersive media, such as an optical fiber. These fields were the Laguerre-Gaussian correlated Schell-model (LGCSM) and Hermite-Gaussian correlated Schell-model (HGCSM) beams, which we derived via a genuine representation approach. We then propagated the model fields, and presented a definition of the temporal far field, which bears a strong similarity to the condition for spatial far field. The model pulses were found to self-split, where the order n of the correlation function plays a vital role: for LGCSM pulses, the field evolves to $n+1$ sub pulses, whereas HGCSM pulses always split into two, but their temporal separation increases with increasing n. Afterwards, we offered an interpretation of this behavior and found that the temporal pulse assumes the form of its power spectrum in the temporal far field, which is analogous to the spatial case.

Paper **VII** introduced a novel method for measuring the two-coordinate spatial coherence properties of arbitrary fields, the grating interferometer. This device works by first dividing the beam in two and then recombining them at some observation plane. In the first iteration of this method we kept the two gratings stationary, and moved the detector in a z-scanning fashion. The greatest advantage of this interferometer is that it measures a whole slice of the spatial coherence function at every value of lateral shear. It also features zero time delay between the recombined beams, and thus it measures only spatial properties of the input light. However, we found that the device produces an interference pattern which has a spectrally varying footprint, that is, each frequency generates a fringe pattern with a different size. Because of this, the device can be used for the measurement of quasi-monochromatic sources as is, and for wide-bandwidth fields an imaging spectrograph is required. The device was demonstrated with several light sources: Gaussian- and Bessel-correlated fields, a broad-area laser diode, an RGB-laser, a white LED and a halogen lamp. In all of these cases, the measured values were compared to ones attained with a Young's interferometer. It was found that the grating interferometer measured the spatial coherence correctly.

In paper **VIII**, the grating interferometer was employed to measure the spatial coherence of an exotic pulsed light source, the wood laser. The wood laser is a relatively novel source, which substitutes the laser cavity for hollow wood fibers, made possible by the realization of transparent wood. The transparent wood is doped with a laser dye and when it is pumped strongly enough, the wood sample will lase. Since the fibers have a partial degree of order, we called this source type a quasi-random laser. During this work, several improvements to the grating interferometer were implemented. Most notably, we decided to change the z-scanning method, from moving the camera to scanning the gratings. The distance between the gratings was kept constant and they were moved in conjunction along the z-direction. This allows for very simple alignment, where the experimenter simply puts the detector in front of the light to be measured (focusing or collimating when necessary) and then places the two gratings between the source and the detector.

Scanning the gratings in the z-direction produces a lateral shear at the detection plane, while keeping the optical path length constant at all measurement points.

Further understanding of the grating interferometer gave insight to an extension on the wavefront folding interferometer (WFI), which was introduced in paper **IX**. The WFI is a popular device for measuring spatial coherence properties. In its traditional form, the device can only measure Schell-model sources. However, just by scanning the beam at the input of the WFI, it is possible to find the complete two-coordinate spatial coherence function. Additionally, we introduced several new WFI designs, where the planar mirror variation shows most promise. This variation is almost polarization insensitive, features no optical obstructions, and it can be generalized to measuring the full three-dimensional coherence function. We employed this device to measure the spatial coherence of a partially polarized multimode helium-neon laser, and a polarized multimode diode laser, both of which agreed well with results from a Young's interferometer. It was also notable that the modified WFI has very high data acquisition speed, since the measurement time scales linearly, whereas for the Young's interferometer it scales quadratically with the number of measurement points. Thus, it was established that a WFI can measure spatial coherence functions with a high resolution, while keeping the measurement time relatively short.

The work in paper **X** considered the temporal coherence properties of nonstationary fields, and what can be measured with relatively simple interferometric experiments. First, it was shown that a field autocorrelation contains information only on the power spectrum of the source, which is caused by time integration at the detector. Then, a recently introduced experimental scheme was evaluated in this context, and it was found that it can detect a decrease in coherence. Further, we introduced an interferometric cross-correlation scheme, which can be used to find the quasi-coherent part of the spectrum. The theoretical expressions were evaluated by characterizing numerically generated supercontinuum and free-electron laser pulses. These two sources were shown to feature very distinct properties, though both of them could be probed with the novel cross-correlation measurement.

We also introduced a method for generating partial temporal coherence in paper **XI**. The method consists of a pulse shaper which is driven with a time varying signal. With this approach, it is possible to take a completely coherent pulse train, and modulate it so that it becomes partially coherent. We also considered the speed at which modulation needs to take place, and it was concluded that since the correlation functions are taken as an ensemble average over the whole train of pulses, it does not matter what the modulation speed is, as long as all of the pulses are accounted for. It was found that this method can be used to produce a large amount of different types of temporally partially coherent pulse trains. Experimental demonstration of the device is under way, and during the preparation I found that measurement methods available to us are not sufficient for retrieving complex pulses. This sparked the development of an improved FROG retrieval algorithm, which was introduced in this thesis. It constitutes a large improvement in the speed, convergence and applicability over the basic algorithm, and it will be demonstrated in the future. While researching other pulse measurement devices, I also happened to realize that the SPIDER can be used to measure the whole spectral correlation function, which has not been examined before. The basic mathematical framework was drafted in this thesis, and a more detailed study is warranted.

Finally, in paper **XII**, we showed that it is possible to increase the temporal and spectral coherence of pulse trains, with simple Fabry–Pérot type devices. The vari-

ation that was covered in this publication is an inteferometer with a short cavity, so that the output pulses temporally overlap with each other. This leads to interference between different parts of the pulse, thus filtering the power spectrum and increasing the coherence of the output pulse train. We numerically demonstrated this effect with a Gaussian Schell-model pulse train, and a realistic supercontinuum ensemble. For very large bandwidth pulses, it may be difficult to produce small enough cavities to achieve this filtering effect, but it should be relatively straightforward with nanosecond pulses. The last novel result in this thesis is the extension of the Fabry–Pérot interferometer to long cavities. When the cavity length is equal to the pulse repetition rate, the incident pulses are superposed within the resonator. This causes the randomly varying parts of the pulses to average out, while the constant components remain. Numerical simulations support this conclusion and a nearly incoherent supercontinuum pulse train was converted to an almost completely coherent one.

6.2 FUTURE PROSPECTS

There are several exciting avenues for future studies. The research covered in this thesis ranges over a wide variety of topics in nonstationary coherence, and their continuation holds great potential. First of all, the use of SPIDER for spectral coherence measurements has to be investigated in detail. The theoretical framework given here shows that at the very least, pulses that are much longer than a single optical cycle can be characterized; what happens for shorter pulses warrants more investigation. Additionally, the experimental implementation will have to be rethought entirely, in order to realize spectral shearing over the whole power spectrum. Once these issues have been tackled, an experimental demonstration of the device has to be carried out. If there are no large obstacles, it is conceivable that the modified SPIDER apparatus will become the gold standard for measuring the spectral coherence properties of pulsed light sources. Comparative measurements could be carried out with the field cross-correlation setup, or single-shot FROG.

Additionally, the idea of increasing temporal coherence of pulse trains is highly appealing. The Fabry-Pérot interferometers discussed here – especially the long variations – could be used to produce ultra stable pulsed light beams. Highly coherent pulse trains have a large variety of uses ranging from metrology to material processing, but the applicability of this scheme needs to be investigated very closely. An experimental realization of these devices would be at least as important as the SPIDER demonstration discussed above. Additionally, the pulse shaper setup for controlling temporal coherence has to be demonstrated in the near future. The setup could be used to characterize the coherence filtering effect of the long Fabry-Pérot interferometer. In the context of temporal coherence control experiments it will also be important to demonstrate the retrieval of very complex pulses from an experimentally measured FROG trace.

Experimental demonstrations are also required in the spatial domain. The various spatial coherence measurement schemes will be employed to characterize a wide variety of light fields, with the WFI having the most attention. This is due to its unparalleled properties, such as measuring the complete coherence function in three dimensions with great resolution and speed, while retaining high light efficiency. Furthermore, it is nearly polarization insensitive and has no obstructions in the mirror configuration. Thus, it can be used to produce specular and anti-

specular fields, which may have interesting properties. Examining lensless imaging is also a compelling avenue, which we have in fact already demonstrated with a WFI setup, and additional experiments are under way. The arsenal of coherence modulation schemes should also be expanded upon. To this end, we intend to examine several schemes where different types of optical elements are rotated in front of a light source. At the moment we are studying the spatiotemporal effects of rotating 3D printed diffusers. These optical elements are rather unique, since they are fabricated with a high precision 3D printer, and we can control the distribution of surface roughness at will. As long as the surface follows some real probability function, it is possible to fabricate such a diffuser. In addition to diffusive elements, we can consider rotating diffractive components, which give another degree of freedom in the design of coherence functions.

Apart from experimental demonstrations, it will also be of interest to theoretically investigate some properties of nonstationary fields. For example, when we considered the generation of cross-spectrally pure fields, it would appear that light which satisfies Wolf's scaling law forms some sort of duality with cross-spectrally pure fields. This is definitely the case for stationary fields, but for nonstationary light the situation is not as clear cut. The first obstacle is that no one has established the nonstationary analogue of Wolf's scaling law. Therefore, we have already begun our investigation into this feature. It also needs to be theoretically checked what happens when the spectral coherence of spatiotemporally coupled field is partial. This is a direct extension to our work in paper **II**, which would generalize the model for a large variety of pulsed beams. Additionally, spatiotemporal coupling effects in other situations would be worth investigating. So far we have only considered laser pulses from stable cavities, but situation such as unstable laser cavities and scattering may be attractive. The properties of self-Fourier transforming fields will need to be examined more closely as well.

In conclusion, research into the coherence properties of nonstationary light is an active and fruitful area of study. It is to be expected that the work carried out in this context will become increasingly important in the future, with new technologies made possible by ever shorter and more intense pulses of light.

BIBLIOGRAPHY

[1] G. de Villiers and E. R. Pike, *The Limits of Resolution* (CRC Press, 2016).

[2] H. E. Burton, "The optics of Euclid," *J. Opt. Soc. Am.* **35**, 357–372 (1945).

[3] A. I. Sabra, *The optics of Ibn al-Haytham* (W. S. Maney and Son, 1989).

[4] A. Tbakhi and S. S. Amr, "Ibn Al-Haytham: father of modern optics," *Ann. Saudi Med.* **27**, 464–467 (2007).

[5] J. Al-Khalili, "In retrospect: Book of Optics," *Nature* **518**, 164 (2015).

[6] M. Born and E. Wolf, *Principles of Optics: Electromagnetic Theory of Propagation, Interference and Diffraction of Light*, 7 ed. (Cambridge University Press, 1999).

[7] A. L. Schawlow and C. H. Townes, "Infrared and optical masers," *Phys. Rev.* **112**, 1940–1949 (1958).

[8] I. A. Walmsley and C. Dorrer, "Characterization of ultrashort electromagnetic pulses," *Adv. Opt. Photon.* **1**, 308–437 (2009).

[9] C. Manzoni, O. D. Mücke, G. Cirmi, S. Fang, J. Moses, S.-W. Huang, K.-H. Hong, G. Cerullo, and F. X. Kärtner, "Coherent pulse synthesis: towards sub-cycle optical waveforms," *Laser Photonics Rev.* **9**, 129–171 (2015).

[10] Y. Kida, R. Kinjo, and T. Tanaka, "Synthesizing high-order harmonics to generate a sub-cycle pulse in free-electron lasers," *Appl. Phys. Lett.* **109**, 151107 (2016).

[11] H. Liang, P. Krogen, Z. Wang, H. Park, T. Kroh, K. Zawilski, P. Schunemann, J. Moses, L. F. DiMauro, F. X. Kärtner, and K.-H. Hong, "High-energy mid-infrared sub-cycle pulse synthesis from a parametric amplifier," *Nat. Commun.* **8**, 141 (2017).

[12] A. V. Pakhomov, R. M. Arkhipov, M. V. Arkhipov, I. Babushkin, and N. N. Rosanov, "On the generation of extremely short light pulses in effectively one-dimensional schemes," *Optics and Spectroscopy* **123**, 913–917 (2017).

[13] R. M. Arkhipov, M. V. Arkhipov, A. V. Pakhomov, I. Babushkin, and N. N. Rosanov, "Collisions of unipolar subcycle pulses in a nonlinear resonantly absorbing medium," *Opt. Spectrosc.* **123**, 610–614 (2017).

[14] R. M. Arkhipov and N. N. Rosanov, "On the splitting of a subcycle pulse upon its coherent propagation in a resonant medium," *Opt. Spectrosc.* **124**, 726–729 (2018).

[15] R. M. Arkhipov, M. V. Arkhipov, I. Babushkin, A. V. Pakhomov, and N. N. Rosanov, "Propagation of a light pulse with a duration of less than one period in a resonant amplifying medium," *Quantum Electron.* **48**, 532–536 (2018).

[16] R. Trebino, *Frequency-Resolved Optical Gating: The Measurement of Ultrashort Laser Pulses* (Kluwer Academic Publishers, 2000).

[17] C. Iaconis and I. A. Walmsley, "Spectral phase interferometry for direct electric-field reconstruction of ultrashort optical pulses," *Opt. Lett.* **23**, 792–794 (1998).

[18] A. Zewail, "Laser femtochemistry," *Science* **242**, 1645–1653 (1988).

[19] A. Zewail, "Femtochemistry: atomic-scale dynamics of the chemical bond," *J. Phys. Chem. A* **104**, 5660–5694 (2000).

[20] A. Zewail, "Femtochemistry. Past, present, and future.," *Pure Appl. Chem.* 2219–2231 (2000).

[21] T. Udem, J. Reichert, R. Holzwarth, and T. W. Hänsch, "Accurate measurement of large optical frequency differences with a mode-locked laser," *Opt. Lett.* **24**, 881–883 (1999).

[22] T. Udem, J. Reichert, R. Holzwarth, and T. W. Hänsch, "Absolute optical frequency measurement of the cesium D_1 line with a mode-locked laser," *Phys. Rev. Lett.* **82**, 3568–3571 (1999).

[23] T. Udem, R. Holzwarth, and T. W. Hänsch, "Optical frequency metrology," *Nature* **416**, 233–237 (2002).

[24] N. R. Newbury and W. C. Swann, "Low-noise fiber-laser frequency combs," *J. Opt. Soc. Am. B* **24**, 1756–1770 (2007).

[25] S. Koke, C. Grebing, H. Frei, A. Anderson, A. Assion, and G. Steinmeyer, "Direct frequency comb synthesis with arbitrary offset and shot-noise-limited phase noise," *Nat. Photonics* **4**, 462–465 (2010).

[26] G. Villares, A. Hugi, S. Blaser, and J. Faist, "Dual-comb spectroscopy based on quantum-cascade-laser frequency combs," *Nat. Commun.* **5**, 5192 (2014).

[27] J. L. Hall, "Nobel Lecture: Defining and measuring optical frequencies," *Rev. Mod. Phys.* **78**, 1279–1295 (2006).

[28] X. Liu, D. Du, and G. Mourou, "Laser ablation and micromachining with ultrashort laser pulses," *IEEE J. Quantum Electron.* **33**, 1706–1716 (1997).

[29] A. M. Morales and C. M. Lieber, "A laser ablation method for the synthesis of crystalline semiconductor nanowires," *Science* **279**, 208–211 (1998).

[30] Y. Shimotsuma, K. Miura, and H. Kazuyuki, "Nanomodification of glass using fs laser," *Int. J. Appl. Glass Sci.* **4**, 182–191 (2013).

[31] L. Mandel and E. Wolf, *Optical Coherence and Quantum Optics* (Cambridge University Press, 1995).

[32] E. Wolf, "Invariance of the spectrum of light on propagation," *Phys. Rev. Lett.* **56**, 1370–1372 (1986).

[33] G. M. Morris and D. Faklis, "Effects of source correlation on the spectrum of light," *Opt. Commun.* **62**, 5–11 (1987).

[34] D. Faklis and G. M. Morris, "Spectral shifts produced by source correlations," *Opt. Lett.* **13**, 4–6 (1988).

[35] T. Hassinen, J. Tervo, T. Setälä, J. Turunen, and A. T. Friberg, "Spectral invariance and the scaling law with random electromagnetic fields," *Phys. Rev. A* **88**, 043804 (2013).

[36] Y. Gu and G. Gbur, "Scintillation of nonuniformly correlated beams in atmospheric turbulence," in *Frontiers in Optics* (2013), p. FW4D.2.

[37] R. Chen, L. Liu, S. Zhu, G. Wu, F. Wang, and Y. Cai, "Statistical properties of a Laguerre-Gaussian Schell-model beam in turbulent atmosphere," *Opt. Express* **22**, 1871–1883 (2014).

[38] H.-F. Xu, Z. Zhang, J. Qu, and W. Huang, "Propagation factors of cosine-Gaussian-correlated Schell-model beams in non-Kolmogorov turbulence," *Opt. Express* **22**, 22479–22489 (2014).

[39] X. Wang, M. Yao, Z. Qiu, X. Yi, and Z. Liu, "Evolution properties of Bessel-Gaussian Schell-model beams in non-Kolmogorov turbulence," *Opt. Express* **23**, 12508–12523 (2015).

[40] J. Yu, Y. Chen, L. Liu, X. Liu, and Y. Cai, "Splitting and combining properties of an elegant Hermite-Gaussian correlated Schell-model beam in Kolmogorov and non-Kolmogorov turbulence," *Opt. Express* **23**, 13467–13481 (2015).

[41] J. Wang, S. Zhu, H. Wang, Y. Cai, and Z. Li, "Second-order statistics of a radially polarized cosine-Gaussian correlated Schell-model beam in anisotropic turbulence," *Opt. Express* **24**, 11626–11639 (2016).

[42] F. Wang and O. Korotkova, "Circularly symmetric cusped random beams in free space and atmospheric turbulence," *Opt. Express* **25**, 5057–5067 (2017).

[43] J. Durnin, J. J. Miceli, and J. H. Eberly, "Diffraction-free beams," *Phys. Rev. Lett.* **58**, 1499–1501 (1987).

[44] J. Turunen, "Space-time coherence of polychromatic propagation-invariant fields," *Opt. Express* **16**, 20283–20294 (2008).

[45] K. Saastamoinen, J. Turunen, P. Vahimaa, and A. T. Friberg, "Spectrally partially coherent propagation-invariant fields," *Phys. Rev. A* **80**, 053804 (2009).

[46] J. Turunen and A. T. Friberg, "Propagation-invariant optical fields," in *Progress in Optics*, Vol. 54 (Elsevier, 2010), pp. 1–88.

[47] F. Gori and C. Palma, "Partially coherent sources which give rise to highly directional light beams," *Opt. Commun.* **27**, 185–188 (1978).

[48] F. Gori, "Collett-Wolf sources and multimode lasers," *Opt. Commun.* **34**, 301–305 (1980).

[49] F. Gori, "Directionality and spatial coherence," *Opt. Acta* **27**, 1025–1034 (1980).

[50] F. Gori, "Mode propagation of the field generated by Collett-Wolf Schell-model sources," *Opt. Commun.* **46**, 149–154 (1983).

[51] R. Simon and N. Mukunda, "Twisted Gaussian Schell-model beams," *J. Opt. Soc. Am. A* **10**, 95–109 (1993).

[52] A. T. Friberg, E. Tervonen, and J. Turunen, "Interpretation and experimental demonstration of twisted Gaussian Schell-model beams," *J. Opt. Soc. Am. A* **11**, 1818–1826 (1994).

[53] Z. Tong and O. Korotkova, "Beyond the classical Rayleigh limit with twisted light," *Opt. Lett.* **37**, 2595–2597 (2012).

[54] C. Liang, G. Wu, F. Wang, W. Li, Y. Cai, and S. A. Ponomarenko, "Overcoming the classical Rayleigh diffraction limit by controlling two-point correlations of partially coherent light sources," *Opt. Express* **25**, 28352–28362 (2017).

[55] M. A. Porras, "Ultrashort pulsed Gaussian light beams," *Phys. Rev. E* **58**, 1086–1093 (1998).

[56] S. Feng, H. G. Winful, and R. W. Hellwarth, "Spatiotemporal evolution of focused single-cycle electromagnetic pulses," *Phys. Rev. E* **59**, 4630–4649 (1999).

[57] V. V. Kozlov, N. N. Rosanov, and S. Wabnitz, "Obtaining single-cycle pulses from a mode-locked laser," *Phys. Rev. A* **84**, 053810 (2011).

[58] V. V. Kozlov and N. N. Rosanov, "Single-cycle-pulse passively-mode-locked laser with inhomogeneously broadened active medium," *Phys. Rev. A* **87**, 043836 (2013).

[59] R. M. Arkhipov, M. V. Arkhipov, I. Babushkin, and N. N. Rosanov, "Self-induced transparency mode locking, and area theorem," *Opt. Lett.* **41**, 737–740 (2016).

[60] V. Torres-Company, H. Lajunen, and A. T. Friberg, "Coherence theory of noise in ultrashort-pulse trains," *J. Opt. Soc. Am. B* **24**, 1441–1450 (2007).

[61] H. Lajunen, J. Tervo, and P. Vahimaa, "Overall coherence and coherent-mode expansion of spectrally partially coherent plane-wave pulses," *J. Opt. Soc. Am. A* **21**, 2117–2123 (2004).

[62] A. Schell, "A technique for the determination of the radiation pattern of a partially coherent aperture," *IEEE Trans. Antennas Propag.* **15**, 187–188 (1967).

[63] A. T. Friberg and E. Wolf, "Relationships between the complex degrees of coherence in the space–time and in the space–frequency domains," *Opt. Lett.* **20**, 623–625 (1995).

[64] F. Gori and M. Santarsiero, "Devising genuine spatial correlation functions," *Opt. Lett.* **32**, 3531–3533 (2007).

[65] P. Pääkkönen, J. Turunen, P. Vahimaa, A. T. Friberg, and F. Wyrowski, "Partially coherent Gaussian pulses," *Opt. Commun.* **204**, 53–58 (2002).

[66] L. Mandel, "Concept of cross-spectral purity in coherence theory," *J. Opt. Soc. Am.* **51**, 1342–1350 (1961).

[67] L. Mandel and E. Wolf, "Spectral coherence and the concept of cross-spectral purity∗," *J. Opt. Soc. Am.* **66**, 529–535 (1976).

[68] D. F. James and E. Wolf, "Cross-spectrally pure light and the spectral modulation law," *Opt. Commun.* **138**, 257–261 (1997).

[69] H. Liu, J. Cheng, and S. Han, "Cross spectral purity and its influence on ghost imaging experiments," *Opt. Commun.* **273**, 50–53 (2007).

[70] M. Lahiri and E. Wolf, "Statistical similarity and cross-spectral purity of stationary stochastic fields," *Opt. Lett.* **37**, 963–965 (2012).

[71] M. Lahiri and E. Wolf, "Effect of scattering on cross-spectral purity of light," *Opt. Commun.* **330**, 165–168 (2014).

[72] T. Hassinen, J. Tervo, and A. T. Friberg, "Cross-spectral purity of electromagnetic fields," *Opt. Lett.* **34**, 3866–3868 (2009).

[73] J. Chen, R. Lu, F. Chen, and J. Li, "Cross-spectrally pure light, cross-spectrally pure fields and statistical similarity in electromagnetic fields," *J. Mod. Opt.* **61**, 1164–1173 (2014).

[74] T. Hassinen, J. Tervo, and A. T. Friberg, "Purity of partial polarization in the frequency and time domains," *Opt. Lett.* **38**, 1221–1223 (2013).

[75] T. Hassinen, J. Tervo, and A. T. Friberg, "Cross-spectral purity of the Stokes parameters," *Appl. Phys. B* **105**, 305–308 (2011).

[76] X. Peng, D. Ye, Y. Xin, Y. Chen, and M. Song, "Cross-spectral purity of Stokes parameters, purity of partial polarization and statistical similarity," *Optik* **145**, 42–48 (2017).

[77] I. Christov, "Propagation of partially coherent light pulses," *Opt. Acta* **33**, 63–72 (1986).

[78] R. W. Ziolkowski and J. B. Judkins, "Propagation characteristics of ultrawide-bandwidth pulsed Gaussian beams," *J. Opt. Soc. Am. A* **9**, 2021–2030 (1992).

[79] L. Sereda, M. Bertolotti, and A. Ferrari, "Coherence properties of nonstationary light wave fields," *J. Opt. Soc. Am. A* **15**, 695–705 (1998).

[80] Q. Lin, L. Wang, and S. Zhu, "Partially coherent light pulse and its propagation," *Opt. Commun.* **219**, 65–70 (2003).

[81] L.-G. Wang, Q. Lin, H. Chen, and S.-Y. Zhu, "Propagation of partially coherent pulsed beams in the spatiotemporal domain," *Phys. Rev. E* **67**, 056613 (2003).

[82] C. Chen, H. Yang, Y. Lou, and S. Tong, "Second-order statistics of Gaussian Schell-model pulsed beams propagating through atmospheric turbulence," *Opt. Express* **19**, 15196–15204 (2011).

[83] Y. Cai, Y. Chen, and F. Wang, "Generation and propagation of partially coherent beams with nonconventional correlation functions: a review," *J. Opt. Soc. Am. A* **31**, 2083–2096 (2014).

[84] G. Gbur and T. Visser, "The structure of partially coherent fields," in *Progress in Optics*, Vol. 55, E. Wolf, ed. (Elsevier, 2010), pp. 285–341.

[85] H. Lajunen and T. Saastamoinen, "Propagation characteristics of partially coherent beams with spatially varying correlations," *Opt. Lett.* **36**, 4104–4106 (2011).

[86] Z. Mei, "Light sources generating self-focusing beams of variable focal length," *Opt. Lett.* **39**, 347–350 (2014).

[87] Z. Song, Z. Liu, K. Zhou, Q. Sun, and S. Liu, "Propagation characteristics of a non-uniformly Hermite–Gaussian correlated beam," *J. Opt.* **18**, 015606 (2015).

[88] Z. Mei and O. Korotkova, "Cosine-Gaussian Schell-model sources," *Opt. Lett.* **38**, 2578–2580 (2013).

[89] Y. Chen, J. Gu, F. Wang, and Y. Cai, "Self-splitting properties of a Hermite-Gaussian correlated Schell-model beam," *Phys. Rev. A* **91**, 013823 (2015).

[90] Y. Chen, S. A. Ponomarenko, and Y. Cai, "Self-steering partially coherent beams," *Sci. Rep.* **7**, 39957 (2017).

[91] O. Korotkova, S. Sahin, and E. Shchepakina, "Multi-Gaussian Schell-model beams," *J. Opt. Soc. Am. A* **29**, 2159–2164 (2012).

[92] S. Sahin and O. Korotkova, "Light sources generating far fields with tunable flat profiles," *Opt. Lett.* **37**, 2970–2972 (2012).

[93] Z. Mei and O. Korotkova, "Random sources generating ring-shaped beams," *Opt. Lett.* **38**, 91–93 (2013).

[94] O. Korotkova, "Random sources for rectangular far fields," *Opt. Lett.* **39**, 64–67 (2014).

[95] Z. Mei, "Two types of sinc Schell-model beams and their propagation characteristics," *Opt. Lett.* **39**, 4188–4191 (2014).

[96] F. Wang and O. Korotkova, "Random sources for beams with azimuthal intensity variation," *Opt. Lett.* **41**, 516–519 (2016).

[97] J. Li, F. Wang, and O. Korotkova, "Random sources for cusped beams," *Opt. Express* **24**, 17779–17791 (2016).

[98] Z. Mei and O. Korotkova, "Random sources for rotating spectral densities," *Opt. Lett.* **42**, 255–258 (2017).

[99] Y. Yuan, X. Liu, F. Wang, Y. Chen, Y. Cai, J. Qu, and H. T. Eyyuboğlu, "Scintillation index of a multi-Gaussian Schell-model beam in turbulent atmosphere," *Opt. Commun.* **305**, 57–65 (2013).

[100] H. Lajunen and T. Saastamoinen, "Non-uniformly correlated partially coherent pulses," *Opt. Express* **21**, 190–195 (2013).

[101] C. Ding, O. Korotkova, Y. Zhang, and L. Pan, "Cosine-Gaussian correlated Schell-model pulsed beams," *Opt. Express* **22**, 931–942 (2014).

[102] C. Ding, O. Korotkova, and L. Pan, "The control of pulse profiles with tunable temporal coherence," *Phys. Lett. A* **378**, 1687–1690 (2014).

[103] E. Wolf and G. S. Agarwal, "Coherence theory of laser resonator modes," *J. Opt. Soc. Am. A* **1**, 541–546 (1984).

[104] C. M. Warnky, B. L. Anderson, and C. A. Klein, "Determining spatial modes of lasers with spatial coherence measurements," *Appl. Opt.* **39**, 6109–6117 (2000).

[105] N. Stelmakh and M. Flowers, "Measurement of spatial modes of broad-area diode lasers with 1-GHz resolution grating spectrometer," *IEEE Photon. Technol. Lett.* **18**, 1618–1620 (2006).

[106] H. Lajunen, P. Vahimaa, and J. Tervo, "Theory of spatially and spectrally partially coherent pulses," *J. Opt. Soc. Am. A* **22**, 1536–1545 (2005).

[107] T. Voipio, T. Setälä, and A. T. Friberg, "Coherent-mode representation of partially polarized pulsed electromagnetic beams," *J. Opt. Soc. Am. A* **30**, 2433–2443 (2013).

[108] A. Starikov and E. Wolf, "Coherent-mode representation of Gaussian Schell-model sources and of their radiation fields," *J. Opt. Soc. Am.* **72**, 923–928 (1982).

[109] Z. Mei, "Hyperbolic sine-correlated beams," *Opt. Express* **27**, 7491–7497 (2019).

[110] M. Santarsiero, R. Martínez-Herrero, D. Maluenda, J. C. G. de Sande, G. Piquero, and F. Gori, "Partially coherent sources with circular coherence," *Opt. Lett.* **42**, 1512–1515 (2017).

[111] B. H. Kolner, "Space-time duality and the theory of temporal imaging," *IEEE J. Quantum Electron.* **30**, 1951–1963 (1994).

[112] J. Lancis, V. Torres-Company, E. Silvestre, and P. Andrés, "Space–time analogy for partially coherent plane-wave-type pulses," *Opt. Lett.* **30**, 2973–2975 (2005).

[113] V. Torres-Company, H. Lajunen, J. Lancis, and A. T. Friberg, "Ghost interference with classical partially coherent light pulses," *Phys. Rev. A* **77**, 043811 (2008).

[114] V. Torres-Company, J. Lancis, and P. Andrés, "Space-time analogies in optics," in *Progress in Optics*, Vol. 56, E. Wolf, ed. (Elsevier, 2011), pp. 1–80.

[115] R. Salem, M. A. Foster, and A. L. Gaeta, "Application of space–time duality to ultrahigh-speed optical signal processing," *Adv. Opt. Photon.* **5**, 274–317 (2013).

[116] S. A. Collins, "Lens-system diffraction integral written in terms of matrix optics," *J. Opt. Soc. Am.* **60**, 1168–1177 (1970).

[117] S. P. Dijaili, A. Dienes, and J. S. Smith, "ABCD matrices for dispersive pulse propagation," *IEEE J. Quantum Electron.* **26**, 1158–1164 (1990).

[118] G. Gbur and E. Wolf, "The Rayleigh range of partially coherent beams," *Opt. Commun.* **199**, 295–304 (2001).

[119] F. Gori, "Far-zone approximation for partially coherent sources," *Opt. Lett.* **30**, 2840–2842 (2005).

[120] A. L. Marec, O. Guilbaud, O. Larroche, and A. Klisnick, "Evidence of partial temporal coherence effects in the linear autocorrelation of extreme ultraviolet laser pulses," *Opt. Lett.* **41**, 3387–3390 (2016).

[121] T. Osaka, T. Hirano, Y. Morioka, Y. Sano, Y. Inubushi, T. Togashi, I. Inoue, K. Tono, A. Robert, K. Yamauchi, J. B. Hastings, and M. Yabashi, "Characterization of temporal coherence of hard X-ray free-electron laser pulses with single-shot interferograms," *IUCrJ* **4**, 728–733 (2017).

[122] A. L. Marec, O. Larroche, and A. Klisnick, "Linear autocorrelation of partially coherent extreme-ultraviolet lasers: a quantitative analysis," *Opt. Lett.* **42**, 4958–4961 (2017).

[123] E. Tervonen, J. Turunen, and A. T. Friberg, "Transverse laser-mode structure determination from spatial coherence measurements: experimental results," *Appl. Phys. B* **49**, 409–414 (1989).

[124] B. L. Anderson and P. L. Fuhr, "Twin-fiber interferometric method for measuring spatial coherence," *Opt. Eng.* **32**, 926–932 (1993).

[125] C. K. Hitzenberger, M. Danner, W. Drexler, and A. F. Fercher, "Measurement of the spatial coherence of superluminescent diodes," *J. Mod. Opt.* **46**, 1763–1774 (1999).

[126] M. Santarsiero and R. Borghi, "Measuring spatial coherence by using a reversed-wavefront Young interferometer," *Opt. Lett.* **31**, 861–863 (2006).

[127] H. Partanen, J. Turunen, and J. Tervo, "Coherence measurement with digital micromirror device," *Opt. Lett.* **39**, 1034–1037 (2014).

[128] H. E. Kondakci, A. Beckus, A. El-Halawany, N. Mohammadian, G. K. Atia, and A. F. Abouraddy, "Coherence measurements of scattered incoherent light for lensless identification of an object's location and size," *Opt. Express* **25**, 13087–13100 (2017).

[129] A. El-Halawany, A. Beckus, H. E. Kondakci, M. Monroe, N. Mohammadian, G. K. Atia, and A. F. Abouraddy, "Incoherent lensless imaging via coherency back-propagation," *Opt. Lett.* **42**, 3089–3092 (2017).

[130] H. W. Wessely and J. O. Bolstad, "Interferometric technique for measuring the spatial-correlation function of optical radiation fields$*$," *J. Opt. Soc. Am.* **60**, 678–682 (1970).

[131] H. Arimoto and Y. Ohtsuka, "Measurements of the complex degree of spectral coherence by use of a wave-front-folded interferometer," *Opt. Lett.* **22**, 958–960 (1997).

[132] A. Bhattacharjee, S. Aarav, and A. K. Jha, "Two-shot measurement of spatial coherence," *Appl. Phys. Lett.* **113**, 051102 (2018).

[133] W. H. Carter, "Measurement of second-order coherence in a light beam using a microscope and a grating," *Appl. Opt.* **16**, 558–563 (1977).

[134] C. Iaconis and I. A. Walmsley, "Direct measurement of the two-point field correlation function," *Opt. Lett.* **21**, 1783–1785 (1996).

[135] Y. Mejía and A. I. González, "Measuring spatial coherence by using a mask with multiple apertures," *Opt. Commun.* **273**, 428–434 (2007).

[136] S. Cho, M. A. Alonso, and T. G. Brown, "Measurement of spatial coherence through diffraction from a transparent mask with a phase discontinuity," *Opt. Lett.* **37**, 2724–2726 (2012).

[137] A. Efimov, "Lateral-shearing, delay-dithering Mach–Zehnder interferometer for spatial coherence measurement," *Opt. Lett.* **38**, 4522–4525 (2013).

[138] K. Saastamoinen, J. Tervo, J. Turunen, P. Vahimaa, and A. T. Friberg, "Spatial coherence measurement of polychromatic light with modified Young's interferometer," *Opt. Express* **21**, 4061–4071 (2013).

[139] R. R. Naraghi, H. Gemar, M. Batarseh, A. Beckus, G. Atia, S. Sukhov, and A. Dogariu, "Wide-field interferometric measurement of a nonstationary complex coherence function," *Opt. Lett.* **42**, 4929–4932 (2017).

[140] L. Pan, X. Chao, Z.-C. Ren, H.-T. Wang, and J. Ding, "Measuring spatial coherence by using a lateral shearing interferometry," *Appl. Opt.* **58**, 56–61 (2019).

[141] H. Cao, Y. G. Zhao, S. T. Ho, E. W. Seelig, Q. H. Wang, and R. P. H. Chang, "Random laser action in semiconductor powder," *Phys. Rev. Lett.* **82**, 2278–2281 (1999).

[142] E. Saldin, E. V. Schneidmiller, and M. V. Yurkov, *The Physics of Free Electron Lasers* (Springer, 2000).

[143] H. Cao, Y. Ling, J. Y. Xu, C. Q. Cao, and P. Kumar, "Photon statistics of random lasers with resonant feedback," *Phys. Rev. Lett.* **86**, 4524–4527 (2001).

[144] R. C. Polson, M. E. Raikh, and Z. V. Vardeny, "Universal properties of random lasers," *IEEE J. Sel. Top. Quantum Electron.* **9**, 120–123 (2003).

[145] D. S. Wiersma, "The physics and applications of random-lasers," *Nat. Phys.* **4**, 359–367 (2008).

[146] B. Redding, M. A. Choma, and H. Cao, "Spatial coherence of random laser emission," *Opt. Lett.* **36**, 3404–3406 (2011).

[147] D. S. Wiersma, "Disordered photonics," *Nat. Photonics* **7**, 188–196 (2013).

[148] H. Partanen, J. Tervo, and J. Turunen, "Spatial coherence of broad-area laser diodes," *Appl. Opt.* **52**, 3221–3228 (2013).

[149] A. Efimov, "Spatial coherence at the output of multimode optical fibers," *Opt. Express* **22**, 15577–15588 (2014).

[150] T. K. Hakala, A. J. Moilanen, A. I. Väkeväinen, R. Guo, J.-P. Martikainen, K. S. Daskalakis, H. T. Rekola, A. Julku, and P. Törmä, "Bose-Einstein condensation in a plasmonic lattice," *Nat. Phys.* **14**, 739–744 (2018).

[151] T. Young, "II. The Bakerian Lecture. On the theory of light and colours," *Philos. Trans. Royal Soc.* **92**, 12–48 (1802).

[152] T. Young, "I. The Bakerian Lecture. Experiments and calculations relative to physical optics," *Philos. Trans. Royal Soc.* **94**, 1–16 (1804).

[153] E. Vasileva, Y. Li, I. Sychugov, M. Mensi, L. Berglund, and S. Popov, "Lasing from organic dye molecules embedded in transparent wood," *Adv. Opt. Mater.* **5**, 1700057 (2017).

[154] I. Burgert, E. Cabane, C. Zollfrank, and L. Berglund, "Bio-inspired functional wood-based materials – hybrids and replicates," *Int. Mater. Rev.* **60**, 431–450 (2015).

[155] M. Zhu, J. Song, T. Li, A. Gong, Y. Wang, J. Dai, Y. Yao, W. Luo, D. Henderson, and L. Hu, "Highly anisotropic, highly transparent wood composites," *Adv. Mater.* **28**, 5181–5187 (2016).

[156] Y. Li, Q. Fu, S. Yu, M. Yan, and L. Berglund, "Optically transparent wood from a nanoporous cellulosic template: combining functional and structural performance," *Biomacromolecules* **17**, 1358–1364 (2016).

[157] M. Zhu, T. Li, C. S. Davis, Y. Yao, J. Dai, Y. Wang, F. AlQatari, J. W. Gilman, and L. Hu, "Transparent and haze wood composites for highly efficient broadband light management in solar cells," *Nano Energy* **26**, 332–339 (2016).

[158] T. Li, M. Zhu, Z. Yang, J. Song, J. Dai, Y. Yao, W. Luo, G. Pastel, B. Yang, and L. Hu, "Wood composite as an energy efficient building material: guided sunlight transmittance and effective thermal insulation," *Adv. Energy Mater.* **6**, 1601122 (2016).

[159] M. Borrega, P. Ahvenainen, R. Serimaa, and L. Gibson, "Composition and structure of balsa (Ochroma pyramidale) wood," *Wood Sci. Technol.* **49**, 403–420 (2015).

[160] J. Motohisa, J. Noborisaka, J. Takeda, M. Inari, and T. Fukui, "Catalyst-free selective-area MOVPE of semiconductor nanowires on (111)B oriented substrates," *J. Cryst. Growth* **272**, 180 – 185 (2004).

[161] W. Lu and C. M. Lieber, "Semiconductor nanowires," *J. Phys. D* **39**, R387–R406 (2006).

[162] J. Arbiol and Q. Xiong, *Semiconductor Nanowires* (Elsevier Science, 2015).

[163] F. Gori, G. Guattari, C. Palma, and C. Padovani, "Specular cross-spectral density functions," *Opt. Commun.* **68**, 239–243 (1988).

[164] H. Partanen, N. Sharmin, J. Tervo, and J. Turunen, "Specular and antispecular light beams," *Opt. Express* **23**, 28718–28727 (2015).

[165] R. Dutta, J. Turunen, and A. T. Friberg, "Michelson's interferometer and the temporal coherence of pulse trains," *Opt. Lett.* **40**, 166–169 (2015).

[166] J. M. Dudley and S. Coen, "Coherence properties of supercontinuum spectra generated in photonic crystal and tapered optical fibers," *Opt. Lett.* **27**, 1180–1182 (2002).

[167] G. Genty, M. Surakka, J. Turunen, and A. T. Friberg, "Complete characterization of supercontinuum coherence," *J. Opt. Soc. Am. B* **28**, 2301–2309 (2011).

[168] G. Stibenz and G. Steinmeyer, "High dynamic range characterization of ultrabroadband white-light continuum pulses," *Opt. Express* **12**, 6319–6325 (2004).

[169] J. Wemans, G. Figueira, N. Lopes, and L. Cardoso, "Self-referencing spectral phase interferometry for direct electric-field reconstruction with chirped pulses," *Opt. Lett.* **31**, 2217–2219 (2006).

[170] J. Bethge, C. Grebing, and G. Steinmeyer, "A fast Gabor wavelet transform for high-precision phase retrieval in spectral interferometry," *Opt. Express* **15**, 14313–14321 (2007).

[171] J. Ratner, G. Steinmeyer, T. C. Wong, R. Bartels, and R. Trebino, "Coherent artifact in modern pulse measurements," *Opt. Lett.* **37**, 2874–2876 (2012).

[172] X. Gu, M. Kimmel, A. P. Shreenath, R. Trebino, J. M. Dudley, S. Coen, and R. S. Windeler, "Experimental studies of the coherence of microstructure-fiber supercontinuum," *Opt. Express* **11**, 2697–2703 (2003).

[173] I. Zeylikovich and R. Alfano, "Coherence properties of the supercontinuum source," *Appl. Phys. B* **77**, 265–268 (2003).

[174] M. Närhi, J. Turunen, A. T. Friberg, and G. Genty, "Experimental Measurement of the Second-Order Coherence of Supercontinuum," *Phys. Rev. Lett.* **116**, 243901 (2016).

[175] Y. Zhang, D. J. Kane, and F. G. Omenetto, "Experimental measurement of supercontinuum coherence in tellurite photonic crystal fibers," *Opt. Lett.* **42**, 4857–4860 (2017).

[176] R. Jafari, T. Jones, and R. Trebino, "100% reliable algorithm for second-harmonic-generation frequency-resolved optical gating," *Opt. Express* **27**, 2112–2124 (2019).

[177] C. Bourassin-Bouchet and M.-E. Couprie, "Partially coherent ultrafast spectrography," *Nat. Commun.* **6**, 6465 (2015).

[178] C. Ding, L. Pan, and B. Lü, "Characterization of stochastic spatially and spectrally partially coherent electromagnetic pulsed beams," *New J. Phys.* **11**, 083001 (2009).

[179] C. Ding, L. Pan, and B. Lü, "Changes in the spectral degree of polarization of stochastic spatially and spectrally partially coherent electromagnetic pulses in dispersive media," *J. Opt. Soc. Am. B* **26**, 1728–1735 (2009).

[180] C. Ding, O. Korotkova, Y. Zhang, and L. Pan, "Sinc Schell-model pulses," *Opt. Commun.* **339**, 115–122 (2015).

[181] H. Lajunen, J. Tervo, J. Turunen, P. Vahimaa, and F. Wyrowski, "Spectral coherence properties of temporally modulated stationary light sources," *Opt. Express* **11**, 1894–1899 (2003).

[182] V. Torres-Company, G. Mínguez-Vega, J. Lancis, and A. T. Friberg, "Controllable generation of partially coherent light pulses with direct space-to-time pulse shaper," *Opt. Lett.* **32**, 1608–1610 (2007).

[183] J. M. Dudley, G. Genty, and S. Coen, "Supercontinuum generation in photonic crystal fiber," *Rev. Mod. Phys.* **78**, 1135–1184 (2006).

[184] S. Lowenthal and D. Joyeux, "Speckle removal by a slowly moving diffuser associated with a motionless diffuser," *J. Opt. Soc. Am.* **61**, 847–851 (1971).

[185] G. Li, Y. Qiu, and H. Li, "Coherence theory of a laser beam passing through a moving diffuser," *Opt. Express* **21**, 13032–13039 (2013).

[186] S. G. Reddy, A. Kumar, S. Prabhakar, and R. P. Singh, "Experimental generation of ring-shaped beams with random sources," *Opt. Lett.* **38**, 4441–4444 (2013).

[187] Y. Chen, F. Wang, L. Liu, C. Zhao, Y. Cai, and O. Korotkova, "Generation and propagation of a partially coherent vector beam with special correlation functions," *Phys. Rev. A* **89**, 013801 (2014).

[188] Y. Chen, F. Wang, C. Zhao, and Y. Cai, "Experimental demonstration of a Laguerre-Gaussian correlated Schell-model vortex beam," *Opt. Express* **22**, 5826–5838 (2014).

[189] F. Wang, C. Liang, Y. Yuan, and Y. Cai, "Generalized multi-Gaussian correlated Schell-model beam: from theory to experiment," *Opt. Express* **22**, 23456–23464 (2014).

[190] S. Cui, Z. Chen, L. Zhang, and J. Pu, "Experimental generation of nonuniformly correlated partially coherent light beams," *Opt. Lett.* **38**, 4821–4824 (2013).

[191] M. W. Hyde, S. Basu, D. G. Voelz, and X. Xiao, "Experimentally generating any desired partially coherent Schell-model source using phase-only control," *J. Appl. Phys.* **118**, 093102 (2015).

[192] J. Lehtolahti, M. Kuittinen, J. Turunen, and J. Tervo, "Coherence modulation by deterministic rotating diffusers," *Opt. Express* **23**, 10453–10466 (2015).

[193] P. Vahimaa and J. Turunen, "Finite-elementary-source model for partially coherent radiation," *Opt. Express* **14**, 1376–1381 (2006).

[194] J. Turunen, "Elementary-field representations in partially coherent optics," *J. Mod. Opt.* **58**, 509–527 (2011).

[195] F. Gori, G. Guattari, and C. Padovani, "Modal expansion for J_0-correlated Schell-model sources," *Opt. Commun.* **64**, 311–316 (1987).

[196] C. Palma and G. Cincotti, "Imaging of J_0-correlated Bessel-Gauss beams," *IEEE J. Quantum Electron.* **33**, 1032–1040 (1997).

[197] R. Borghi, "Superposition scheme for J_0-correlated partially coherent sources," *IEEE J. Quantum Electron.* **35**, 849–856 (1999).

[198] F. Gori, M. Santarsiero, and R. Borghi, "Modal expansion for J_0-correlated electromagnetic sources," *Opt. Lett.* **33**, 1857–1859 (2008).

[199] H. Kandpal, "Generation of cross-spectrally pure light by two diffusers moving in opposite directions and determination of diffuser surface roughness," *Opt. Commun.* **207**, 73–76 (2002).

[200] R. H. Katyl, "Compensating optical systems. Part 3: achromatic Fourier transformation," *Appl. Opt.* **11**, 1255–1260 (1972).

[201] G. M. Morris, "Diffraction theory for an achromatic Fourier transformation," *Appl. Opt.* **20**, 2017–2025 (1981).

[202] G. M. Morris, "An ideal achromatic fourier processor," *Opt. Commun.* **39**, 143–147 (1981).

[203] C. Brophy, "Design of an all-glass achromatic-fourier-transform lens," *Opt. Commun.* **47**, 364–368 (1983).

MATIAS KOIVUROVA

This thesis considers the spatial, temporal, and spectral coherence properties of pulsed light. The theoretical investigation extends the concept of cross-spectral purity to nonstationary fields. Additionally, spatiotemporally coupled, self-focusing, as well as self-splitting model fields are introduced. Several novel measurement modalities for characterization of pulsed light are considered in detail, and lastly, methods for controlling coherence properties are discussed.

UNIVERSITY OF
EASTERN FINLAND

uef.fi

PUBLICATIONS OF
THE UNIVERSITY OF EASTERN FINLAND
Dissertations in Forestry and Natural Sciences

ISBN 978-952-61-3115-3
ISSN 1798-5668